Coordination of the cell cycle and the cytoskeleton during oocyte meiosis

Dissertation

for the award of the degree

“Doctor rerum naturalium”

of the Georg-August-Universität Göttingen

within the doctoral program

International Max-Planck Research School

of the Göttingen Graduate School for Neurosciences,

Biophysics, and Molecular Biosciences (GGNB)

submitted by

Ivan Avilov

from Nikopol, Ukraine

Göttingen, 2023

Thesis Committee

Dr. Peter Lenart
Research group Cytoskeletal Dynamics in Oocytes,
Max Planck Institute for Multidisciplinary Sciences

Prof. Dr. Henning Urlaub
Research group Bioanalytical Mass Spectrometry,
Max Planck Institute for Multidisciplinary Sciences

Dr. Melina Schuh
Department of Meiosis,
Max Planck Institute for Multidisciplinary Sciences

Dr. Ufuk Günesdogan
Department of Developmental Biology,
Göttingen Center for Molecular Biosciences

Members of the Examination Board

1st Referee: **Dr. Peter Lenart**
Research group Cytoskeletal Dynamics in Oocytes,
Max Planck Institute for Multidisciplinary Sciences

2nd Referee: **Prof. Dr. Henning Urlaub**
Research group Bioanalytical Mass Spectrometry,
Max Planck Institute for Multidisciplinary Sciences

Dr. Melina Schuh
Department of Meiosis,
Max Planck Institute for Multidisciplinary Sciences

Dr. Ufuk Günesdogan
Department of Developmental Biology,
Göttingen Center for Molecular Biosciences

Prof. Dr. Jan Huisken
Laboratory of Multiscale Biology
Georg-August-Universität Göttingen

Prof. Dr. Timo Betz
Third Institute of Physics– Biophysics,
Georg-August-Universität Göttingen

Date of oral examination: 1st of June 2023

“And the light shineth in darkness; and the darkness comprehended it not”

- John 1:5

Table of contents

Acknowledgments

First of all, I would like to thank my supervisor Dr. Peter Lenart for giving me the opportunity to work together and discover the developmental biology universe. Without your infinite patience and continuous guidance, I would not be able to finalize my manuscripts and the doctor's thesis work.

I am grateful to the International Max Planck Research School of Molecular Biology for giving me the opportunity to do my Master's and PhD studies in the excellent scientific environment and for the valuable financial support in the past years.

I want to mention and show my gratitude to Prof. Dr. Henning Urlaub Dr. Melina Schuh and Dr. Ufuk Günesdogan for their support as thesis advisory committee members as well as Prof. Dr. Jan Huisken and Prof. Dr. Timo Betz for kindly participating in my examination board.

I would also like to thank the former and present members of the research group of Cytoskeletal Dynamics in Oocytes where one always can find valuable advice, share some jokes or food, and have a really good time together. Especially I want to say thank you to Antonio and Jasmin for being my friends and supporting me in my hour of need.

My work would not be possible without the help of my colleagues from MPI-NAT. Special thanks to members of the animal facility Sascha Krause and Ulrike Teichmann for taking care of the starfish, to Kseniia Lysakovskaia, Jens Krull, Mireia Sola, Liran Fu, and Dr. Dirk Görlich for infinite support with the molecular biology experiments, to members of the Department of Meiosis and especially Chun So (Nick) for their support with the oocyte manipulation technics, to members of the Bioanalytical Mass Spectrometry group: Luisa Welp and Monika Raabe for the help with my MS experiment and to Dr. Juliane Liepe for her support with starfish proteomics.

I want specially thank my girlfriend Nyam-Erdene and the members of the Petrichenko family: Valentyn, Lilia, and Jeka for sharing with me the happiest and saddest moments during my PhD. I am also grateful to Yehor and Aleksander, who in addition to their direct help with my PhD project are also my friends on which I can always rely on. My work and my life would not be possible without my mother. Thank you for your support and encouragement whenever life was not going well.

Abstract

Meiosis serves to reduce ploidy, to half the genetic content of germ cells before they unite again at fertilization. This is achieved by two subsequent divisions called meiosis I and II without an intermittent S-phase. In oocytes, the meiotic divisions are extremely asymmetric and characterized by the emission of small polar bodies.

Mos is a conserved kinase that is exclusively expressed in the oocytes of most animal species and is degraded after fertilization. Mos activates the ERK/MAPK pathway through the phosphorylation of MEK, that in turn phosphorylates MAPK. During meiosis, activation of Mos-MAPK mediates important functions: it is rendering the meiotic divisions highly asymmetric and it regulates the cell cycle machinery to suppress S-phase in between the two meiotic divisions. Thus, Mos can be seen as a universal switch between meiotic and mitotic types of cell division. However, the molecular mechanisms that underlie these highly conserved functions mediated by Mos-MAPK remain poorly understood.

In my work, I used the well-established and specific inhibitor, U0126 to block the Mos-MAPK pathway in starfish oocytes. I showed that U0126-treated starfish oocytes display mitotic-like spindle phenotype during metaphase I, followed by an exit from the meiotic program instead of undergoing meiosis II. This indicates that Mos-MAPK activity at metaphase I triggers key meiotic events: the second division without an S-phase and it also ensures the asymmetry of division. To identify the downstream molecular and cellular mechanisms, I then combined phospho-proteomic profiling of Mos-MAPK-inhibited oocytes with high-resolution live-cell imaging. Thereby, I was able to correlate changes in spindle morphology and cell cycle progression with the phosphorylation of specific proteins.

This led me to discover that, firstly, Mos-MAPK is responsible for the stimulation of Cyclin B synthesis through inhibition of the CPEB module, known to suppress Cyclin B translation. I have shown that injection of active Cdk1-Cyclin B complex at the meiosis I-to-II transition rescues Mos-MAPK inhibition and restores meiosis II. This indicates that Mos-MAPK-dependent synthesis of Cyclin B at the meiosis I-to-II transition is indeed sufficient to drive meiosis II. Rapid reactivation of Cdk1-Cyclin B prevents the interphase entry and therefore allows skipping the S-phase, leading to the reduction of genomic content.

Secondly, phospho-proteomic profiling identified multiple proteins under the control of Mos-MAPK that are involved in the regulation of the microtubule and actin cytoskeleton. These included proteins responsible for the recruitment and organization of the pericentriolar material at centrosomes as well as proteins that nucleate and regulate the growth of astral microtubules. Mos-MAPK-dependent regulation of these proteins explains how Mos-MAPK suppresses astral microtubules, which in turn enables the positioning of the meiotic spindle to the cortex and thereby the asymmetric meiotic divisions.

Besides the regulation of meiosis by Mos-MAPK, I studied the mechanisms of nuclear envelope breakdown (NEBD) in the unusually large nuclei of oocytes. In starfish, nuclear membrane fragmentation is dependent on the Arp2/3-nucleated F-actin 'shell'. By using super-resolution microscopy, I contributed to revealing the mechanisms by which this F-actin shell ruptures the nuclear membrane. Firstly, I found that the nuclear membrane separates into pore-free and pore-dense regions. Then, F-actin nucleates within the lamina under the pore-free membrane and forms filopodia-like spikes toward the cytoplasm. These spikes protrude and rupture the pore-free nuclear membrane, converting the pore-dense membrane regions into an ER-like network that is associated with the still-intact lamina.

Taken together, in my PhD project I identified the molecular mechanisms of how the second meiosis and the asymmetric divisions are controlled by Mos-MAPK in oocytes. I expect that the identification of the conserved molecular modules controlling meiotic functions in starfish will have important general implications for understanding meiosis in other species including humans.

Introduction

Cell cycle regulation

In eukaryotes, there are two types of the cell cycle: mitosis and meiosis. The mitotic cell cycle occurs in somatic cells and serves to maintain ploidy (Flemming, 1882), while meiosis occurs only in germ cells and functions in sexual reproduction by reducing the chromosome content by half (Farmer and Moore, 1905). In principle, the meiotic division consists of two mitotic divisions without DNA replication in between.

Mitotic progression

While most of the cell's components duplicate continuously during the cell cycle the chromosomes and centrioles duplicate during the S-phase (synthetic phase). During the M-phase, the cellular contents are segregated into two daughter cells. The S-phase and M-phase are intervened by two gap phases G1 and G2 in which the cell functions in the tissue and accumulates various components needed for division (Nurse, 2000).

After DNA duplication and transition through the G2 phase, the cell enters mitosis, which is traditionally divided into 5 stages based on chromosome morphology observed under the microscope: prophase, prometaphase, metaphase, anaphase, and telophase. When mitosis is completed, the cytoplasm is equally divided during cytokinesis. In prophase, the replicated chromosomes condense into mitotic chromosomes, and the centrioles move apart and initiate mitotic spindle formation. While the beginning of the prophase remains still poorly defined, the prometaphase starts with a major event, well visible under the microscope – nuclear envelope breakdown (NEBD). After NEBD, chromosomes attach to the kinetochore microtubules and help to nucleate additional microtubules in the spindle via the Ran pathway. At metaphase, the chromosomes align at the spindle equator. The anaphase consists of two sub-phases: anaphase A followed by anaphase B, both contributing to chromosome separation (FitzHarris, 2012). In anaphase A, the kinetochores synchronously pull the attached chromosomes to the opposing poles. In anaphase B, the opposing poles are separated by pushing forces generated by interpolar microtubules. During telophase, the chromosomes arrive at the poles and decondense. The nuclear envelope reassembles around each set of chromosomes indicating the end of mitosis. Cytokinesis is characterized by the significant involvement of actin instead of microtubules. Actin and myosin form the contractile ring that pinches the cytoplasm into the two daughter cells.

Mitotic regulation

The coordination and proper timing of the mitotic progression are ensured by a cell-cycle control system that responds to extracellular signals as well as intracellular conditions (Nurse, 2000). The main component of this system are proteins called cyclins and respective cyclin-dependent kinases (Cdks). The activity oscillations of different Cdks control multiple cellular events. For example, in animals, Cdk1-Cyclin B complex controls mitosis entry and M-phase, while Cyclin D-Cdk4/6 functions in G1-phase, Cyclin A/E-Cdk2 complex initiates the S-phase, and cyclin A-Cdk1 is implicated in G2-phase (Malumbres and Barbacid, 2005; Nigg, 2001). While the regulation of cyclin-Cdk heterodimers is very complex it shares multiple common principles among different cyclin-Cdk complexes. The control mechanisms include the translation/degradation of the cyclins and phosphorylation/dephosphorylation of the Cdks.

In addition, the cell cycle progression and its irreversibility are maintained by cell cycle checkpoints (Hartwell and Weinert, 1989). The first checkpoint or restriction point occurs at the G2-M transition and triggers mitosis only if all DNA is replicated and the environment is favorable. The second

governs the metaphase-to-anaphase transition only if all chromosomes are attached to kinetochores. Finally, the third checkpoint controls whether the cell can proceed to the S-phase.

Regulation of Cdk1-Cyclin B activity

The Cdk1-Cyclin B complex controls mitotic entry and progression until metaphase. The dramatic morphological transition from interphase to mitosis is ensured by Cdk1 kinase activity that phosphorylates almost half of the proteome (Olsen et al., 2010). At the same time, Cdk1-Cyclin B is one of the most regulated complexes in the cell (Lew and Kornbluth, 1996) (Fig. 1). During interphase, Cdk1 is maintained in the inhibited state by Wee1- and Myt1-mediated phosphorylation of the Cdk1 at the conserved Tyr15 (Fig. 1A). Upon binding to Cyclin B, the Cdc25 phosphatase dephosphorylates Cdk1 at the Tyr15 site resulting in Cdk1 activation.

Moreover, the activation of Cdk1-Cyclin B consists of initiation and autoregulation phases. At the initiation phase, the upstream signaling shifts the balance of Cdk1 phosphorylation/dephosphorylation towards the activation of a small population of Cdk1-Cyclin B complexes. In the second phase, Cdk1 initiates the autoregulatory activation loop by direct phosphorylation of Cdc25 and Wee1/Myt1 resulting in their respective activation and inhibition. This autoregulation loop activates all the Cdk1-Cyclin B pool and results in M-phase entry.

While the Cdk1-Cyclin B activation requires the Cdk1 dephosphorylation, the further progression from metaphase to anaphase requires ubiquitin-mediated Cyclin B degradation (Glotzer et al., 1991; Peters, 2006) (Fig. 2B). This process involves Cyclin B polyubiquitination by anaphase-promoting complex/cyclosome (APC/C) associated with Cdc20 and subsequent proteolysis in the proteasome. The activation of Cdk1-Cyclin B is self-destructing since the APC/C requires Cdk1 phosphorylation and the presence of a so-called “destruction box” or D-box on Cyclin B protein.

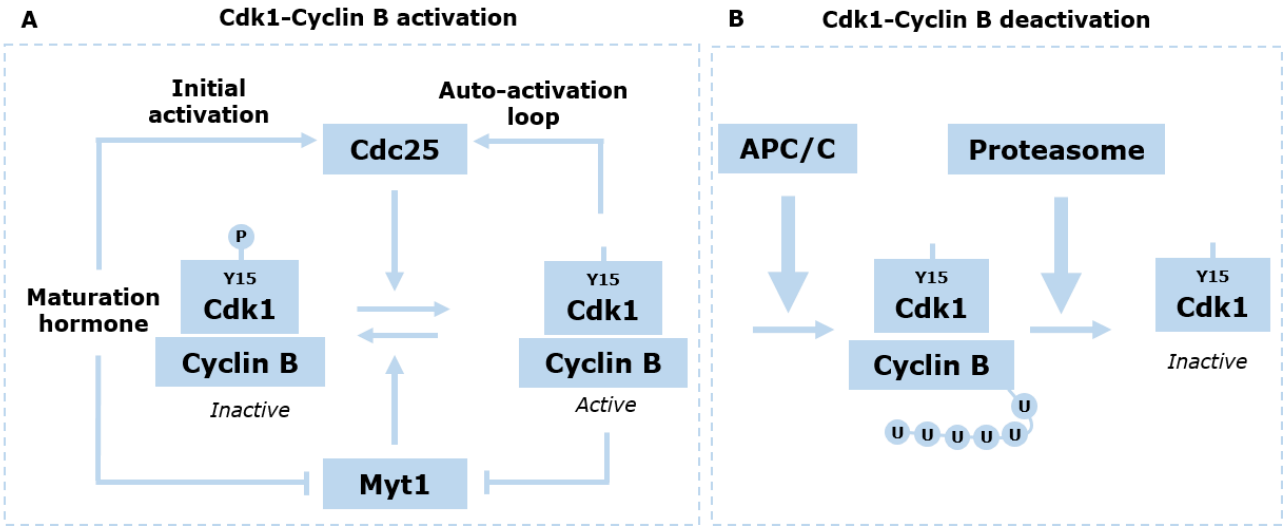

Figure 1. Regulation of the Cdk1-Cyclin B complex in meiosis.
(A) The Cdk1-Cyclin B activation consist of initial activation and auto-activation steps that regulate the Cdk1 activity by phosphoregulation.
(B) Cdk1-Cyclin B complex deactivation is occurred through Cyclin B degradation
Figure adapted form (KISHIMOTO, 2018)

Meiosis is a specialized type of cell division

Meiosis consists of two subsequent divisions called meiosis I (MI) and meiosis II (MI) without a S-phase in-between (Fig. 2). Apart from the absence of replication, which makes the meiosis reductional, there are several other important differences between meiosis and mitosis. In the current study, I am focusing on female oocyte meiosis, which in addition to differences from mitosis also differs from meiosis in male germ cells meiosis during spermatogenesis. Fertilization then restores ploidy and reverts the meiotic division pattern back to mitosis. The mechanisms of asymmetric cell division and S-phase skipping in meiosis are discussed in more detail in chapters 1 and 2.

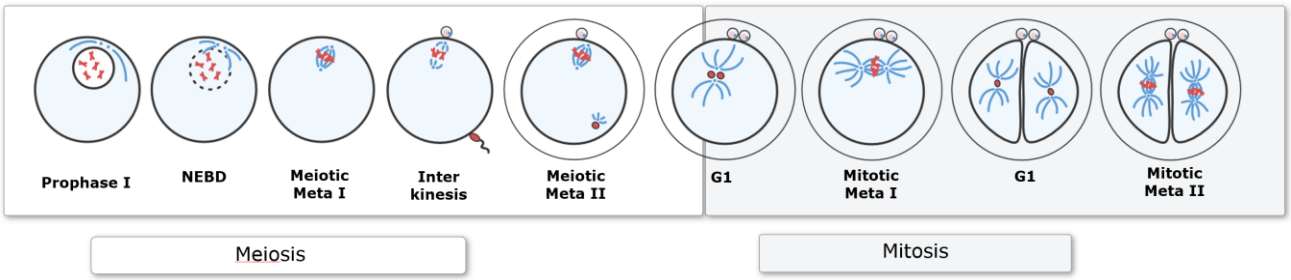

Figure 2. In oocytes, meiosis is followed by mitosis.
Meiotic divisions characterized by extreme asymmetry with extrusion of polar bodies. After pronuclear fusion the divisions reverted back mitosis with symmetric division of blastomeres.

Meiotic recombination

In meiosis, the prophase I is prolonged, and in some species like humans may take even decades (MacLennan et al., 2015). During this stage, the two homologous chromosomes each consisting of two sister chromatids pair up and become tightly juxtaposed (Baudat et al., 2013). During meiotic recombination, double-strand breaks in the DNA allow the exchange of genetic material between the homologous chromosomes. The crossovers a.k.a. chiasmata appear after homologous recombination between the homologs and holding each pair of homologs together. The sister chromatid cohesion complexes help the chiasmata to hold the homologs and orient the bivalents during metaphase I. Removal of the sister chromatid cohesion and chiasmata resolution allows the homologous chromosomes to segregate in anaphase I. The meiosis-specific kinetochore proteins ensure that the homologs remain connected at their centromeres during anaphase I. This results in the homologs separation rather than sister chromatids separation that contrast meiosis from mitosis. After meiosis I, the second meiotic division (MII) initiates rapidly without interphase and the removal of centromeric cohesion allows sister chromatid separation similar to mitosis (Baudat et al., 2013).

Meiotic maturation depends on Cdk1-Cyclin B

The oocyte meiotic division is characterized by the absence or weakening of cell cycle checkpoints (Chenevert et al., 2020). Instead, the oocytes have two cell cycle arrests (Costache et al., 2014; Jessus et al., 2020; Sagata, 1996). The first arrest occurs at prophase I, which is equivalent to late mitotic G2 and controls meiosis entry. Oocytes arrested at prophase I are called immature and as oocytes are released from this arrest is defined as meiosis resumption. The meiosis resumption is triggered by maturation hormone that differs between animal species. For example in mammals, upon luteinizing hormone (LH) surge the follicle cells that surround the oocyte release the cGMP that causes meiosis entry (Strączyńska et al., 2022). In *Xenopus*, the maturation hormone is progesterone, and in starfish 1-

methyladenine (KANATANI et al., 1969). The maturation hormone treatment initiates the intracellular signaling cascade that activates the Cdk1-Cyclin B complex stored in the cytoplasm in an inactive form as well as translation of the new Cyclin B. The activated Cdk1-Cyclin B complex provokes NEBD – as a visual indication of meiotic maturation. The ability of Cdk1-Cyclin B to initiate NEBD allowed concluding that the Cdk1-Cyclin B complex is equivalent to the maturation promoting factor (MPF) (Kishimoto, 2015).

Although, the starfish (Hara et al., 2012) and mouse oocyte (Adhikari et al., 2014) injection with an excess of purified Cdk1-Cyclin B can induce NEBD, the subsequent spindle formation is abortive (Hara et al., 2012; Okumura et al., 1996) which similar to the somatic cells (Álvarez-Fernández et al., 2013; Cundell et al., 2013). In addition to Cdk1-Cyclin B, full meiotic maturation and spindle formation requires the activation of the nuclear protein Greatwall kinase (Gwl aka MASTL) (Hara et al., 2012). Gwl activates Arpp19, which in turn inhibits the PP2A phosphatase that antagonizes Cdk1-Cyclin B activity (Hara et al., 2012). In other words, activation of Gwl stimulates Cdk1-Cyclin B activity. Following meiotic resumption, the Cdk1-Cyclin B autoactivation loop inhibits PP2A (Mochida et al., 2009). Taken together MPF consists of two components: the cytoplasmic Cdk1-Cyclin B and the nuclear Gwl (Kishimoto, 2015).

The cytostatic factor arrest

The second cell cycle arrest a.k.a. cytostatic factor (CSF) arrest synchronizes the meiotic progression in the oocytes with the event of fertilization (Costache et al., 2014; Jessus et al., 2020). The mechanism of CSF arrest varies in different species. While in vertebrates it occurs at metaphase II, in invertebrates it can take place at any stage of meiosis (Costache et al., 2014). In vertebrates, the metaphase II-arrest of oocytes is released by activation of APC/C and Cdk1-Cyclin B destruction, thus allowing the onset of anaphase II (Jessus et al., 2020). In starfish, the arrest occurs at G1-phase and is released by breaking the Rsk-mediated S-phase inhibition and suppression of Cyclin A/B synthesis, resulting in pronuclear fusion and S-phase (Hara et al., 2009). Despite the species-specific differences, the CSF arrest is established by mitogen-activated protein kinase activity (MAPK a.k.a. ERK) and released by sperm-oocyte interactions at fertilization.

Asymmetric division in meiosis

As first recognized by Theodor Boveri (Boveri, 1895), in the oocyte meiotic divisions the cytoplasm instead of splitting in half separates between the large oocyte and the small polar bodies. This makes the division extremely asymmetric. The asymmetric division differentiates oocytes not only form the somatic cells but also from the male germs cells that divide equally during spermatogenesis (Brunet and Verlhac, 2011). The obvious reason for such an unusual type of cell division is to preserve as many nutrients and maternal morphogens as possible, which are needed later for the embryo (Brunet and Verlhac, 2011). However, possibly an even more important reason for the asymmetric divisions is the control of embryo number. Minimizing the cytoplasmic volume prevents the further division of polar bodies (Saiki and Hamaguchi, 1997) and results in their degradation. There are two reasons why the elimination of polar bodies is necessary. Firstly, it prevents competition with the egg for fertilization, supported by evidence in the human oocytes where polar body fertilization is leading to parasitic twin formation (Bieber et al., 1981). Secondly, the formation of the two mature eggs within the same *Zona pellucida* may result in the mixing of the blastomeres of the two embryos (Otsuki et al., 2012). Therefore, there are multiple mechanisms to ensure the asymmetry of divisions in meiosis discussed in chapters 1 and 2 below.

Functions of actin in meiosis

The asymmetric cell division in oocyte meiosis relies on highly specialized cytoskeletal functions. Uraji and colleagues summarized the functions of F-actin in mouse oocytes identified to date (Uraji et al., 2018). The actin functions in mouse oocytes include long-range vesicular transport (Schuh, 2011), positioning of the nucleus at the center of the oocyte (Almonacid et al., 2015), migration of the meiosis I spindle towards the oocyte cortex (Dumont et al., 2007; Schuh and Ellenberg, 2008), supporting chromosome alignment and segregation (Mogessie and Schuh, 2017), cortical polarization with the formation of the so-called actin cap at the polar body extrusion site (Dehapiot et al., 2013; Deng et al., 2007), cytokinesis during polar body extrusion similarly to mitosis (Dehapiot et al., 2013), spindle anchorage to the cortex during metaphase II arrest (Yi et al., 2011) and finally spindle rotation at anaphase II (Wang et al., 2011; Zhong et al., 2005). While some of these functions remain mouse-specific, they indicate a diversity of new roles of actin, which in mitotic systems are typically associated with microtubules.

Actin regulators in meiosis

Several regulatory proteins modulate actin in oocyte meiosis. One group of these regulators are actin nucleators, namely the formin family and the Arp2/3 complex that nucleates branched or unbranched actin filaments respectively (Pollard, 2016). Another group is actin motors, myosin-2 and myosin-5 that are able to slide along the actin fibers in an ATP-dependent manner (Masters et al., 2016). Localization and activation of actin regulators depend on small GTPases: Rho, Cdc42, and Rac, and in oocytes there is evidence that the small GTPase Ran is involved.

The Arp2/3 complex consists of seven subunits, including Arp2 and Arp3 proteins. The complex is maintained in its inactive state by the sequestration of Arp moieties by the other subunits (Robinson et al., 2001). Upon actin filament binding, Arp2 and Arp3 move closer together and nucleate the base for a daughter filament (Rouiller et al., 2008). The further elongation of this filament results in an actin branch. Multiple nucleation-promoting factors activate the Arp2/3 complex including WASP, N-WASP, Scar, WAVE, and WASH (Rotty et al., 2013). Intramolecular sequestration of their Arp2/3 complex and actin-binding sites keeps them intrinsically inactive. Rho-family GTPases overcome the intramolecular interaction that inhibits WASP and N-WASP and stimulates the Arp2/3 complex activity (Chen et al., 2010). Similarly, Rac-GTP regulates WAVE and WASH (Campellone and Welch, 2010).

Formins are multidomain proteins that carry a formin homology 2 domain (FH2) that form head-to-tail homodimers (Paul and Pollard, 2009; Xu et al., 2004). There are 15 isoforms of formins in mammals that possess overlapping functions in the nucleating unbranched filaments for the filopodia, stress fibers, and contractile ring (Pollard, 2016). Most of the formins are autoinhibited by intramolecular interaction of the diaphanous autoinhibitory domain (DAD) at the N-terminus and a DAD-interacting domain (DID) at the C-terminus (Alberts, 2001). Similarly to WASP and N-WASP, the Rho-GTPase breaks this interaction and activates the formin homodimer.

NEBD in starfish depends on actin

Nuclear envelope breakdown (NEBD) dissolves cytoplasmic and nuclear compartmentalization, which contributes to the dramatic cellular reorganization at the cell division entry (Güttinger et al., 2009). In multiple animal systems, including oocytes and somatic cells, NEBD consists of two phases (Dultz et al., 2008; Lénárt et al., 2003; Linder et al., 2017; Martino et al., 2017). In phase I, the nuclear envelope remains intact while the nuclear pore complexes undergo phosphorylation-driven partial disassembly (Lénárt et al., 2003; Terasaki et al., 2001). This allows small particles up to ~70 kDa or 40 nm to leak through the nuclear membrane and potentially trigger the next phase (Mori et al., 2014). In phase II, the nuclear envelope undergoes rapid fragmentation and results in complete cyto- and

nucleoplasm intermixing (Lénárt et al., 2003). This dramatic event defines the prophase-to-prometaphase transition (Beaudouin et al., 2002).

In mammalian somatic cells, nuclear membrane fragmentation depends on microtubules and dynein (Beaudouin et al., 2002). However, in starfish oocytes, this process diverged and depends rather on actin than on microtubules (Mori et al., 2014). Prior to fragmentation, F-actin forms a shell-like structure on the inner side of the nuclear membrane (Mori et al., 2014). This actin ''shell'' is nucleated by the Arp2/3 complex and characterized by spike-like protrusions that pierce the nuclear membrane and may play a key role in membrane fragmentation (Mori et al., 2014). Inhibition of the Arp2/3 complex prevents actin "shell" formation and consequently the membrane fragmentation that eventually results in aneuploidy in starfish (Mori et al., 2014). At the moment, the exact mechanism of cytoskeletal-driven NEBD in somatic cells and starfish oocytes is poorly understood and discussed in more detail in chapter 3.

Although in other species actin-driven nuclear membrane breakdown has not been evidenced yet neither in somatic cells nor in oocytes this remains a prominent example of actin cytoskeleton adaptation to the oocyte-specific function.

Actin-driven capture of chromosomes

Capturing chromosomes by microtubules is an important step during the spindle assembly. Defects in this process may lead to chromosome loss and eventually aneuploidy. In comparison to small somatic cells, in the *Xenopus* or starfish oocyte chromosome capturing may be more error-prone due to the longer distances that chromosomes need to travel across the extremely large oocyte nucleus, the germinal vesicle (Burdyniuk et al., 2018; Harasimov et al., 2023). Therefore, in these cells, there are additional mechanisms that ensure proper chromosome delivery to the spindle assembly site.

In *Xenopus* oocytes, acentrosomal microtubule organizing centers (aMTOCs) capture the condensed chromosomes distributed in the former nucleus volume and deliver them to the animal pole, where these chromosomal-microtubule aggregates reorganize into the meiotic spindle (Gard, 1992). In contrast to *Xenopus*, in starfish oocytes, chromosome capturing depends on actin rather than microtubules (Lénárt et al., 2005). After NEBD, the F-actin forms a mesh on the former nuclear site (Lénárt et al., 2005). At the same time, the Arp2/3-nucleated F-actin encloses chromosomes into the dense actin "patches" by Ran-GTP–dependent mechanism (Burdyniuk et al., 2018). Then the enclosed chromosomal patches link to the F-actin mesh (Lénárt et al., 2005). Contraction of this mesh delivers the chromosomes to microtubules by a myosin-independent mechanism (Bun et al., 2018). Distortion of this process in starfish results in chromosome loss and aneuploidy (Burdyniuk et al., 2018).

Although apart from starfish the actin structures around chromosomes in oocytes have been visualized in jellyfish (Amiel and Houliston, 2009), tunicates (Prodon et al., 2006), *Xenopus* (Weber et al., 2004; Yamagishi and Abe, 2018), and mouse (Mogessie and Schuh, 2017), the role of actin in chromosome capturing in these animals have been investigated to a lesser detail. Nevertheless, the recent study in porcine and human oocytes indicates that chromosome clustering and capturing are driven by a dynamic network of formin-nucleated actin cables (Harasimov et al., 2023). Additionally, in human mitotic cells the actin network forms on the former nuclear membrane site after NEBD. Myosin-2-dependent contraction of this network helps to congress the chromosomes to facilitate spindle assembly (Booth et al., 2019).

Visualization of cellular processes is meiosis

Starfish as a model organism for studying meiosis

When studying biological processes, the choice of the model organism is a critical decision. While in recent times the ultimate purpose of biological research has been declared to understand and cure human disease, researching the plethora of model species gave new insights into understanding the diversity of life forms across species. While there is no perfect model organism, some are better suited for studying a certain biological question than others. For more than a century, the research in starfish helped to understand key principles of developmental biology (Fig. 3).

There are multiple advantages of studying reproduction in starfish eggs. Firstly, the echinoderms including starfishes are deuterostomes. Thus, starfish are much more closely related to vertebrates than other commonly used developmental biology models like *Drosophila* and *C. elegans*, which are protostomes. Secondly, starfish oocytes are very easy and robust in handling. They spawn, maturate, and are fertilized at room temperature in seawater without the need for incubators or special culture media. Instead of sacrificing the animal for the experiments, it is possible to collect a small piece of the ovary that promptly regenerates (Wessel et al., 2010). The process of meiosis takes less than 2 hours in comparison to days in mammals. Thirdly, starfish possess a unique feature in combining the ability to provide grams of the egg material like *Xenopus*, while having optically transparent oocytes like mice or jellyfish. This allows for conducting high-resolution microscopy and biochemical assays, including mass spectrometry in the same organism.

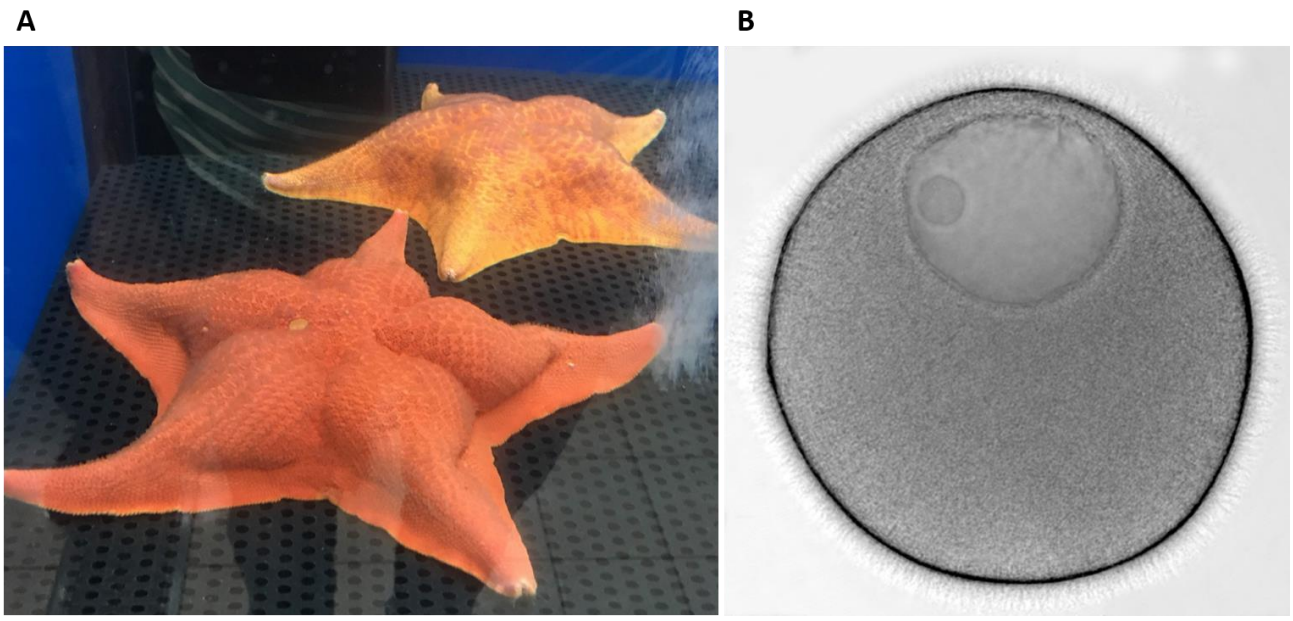

Figure 3. Bat star *Patiria miniata.*
(A) Adult bat star females in the feeding reservoir.
(B) Freshly isolated immature starfish oocyte at prophase I.

Visualization of cellular components in starfish eggs

Live-cell imaging is one of the least intrusive approaches to study meiosis progression. In addition to direct visualization of cellular processes, it allows establishing the order of events, which is crucial in perturbation experiments. There are multiple tools for labeling various cellular components tested in starfish oocytes (Dassow et al., 2018). One method is an injection of synthetic mRNA that

encodes a protein of interest tagged with fluorescent proteins like EGFP or mCherry, which can be later imaged by microscopy. The *de novo* gene synthesis, cloning, and *in vitro* transcription take less than a month. Therefore, this method allows the quick localization of proteins in oocytes. In starfish, this method has an additional advantage over immunostaining since the repertoire of available antibodies for the starfish is limited in comparison mouse or humans, for example. Nevertheless, the exogenous expression of synthetic mRNAs still has several challenges in starfish. Firstly, starfish oocytes are translationally inert which requires injecting higher amounts of mRNA that can be toxic to the oocytes. Secondly, the fluorescent proteins are optimized for the cytoplasm of mammalian cells cultured at 37 ^{0}C and are less efficient in starfish oocytes cultured at room temperature. Thirdly, the starfish animals are not a lab strain and are caught in the wild. This makes the translational efficiency vary from animal to animal. This complicates the optimization of mRNA injection dose that provides a decent signal from fluorescent protein but is not toxic for the oocytes. In addition, the increase of genetic variability of wild-caught animals makes the quantitative analysis and search space choice more challenging in mass spectrometry

Injection of recombinant proteins tagged with chemical fluorescent dyes can overcome some of the limitations of the method of mRNA expression. Additionally, chemical dyes are more photostable. In combination with the strong light resistance of starfish oocytes, it allows using high laser illumination that greatly increases the resolution of microscopy imaging. Nevertheless, expressing the recombinant proteins in *E.coli* with subsequent fluorescent dye coupling is more challenging in comparison to the *in vitro* transcription. Another challenge of using chemical fluorescent dyes is their hydrophobic nature that causes unspecific signal in the oocyte cytoplasm in comparison to the hydrophilic fluorescent proteins.

The alternative to the live imaging is fixation in aldehyde solutions followed by immunostaining with antibodies or other labeling agents. Fixation is extremely beneficial for visualizing transient cellular events. For example, the nuclear membrane rupture in starfish oocytes occurs within 35 seconds and fixation allows to “catch” this process. Additionally, fixation provides significantly higher microscopic resolution since cell immobilization allows much longer exposure times for laser illumination. Nevertheless, similarly to live imaging methods, fixation causes method-specific artifacts. In particular, in starfish oocytes treatment with aldehydes dramatically decreases permeability for the antibodies during the immunostaining step, resulting in uneven staining of the cellular components. This problem can be solved by using nanobodies (Pleiner et al., 2018) or Fab domains of the antibodies instead of traditional secondary antibodies. Due to their small size, they are able to penetrate deeper the starfish oocytes cytoplasm.

Overall, in my work, I used both approaches to localize different structures and their dynamics in starfish oocytes. Confirmation of the cellular phenotypes with both imaging methods allows better characterization of the cellular processes by overcoming their limitations and potential artifacts.

Mass spectrometry as a tool to study protein regulation

In recent years, mass spectrometry (MS) became a powerful tool for the identification and quantification of thousands of proteins. While being more technically challenging in oocyte biology, MS may eventually take over the conventional low-throughput methods of protein analysis like western blots (Kronja et al., 2014; Shaik et al., 2014; Swartz et al., 2021; Wang et al., 2010; Wühr et al., 2014).

The commonly used tandem mass spectrometry analysis, also known as MS2 consists of several steps (Hunt et al., 1986; Pappireddi et al., 2019). During the first step, the biological sample is prepared for MS. The sample undergoes protein denaturation, followed by protease treatment to fragment the denatured protein into peptides. If necessary, the sample can be enriched in phosphorylated peptides by affinity chromatography. Finally, peptides are separated by high-throughput liquid chromatography that

ensures peptide loading into the mass spectrometer one by one. In the second step, the peptides enter the first module of the mass spectrometer (referred as MS1) in which undergo ionization and separation depending on their mass-to-charge ratio (m/z). Before entering the second mass spectrometer module or MS2, the peptide ions coming from MS1 undergo additional fragmentation. In MS2, the ionized peptide fragments are separated again based on m/z values. The detector in MS2 measures the m/z values and intensity of each fragment. In the third and last step, the mass spectra are searched and matched to the peptides and quantification of ion intensities is performed by a special software, for example, MaxQuant (Cox and Mann, 2008). In order to function the proteomics platforms require a priori information about m/z values generated in the mass spectrometer. This information is generated computationally by *in silico* digestion of proteome database and prediction of the m/z values of fragmented peptides. The proteomic software identifies the peptides present in the sample by matching the predicted m/z values with the detected ones. The intensities of the peptide fragment m/z values represent the abundance of the given peptide in the sample. After testing the probability of the correct peptide identification and quantification the proteomic software uses this information to assemble a table of protein abundance in the sample.

One significant limitation of the conventional MS2 is matching the peptide intensities between several runs of MS. During each run of MS, the selection pattern of peptides that undergo ionization in MS1 is different. Comparing the non-overlapping peptide intensity patterns from different runs results in so-called missing values. The problem of missing values and MS multiplication can be solved by isobaric tandem mass tags (TMT) that allow the quantification of multiple samples in a single MS run (Dayon et al., 2008; Dayon and Affolter, 2020). The principle of the method lays in labeling the digested peptides with Tandem mass tags; each sample with a different tag. The labels are isobaric, this means that they have the same mass. Since they also have the same amino acid sequence, TMT-labelled peptides will behave the same during MS1 fragmentation and liquid chromatography. MS2 fragmentation resolves the reporter ion intensities, which are proportional to the analyte ratios in samples before mixing in LC-MS (Dayon et al., 2008; Dayon and Affolter, 2020).

Chapter 1. How does the Mos-MAPK pathway control oocyte meiosis?

(Article is in preparation for publication)

Ivan Avilov and Peter Lenart

Research Group Cytoskeletal Dynamics in Oocytes, Max Planck Institute for Multidisciplinary Sciences, Am Fassberg 11, 37077 Göttingen, Germany

Correspondence to: peter.lenart@mpinat.mpg.de

Abstract

The Mos protein is specifically expressed in oocytes and degraded upon fertilization. When present, Mos constitutively activates the ERK/MAPK pathway. This atypical activation of the ERK/MAPK during meiotic divisions has been observed across animal phyla, from the early branching cnidarians to mammals. While it is clear that Mos-MAPK controls key meiotic functions, the inherent diversity of reproductive strategies and the consequent variability in timing and morphology of meiotic divisions complicates the identification of core functions and conserved molecular mechanisms under the control of Mos-MAPK. In this review, we attempt to synthesize data from different species to first highlight the specialized cellular functions necessary for oocyte meiosis. We then discuss which of these may be under the control of Mos-MAPK. Specifically, we discuss how Mos-MAPK may control the meiotic cell cycle leading to haploidization, and entertain the hypothesis that this function may largely be mediated by translational control of Cyclin B levels. Secondly, we discuss how Mos-MAPK contributes to rendering the meiotic divisions highly asymmetric by acting on astral microtubules of the spindle, and on the cytokinetic machinery.

Conservation and diversity in oocyte meiosis

Oocyte meiosis is a specialized form of cell division that serves to produce the fertilizable egg

The female gamete, the oocyte is an exceptionally large cell that stores nutrients to support embryo development and features a very large nucleus, commonly referred to as the germinal vesicle (GV). After fertilization by the sperm, the zygote uses stored proteins, mRNAs, lipids, and other nutrients to head-start embryo development. Male and female gametes are highly specialized in adaptation to this 'division of labor' between small and motile sperm cells produced in large numbers having to find the few, large and immotile eggs. Consequently, the processes of spermatogenesis and oogenesis differ substantially in their morphology and timing.

In oocytes, the meiotic prophase, during which homologous chromosomes pair and recombine, is temporally separated from the actual meiotic divisions. This often involves a selection process whereby, the mother organism only 'invests' into growing those oocytes to full size, in which meiotic recombination has been successfully completed. The entire process of oocyte growth occurs then later in the meiotic prophase, which is generally referred to as the prophase arrest state.

In this review, we will focus on the subsequent steps of the actual oocyte divisions, commonly referred to as oocyte maturation and the roles of the Mos-MAPK pathway in its regulation. For an extensive discussion of oogenesis, including its earlier steps, we refer the reader to a recent excellent review by Jessus and co-workers (Jessus et al., 2020).

Conserved features of oocyte meiosis: reductional, asymmetric, and coordinated with fertilization

Undoubtedly, the most important function of meiotic divisions – equally for sperm and egg – is the reduction of the genomic content before male and female gametes fuse during fertilization, i.e. haploidization. This is achieved by running two division cycles without DNA replication in between: during meiosis the oocyte undergoes two divisions (M-phases), meiosis I (MI) and meiosis II (MII) without an intervening S-phase. Biochemically, it is well understood that these M-phases are driven by the conserved cell cycle module culminating in the activation of the Cdk1-Cyclin B complex (also known as MPF, i.e. M-phase or maturation promoting factor) (Dorée and Hunt, 2002). Indeed, MPF was first and best characterized in oocytes (KISHIMOTO, 2018). The key to meiotic function here is that Cdk1-Cyclin B is reactivated after meiosis I in such a way that the oocyte does not enter an interphase state and does not undergo an S-phase, as would be the case in mitosis. At the cellular level, this tightly correlates with the absence of nuclear reformation between meiosis I and II. Strikingly, after fertilization, just a few hours later in the same egg cytoplasm, rapid mitotic cell cycles take place with alternating M- and S-phases, and with the nuclear envelope disassembling and re-forming in every cycle. Thus, one critical and specific meiotic function is the reactivation of Cdk1-Cyclin B to drive meiosis II, an extra division cycle without an S-phase – fundamentally different from subsequent mitotic cycles.

The second key meiotic feature, specific to female gametes, is that the division is highly asymmetric – as recognized by Theodor Boveri early on. The purpose of this is to preserve all accumulated nutrients in a single large egg, rather than producing four equal daughter cells as is typically the case for spermatogenesis (Brunet and Verlhac, 2011). Therefore, in oocytes, the extra genomic content is expelled into small and unviable polar bodies (Maddox et al., 2012). Half of the genome, a complete set of chromosomes is segregated into the first polar body in meiosis I. Chromatids of replicated chromosomes are then segregated into the second polar body in meiosis II.

It is important to recognize that polar body divisions are fundamentally distinct in their function from other forms of asymmetric division. Asymmetric divisions produce two viable daughter cells with different sizes and typically also different fates. The function of polar body divisions is instead to produce

the smallest possible 'container' to remove the extra genomic content while minimizing cytoplasmic volume to prevent the further development of polar bodies, and thereby control embryo number. In other words, in the case of polar bodies, it is an important part of the function that polar bodies actually do not survive. If they were, they would compete with the egg for fertilization and development. In humans, for example, polar body fertilization can lead to parasitic twin formation (Bieber et al., 1981). The mechanisms that drive the specialized polar body divisions are just starting to emerge and will be discussed later in this review (Bourdais et al., 2022).

Thirdly, oocyte meiosis has to be coordinated with other events of reproduction. It is a general feature of oocyte meiosis that maturation is timed to start just before fertilization is expected to occur. Thus, the induction of the meiotic divisions is directly linked to the hormonal stimuli regulating mating and reproduction (Jessus et al., 2020). Only fully-grown oocytes are receptive to this hormonal stimulus, which automatically ensures that only those oocytes enter meiosis, which are able to support embryo development. In most species, there is then a second synchronization event to halt meiotic progression awaiting fertilization or spawning (the release of the mature egg from the ovary). In vertebrates, this arrest point is at the metaphase of meiosis II and is referred to as CSF arrest (cytostatic factor arrest), and is relieved by fertilization. In other species, oocytes may arrest at the metaphase of meiosis I or at the G1 stage after both meiotic divisions are completed (Jessus et al., 2020).

Diversity in meiosis as a result of adaptation to variable reproductive strategies

While the above three functions are essential features of oocyte meiosis across animal species, there are major species-to-species differences in the way they are executed, in their morphology, and in their timing. This should not come as a surprise, as animals show an enormous diversity in reproductive strategies. Oocyte meiosis needs to continuously 'keep up' with these changes, i.e. cellular mechanisms need to evolve that ensure the production and survival of the gametes in diverse environments and adapted morphologies.

As a prominent example, oocytes and eggs have very different sizes ranging from tens of micrometers to centimeters. There are large differences even between closely related species driven by the amount of nutrients they need to store until the embryo is able to feed on its own – which in turn is highly dependent on the lifestyle of the species. How do cytoskeletal systems adapt to cope with this enormous cytoplasmic volume?

We now understand the basic laws of how microtubule structures how are built, what determines their shape, and what limits their size (Mitchison, 2020). This predicts, for example, that in cells smaller than approximately 140 micrometers in diameter, astral microtubules of the spindle are able to reach the cell cortex (Wühr et al., 2008). Therefore, microtubules interacting with the cell cortex can directly position the spindle in a relatively small egg cell, in *C. elegans*, for example (Grill et al., 2003). However, the same model also clearly predicts that the majority of species with oocytes larger than 140 micrometers must have evolved different mechanisms for spindle positioning – which remain still largely uncharacterized. A similar scaling problem exists early in cell division: the efficiency of chromosome capture is highly dependent on the distance between chromosomes and microtubule nucleation centers (centrosomes or acentrosomal MTOCs) (Lancaster et al., 2013). Across species and cell types, the capture range of microtubule asters appears to be rather universal and is approximately 30 micrometers (Wollman et al., 2005). In oocytes, chromosomes scattered in the large oocyte nucleus (the germinal vesicle) often need to be collected from much larger distances of up to several hundreds of micrometers. This necessitated the evolution of diverse additional mechanisms to facilitate chromosome capture, including additional microtubule structures, in *Xenopus*, for example, and actin-driven mechanisms that have been characterized in starfish and more recently in mammalian species (Lénárt et al., 2005; Harasimov et al., 2023).

Besides the variable physical size of oocytes, the timing of meiosis also shows substantial diversity: whether fertilization occurs internally or externally, whether on the land or in a marine environment, there are substantial differences in when and where oocytes need to be released from the ovary and in what stage and for how long should they be waiting for fertilization. Therefore, while the fact that maturation needs to be coordinated with fertilization is a universal requirement, the actual schedule of meiotic progression is widely variable among animal species. For example, the time from hormone stimulus to maturation varies from many hours (e.g. frogs or mammalian species) to just about 10-20 minutes in marine species such as starfish or the jellyfish *Clytia*. When and for how long oocytes then arrest awaiting fertilization is also highly variable. In vertebrate oocytes, the MII arrest is released by fertilization which may be correlated with the fact that vertebrate species typically mate, so spawning is reliably followed by fertilization. Starfish oocytes instead sense the event of spawning by responding to the change in pH upon release from the ovary to the outside environment. This pH change then releases oocytes from the MI arrest, and thereafter mature eggs wait for hours for fertilization to occur (Harada et al., 2003).

Taken together, meiotic divisions produce the fertilizable egg that necessitates specialized functions such as reduction of the genomic content, the highly asymmetric divisions to produce a single, large egg cell, and the coordination of maturation with fertilization and other events of reproduction. These features are common to animal species. At the same time, there is a huge diversity in the size and geometry of oocytes and the timing of divisions across animal species adapted to their widely diverse reproductive strategies. This raises the exciting question of to what extent are the underlying molecular mechanisms evolutionarily conserved, and in which cases species evolved new solutions to carry out the same essential function in a different geometry or with a different timing.

Mos-MAPK is a conserved regulator of oocyte meiosis

Mos is a constitutive activator of the ERK/MAPK cascade exclusively expressed in oocytes

Mos is a constitutive activator of the ERK/MAPK (extracellular signal regulated kinase / mitogen-activated protein kinase) cascade. Specifically, Mos is a MAPKKK, a kinase that directly phosphorylates MEK1, the MAPK-kinase. In somatic cells, the ERK pathway is regulated by extracellular signals, such as growth factors, and is thereby one of the main pathways controlling proliferation, survival, and differentiation. Therefore, if Mos is expressed in somatic cells, it acts as a potent oncogene through the overactivation of ERK that originally led to its identification as the transforming gene of the Moloney murine sarcoma virus.

However, under physiological conditions Mos is not expressed in somatic cells; the Mos protein is present exclusively in meiotic oocytes and is degraded upon fertilization. This expression pattern appears to be strictly conserved across animal species, with very few exceptions (for example, in mice Mos is also expressed in developing spermatids). Mos is found in oocytes of all vertebrate species investigated, it is present in tunicates, and it has been extensively characterized in the echinoderm starfish, as well as in the early branching, non-bilaterian cnidarian jellyfish, *Clytia hemisphaerica*. While Mos is also found in *Drosophila*, it appears to play a less important role, and in *C. elegans* the Mos gene is absent. Overall, this indicates that the Mos-MAPK pathway is an ancient essential regulator of oocyte meiosis across Eumetazoa, that appears to have secondarily lost its importance in some Protostomes.

The Mos-MAPK pathway mediates key meiotic functions

What are the functions of this atypical activation of ERK/MAPK in meiosis? Broadly, Mos-MAPK is involved in two types of functions: control of cell cycle progression and cytoskeletal regulation. For the former, Mos-MAPK is known to have a role in (*i*) initiating meiotic maturation in response to the

maturation hormone; (*ii*) in reactivation of cdk1-cyclin B right after meiosis I and thereby mediating the skipping S-phase between MI and MII; and finally, (*iii*) Mos-MAPK also plays a critical role in the maintenance of the arrest awaiting fertilization. As for cytoskeletal regulation, Mos-MAPK's functions generally appear to be centered around ensuring the asymmetry of polar body divisions by regulating both the microtubule spindle and the actin cytoskeleton.

However, as explained above, oocyte meiosis is inherently diverse, and so are Mos' functions. For example, Mos was first characterized in *Xenopus* oocytes, where the most prominent phenotype is the block of meiotic maturation (Sagata et al., 1988). However, as it turned out later, this phenotype is rather specific to frogs. *Xenopus* belongs to the minority of species in which the response to the maturation hormone is strictly dependent on the translation of new protein. Mos itself is one of the first proteins translated in response to the maturation hormone, and it is then essential to facilitate the translation of key cell cycle regulators, prominently cyclin B2 and B5. In most species maturation either does not require translation at all, or translation is not strictly required for maturation causing no effect or a minor delay of maturation if the translation is inhibited (Minshull et al., 1991; Galas et al., 1993; Lévesque and Sirard, 1996; Hochegger et al., 2001; Ledan et al., 2001; Kuroda et al., 2004).

As another example, Mos-MAPK is clearly required for reactivation of Cdk1-Cyclin B after meiosis I in starfish and *Xenopus* oocytes: upon inhibition of Mos-MAPK, oocytes exit after meiosis I, reform the nucleus and initiate S-phase. Whether Cdk1-Cyclin B reactivation is under the control of Mos-MAPK is less clear in some other species. In mouse oocytes, results are somewhat varied as in one of the knockout lines Mos does not seem to be required for Cdk1-Cyclin B reactivation, whereas in another knockout line reformation of the nucleus after meiosis I is observed in a substantial proportion of the oocytes. In the jellyfish, *Clytia* meiosis II appears to occur normally even when Mos-MAPK is inhibited.

There is an even greater degree of diversity in the regulation of meiotic arrest points. On the one hand, it is remarkable that Mos-MAPK is required for the CSF-type arrest in all species investigated so far. Indeed, the most prominent and most common phenotype of Mos-MAPK inhibition is the override of CSF-like arrest and induction of parthenogenetic development. This clearly indicates conservation. On the other hand, the timing of the arrest, whether the arrest occurs in meiosis I, meiosis II, or the G1 phase following meiosis, is variable, and as far as we know, there is significant diversity in the underlying molecular mechanisms as well.

Mos-MAPK's functions in the regulation of the asymmetric divisions appear similarly conserved and diverse at the same time. Mos-MAPK inhibition leads to the formation of enlarged polar bodies across species, but the size of the oocytes, their spindles, the morphology of spindles, and the way spindles are positioned in the oocytes vary widely.

In the subsequent sections, we will discuss what might be the evolutionarily conserved core of molecular mechanisms under the control of the Mos-MAPK pathway mediating this wide range of meiotic functions. As detailed above, the conservation of the Mos protein, its expression pattern, the almost universally observed meiotic activation of ERK/MAPK, as well as the conservation of functions controlled by Mos-MAPK all argue for the conservation of underlying molecular mechanisms. At the same time, this conserved core must have diversified substantially, lost some, and gained additional functions in adaptation to the diverse reproductive strategies of species.

Specifically, we will follow up on two hypotheses:

(*i*) We hypothesize that in the regulation of the meiotic cell cycle, the core functions of the Mos-MAPK pathway may be the translational regulation of Cyclin B levels. This is consistent with earlier proposals that Mos-MAPK generally acts as a stabilizer of Cdk1-Cyclin B activity.

(*ii*) We will discuss which conserved molecular modules may be regulating the meiotic spindle and cytokinesis under the control of Mos-MAPK, and thereby serve as a 'switch' between the equal mitotic and the highly asymmetric meiotic divisions.

Regulation of translation by the Mos-MAPK pathway

Cytoplasmic polyadenylation regulates translation in oocyte meiosis

Oocytes store large amounts of maternal mRNA while being transcriptionally inactive. This renders the translational of maternal mRNAs the predominant mechanism to control protein amounts in oocytes. Indeed, meiotic progression is guided by the translation of mRNAs of cell cycle regulatory proteins and their targeted degradation (Mendez and Richter, 2001). Before maturation, most stored maternal mRNAs are translationally inactive due to their relatively short (<20 bases) poly(A) tails (Barkoff et al., 1998). It is the extension of this tail to >150 bases by the poly(A) polymerase enzyme (PAP) that renders the mRNAs competent for translation. Polyadenylation of maternal mRNAs depends on their 3' untranslated regions (UTRs). 3'-UTRs carry short conserved sequences recognized by specific RNA-interacting proteins, that in turn recruit PAP (Reyes and Ross, 2016). Among these, best studied are the highly conserved polyadenylation signal hexanucleotide (AAUAAA, a.k.a. HEX) recognized by cleavage and polyadenylation specificity factor (CPSF). Second is the meiosis-specific U-rich cytoplasmic polyadenylation element (CPE), which is regulated by the CPE-binding protein CPEB (Stebbins-Boaz et al., 1996).

CPEB plays a dual role in the storage of maternal mRNAs by both protecting them from degradation and preventing their translation. CPEB binds two adjacent (<100 bases apart) CPE elements and forms a dimer that assembles a translation repression complex. This complex controls the polyadenylation of the CPE-containing mRNAs in several ways. Firstly, the CPEB homodimer binds Maskin (the closest human homolog of which is transforming acidic coiled-coil containing protein 3, TACC3). In oocytes, Maskin binds the 5'cap-binding protein, eIF4E, and thereby sequesters the limiting factor required for translation initiation from the eIF4F complex (Stebbins-Boaz et al., 1999; Cao and Richter, 2002). Secondly, CPEB also recruits an eIF4E-binding protein, 4E-T (a.k.a. EIF4ENIF1) (Minshall et al., 2007). 4E-T prevents mRNA de-capping *via* interaction with eIF4E and physically links the 5' and 3' termini of the mRNA. In particular, in sea urchins, 4E-T is a specific translation inhibitor of the cyclin B mRNA (Chassé et al., 2016). Thirdly, CPEB binds the poly(A)-specific ribonuclease PARN that deadenylates the repressed mRNA (Kim and Richter, 2006).

While un-phosphorylated form CPEB inhibits translation by the mechanisms outlined above, phosphorylation switches CPEB into a translational activator. Upon phosphorylation, CPEB's affinity to CPSF is increased which results in the activation of the cytoplasmic poly(A) polymerase GLD-2, and displacement of PARN(Kim and Richter, 2006). The elongated poly(A) tail is covered by poly(A)-binding protein (PABP), which in turn binds eIF4G and breaks the interaction of Maskin and eIF4E, resulting in translation (Stebbins-Boaz et al., 1999; Cao and Richter, 2002).

In Xenopus, two distinct waves of polyadenylation define phases of meiosis

In *Xenopus*, the model system in which translational regulation is best studied, two major polyadenylation waves have been distinguished each driving the translation of a specific subset of meiotic regulators (Belloc et al., 2008; Reyes and Ross, 2016). While there are substantial species-specific variations, *Xenopus* serves as a good example of how translational regulation can guide multiple events and ensure their temporal order.

The maturation hormone, progesterone induces the "early" polyadenylation wave, which drives entry to meiosis. In *Xenopus,* these "early" proteins include the cyclins B2 and B5, Mos, and the APC/C

inhibitor Emi1, all of which are required for the meiosis entry. The "early" wave involves transcripts that contain the early-acting Musashi binding element (MBE) in their 3'-UTR (Arumugam et al., 2009) and contains an "early" CPE configuration of two adjacent CPEs. These CPE elements are populated by excess CPEB that is phosphorylated in a Cdk1-independent manner. Initial reports suggested that upon stimulation by progesterone, CPEB is phosphorylated by the Aurora A kinase (Mendez et al., 2000; Sarkissian et al., 2004). However, there is evidence that CPEB at this stage is phosphorylated by other kinesis, namely xGEF and xRINGO (Keady et al., 2007).

As mentioned above, the strict dependence of meiotic maturation on translation is rather specific to *Xenopus*. Consistently, the "early" wave shows species-specific features. In *Xenopus* Mos translation strongly depends on the early 3'UTR binding protein Musashi (Charlesworth et al., 2006; Weill et al., 2017), which is not the case for other species. Another specific feature appears to be an opposing feedback loop that is mediated by C3H4, a zinc-finger protein involved in the destabilization of AU-rich element (ARE)-containing mRNAs. In meiosis I, this results in de-adenylation of Emi1 mRNA, the subsequent degradation of Emi1 protein, which in turn is required to allow exit from metaphase I.

The second, "late" wave of polyadenylation occurs at metaphase I and is responsible for the meiosis-specific skipping of the S-phase, i.e. driving the reactivation of cdk1-cyclin B through the translation of transcripts including cyclin B1 and B4 (Belloc et al., 2008) The "late" wave is characterized by cdk1-mediated CPEB phosphorylation, resulting in partial degradation of CPEB. Furthermore, the "late" mRNAs feature a CPE overlapping with the polyadenylation signal (HEX). In the "late" wave, CPEB destruction opens these HEX-overlapping CPEs, creating a binding site for CPSF. In addition, while the "early" CPEs are predominantly regulated by CPEB1, this is gradually replaced by CPEB4 for "late" mRNAs (Igea and Méndez, 2010)

Thus, in *Xenopus* "early" cyclins B5 and B2 with an "early" CPE configuration are translated in an MBE-dependent manner and are driving hormone-induced maturation. By contrast, the "late" cyclins B1 and B4 with a "late" CPE configuration drive cdk1-cyclinB reactivation between meiosis I and meiosis II(Arumugam et al., 2009). In contrast, in mouse oocytes, hormone-induced translation is not required for maturation. Correspondingly, cyclin B1 transcripts contain either short 3'UTRs without a CPE, likely responsible for baseline, unregulated cyclin B1 synthesis. The other form of cyclin B1 mRNAs contains a long 3'UTR with multiple CPE elements, which appear to be translated in a Mos-MAPK-dependent manner (Igea and Méndez, 2010; Jansova et al., 2018; Cao et al., 2020).

Temporal control of cyclin B translation as a key component in meiotic cell cycle regulation

Thus, it is clear that translational regulation is critical for meiotic progression. From many studies in multiple species, a consistent picture emerges that the translation of Cyclin B from stored mRNA is one of the main drivers of meiotic events. On the one hand, this is expected because the meiotic M-phases, as mitotic M-phase, are driven by activation of Cdk1-Cyclin B, and oocytes are typically transcriptionally inactive, therefore Cyclin B needs to be produced from stored mRNAs. On the other hand, it is very intriguing to consider how meiosis-specific regulation of cyclin B synthesis could underlie meiosis-specific features of the cell cycle.

Firstly, cyclin B synthesis is clearly an essential component in *Xenopus* where the translation is required for hormone-induced maturation. Secondly, maintenance of high Cdk1-Cyclin B activity through the meiosis I to II transitions is critical for skipping the S-phase between the two meiotic divisions clearly demonstrated in *Xenopus* oocytes (Iwabuchi et al., 2000; Hochegger et al., 2001). It is the above detailed "late" polyadenylation wave in meiosis that is driving the continued synthesis of new Cyclin B protein after meiosis I. The excess Cyclin B protein overrides degradation by the anaphase-promoting complex (APC/C) in anaphase I and thereby prevents the total Cdk1-Cyclin B activity drops below the threshold to initiate interphase. Thirdly, in the majority of species, the CSF-type cytostatic

arrest halts the cell cycle progression in the metaphase of the first or the second meiotic division. This means that high cdk1-cyclin B activity is maintained during the CSF arrest, which requires a shifted balance between production and degradation of Cyclin B – in many ways similar to the meiosis I to II transition. Continuous synthesis of Cyclin B is thus essential for the maintenance of CSF arrest.

Taken together, translational regulation of Cyclin B levels appears to be one core common module of the meiotic cell cycle contributing to almost all aspects of meiosis-specific features, including induction of meiotic maturation, driving the second meiotic division and CSF-type cell cycle arrests.

There are certainly additional mechanisms that contribute to these meiotic functions, but these seem less universal. In several cases, it is also plausible to imagine how these may have evolved by diversification of the core function. For example, the "late" polyadenylation wave in *Xenopus* is known to additionally enhance the synthesis of the APC/C inhibitor Emi2 (Schmidt et al., 2006). This helps to prevent the degradation of Cyclin B that, in addition to cyclin B synthesis, further shifts the balance towards Cdk1-Cyclin B activation during the meiosis I to II transition.

Evidence for the regulation of cyclin B translation by Mos-MAPK

First, there is a strong correlation between the above functions mediated by Cyclin B translation and those under the control of Mos-MAPK. In *Xenopus* oocytes, Mos-MAPK is essential for all three main functions: Mos is required for meiotic maturation, reactivation of Cdk1-Cyclin B after meiosis I, and Mos inhibition also overrides the CSF arrest. While the essential role of Mos-MAPK in meiotic maturation has been challenged by more recent studies, these are very much consistent with the picture that Mos-MAPK is a potent enhancer of Cdk1-Cyclin B activation – by facilitating Cyclin B synthesis – and therefore required for timely maturation. In the absence of Mos-MAPK activity maturation is much slower and less robust.

In mouse oocytes, observations are somewhat varied which may require further clarification of Mos-MAPK function in this species. Mos depletion by morpholinos, data from two different knock-out strains, and inhibition of the Mos-MAPK pathway by small-molecule inhibitors resulted in slightly different phenotypes. Nevertheless, there is consensus that in mice Mos is not required for induction of maturation, but it may be needed for reactivation of Cdk1-Cyclin B, and it is certainly required for maintenance of CSF arrest.

In starfish oocytes, Mos is not required for meiotic maturation, which in starfish is completely mediated by the post-translational signaling pathway. However, Mos is clearly essential for the reactivation of Cdk1-Cyclin B and driving meiosis II in starfish, as well as for the maintenance of the CSF-like arrest in G1. In the jellyfish *Clytia*, Mos-MAPK is also required for maintenance of the CSF arrest.

Taken together, whenever data is available, there is an almost one-to-one correlation between functions dependent on Mos-MAPK activity and those requiring translation of Cyclin B. How much evidence there is for a direct molecular link between these processes?

Without a known exception, CPEB emerges as a widely conserved regulator of meiotic translation. Indeed, in *Xenopus* oocytes, Mos-MAPK activity promotes CPEB phosphorylation (Keady et al., 2007), and in mouse oocytes degradation of CPEB is also dependent on Mos-MAPK activity (Cao et al., 2020). Interestingly, the Mos protein itself has been shown in several species to be under the control of the same translational regulation. This suggests that Mos-MAPK may act in a positive feedback loop to facilitate cyclin B translation.

Additional evidence comes from more recent phospho-proteomic studies. Overall, it appears that protein levels change only very little during meiosis. Interestingly, in starfish oocytes meiosis I proceed normally even when translation is completely inhibited (Swartz et al., 2021). Strikingly, the very few

proteins that show changes in protein levels are CPEB and some of its regulators and, prominently, Cyclin B (Swartz et al., 2021).

Mos-MAPK's functions in the regulation of asymmetric meiotic divisions

The organization of the microtubule spindle

The molecular mechanisms underlying the organization of the microtubule spindle are beginning to be rather well understood, detailed in recent excellent reviews, for example(Valdez et al., 2023). While historically centrosomes were considered as essential constituents of spindle assembly in animal species, it is now clear that a bipolar spindle can also assemble without centrosomes. As prominent example, most oocytes centrioles are eliminated during the meiotic prophase, nevertheless oocytes are able to form a bipolar spindle and faithfully segregate chromosomes. We now understand the mechanisms of acentrosomal spindle formation that have been studied extensively both in vertebrate and invertebrate animals, reviewed in (Severson et al., 2016; Blengini and Schindler, 2021). One possibility is that in the absence of centrioles and thus proper centrosomes, aMTOCs (acentriolar microtubule-organizing centers) take over the function of centrosomes. Alternatively, chromatin-dependent, Ran-GTP-mediated microtubule nucleation mechanisms appear to gain higher importance in the absence of centrosomes (Heald et al., 1996). Indeed, there seems to be a large variability between species in the extent to which aMTOCs *versus* chromatin-mediated microtubule nucleation contributes to meiotic spindle assembly. For example, within mammalian species, the mouse meiosis I spindle is dominated by aMTOCs, and correspondingly only weakly affected by inhibition of the Ran pathway (Schuh and Ellenberg, 2007). By contrast, human oocyte spindles appear to almost fully depend on chromatin and Ran-GTP-dependent microtubule nucleation (Holubcová et al., 2015).

The aMTOCs can be seen as organelles largely equivalent to centrosomes. Apart from the fact that they are not nucleated by centrioles, they contain a very similar set of pericentriolar material proteins as proper centrosomes. These include the pericentriolar material components pericentrin, CEP120, CEP192, and NEDD1, as well as the microtubule nucleator γ-tubulin. As shown recently in mouse and other mammalian oocytes, aMTOCs are organized at spindle poles into a liquid-like spindle domain (LISD), a phase-separated condensate of key microtubule regulators, functionally largely equivalent to centrosomes (So et al., 2019).

As for the chromosomal nucleation pathway, Ran-GTP produced by its chromatin-bound exchange factor RCC1 is responsible for the activation of several spindle assembly factors including HURP, NuMa, and TPX2 (Breuer et al., 2010; Brunet and Verlhac, 2011; Kolano et al., 2012). HURP is a microtubule-associated protein that stabilizes microtubules near mitotic chromosomes and helps sort the aMTOCs into the bipolar structure (Breuer et al., 2010). The NUMA protein anchors microtubule minus ends at the spindle poles (Kolano et al., 2012). In mouse oocytes, NuMa knockout results in elongated highly pointed spindles instead of normal barrel shape (Kolano et al., 2012). The third Ran-dependent factor is TPX2, which has several roles in spindle assembly. Firstly, it is a microtubule nucleation factor itself, secondly, it phosphorylates the spindle pole regulator TACC3 and thirdly it binds AURKA, enchases its activity, and as a heterodimer translocates to the spindle poles (Eyers et al., 2003; Tsai et al., 2003; Brunet et al., 2008).

The roles of Aurora A in acentriolar spindle assembly

In vertebrates, the Aurora kinase family consists of Aurora A (AURKA), Aurora B (AURKB), and Aurora C (AURKC) (Willems et al., 2018). These three genes are paralogs that evolved from a single Aurora found in earlier branching deuterostome groups, namely in echinoderms and tunicates (Abe et

al., 2010; Hebras and McDougall, 2012). Therefore, the multiple Aurora kinases found in protostomes cannot be direct orthologues of vertebrate Aurora kinases.

AURKA (Eg2 in *Xenopus*) is a critical factor for the spindle assembly and the only Aurora kinase that is essential for meiotic progression in the mouse. Inhibition of AURKA in mouse oocytes results in three characteristic events: reduced spindle length, impaired aMTOCs fragmentation, and even distribution of the aMTOCs along the spindle instead of localization at the poles (Saskova et al., 2008; Ding et al., 2011; Solc et al., 2012; Blengini et al., 2021). AURKA overexpression has a reverse effect causing spindle elongation, the formation of additional aMTOCs that disrupt spindle bipolarity, and pointy spindle poles (Saskova et al., 2008; Ding et al., 2011; Solc et al., 2012). These observations together indicate that the main functions of AURKA are spindle bipolarization through regulation of aMTOC fragmentation and regulation of spindle length.

AURKA phosphorylates a large number of substrates that mediate these functions in spindle assembly. Firstly, AURKA phosphorylates another key mitotic kinase, polo-like kinase 1, Plk1. Plk1 has a multitude of functions including general regulation of cell cycle entry. However, in this context, the most relevant function may be that Plk1 releases CEP250 (C-NAP1), a cross-linker protein that triggers the decondensation of multiple aMTOCs nucleated around the nucleus (Schuh and Ellenberg, 2007; Clift and Schuh, 2015).

The second main target of AURKA is kinesin-5. After NEBD, aMTOCs are fragmented in a kinesin-5-dependent manner (Clift and Schuh, 2015). Kinesin 5 is an antiparallel microtubule-sliding motor that gradually clusters aMTOCs into the two distinct poles by pushing the aMTOCs outwards (Clift and Schuh, 2015). In other words, kinesin 5 sorts the aMTOCs gradually converting the initial 'microtubule ball' into a bipolar spindle. In addition, kinesin-5 HURP to the spindle midzone, further enhancing bipolarity (Breuer et al., 2010). In contrast to mouse and *Xenopus*, in *C. elegans* kinesin-5 (BMK1) and NuMa (LIN5) are not required for spindle bipolarization, however, NuMa and dynein are required for meiotic spindle positioning (Crowder et al., 2015a).

Thirdly, AURKA phosphorylates TACC3, a main component of the phase-separated spindle pole structure, LISD (So et al., 2019). TACC3 is localized to spindle poles, and it promotes microtubule polymerization at spindle poles (Kinoshita et al., 2005; Kettenbach et al., 2011). This localization of TACC3 is lost if AURKA or Plk1 is inhibited. One important function of the TACC3 in mitosis is binding microtubule plus tip stabilizing protein XMAP215 (aka chTOG) at centrosomes (Kinoshita et al., 2005). This brings a paradox where a plus end protein XMAP215 binds a minus end TACC3, the probable solution of this paradox can be TACC3-mediated "loading" of the XMAP215 onto microtubule plus tips (Lee et al., 2001; Barros et al., 2005).

In protostomes, AURKA is not a direct orthologue of its vertebrate counterpart but still is responsible for TACC3 orthologue phosphorylation and spindle pole regulation. In *Drosophila* mitosis AURKA localize to the centrosome and specifically activates the orthologues of the TACC3 and XMAP215 (D-TACC and MSPS respectively) (Giet et al., 2002; Barros et al., 2005). Alike in *Xenopus* during meiosis, the TACC3-XMAP215 complex is transported to the microtubule minus end and promotes acentrosomal spindle assembly and bipolarity (Gergely et al., 2000; Cullen and Ohkura, 2001). Similarly, in *C. elegans* it was shown that TACC3 forms a complex with XMAP215 (D-TACC and MSPS respectively) to promote pole assembly, bipolarization, and suppressing ectopic pole formation in meiosis I and II (Harvey et al., 2023).

Meiotic spindles have much-reduced asters and lack interpolar microtubules

Theodor Boveri recognized the fundamental difference between the asymmetric meiotic divisions and subsequent embryonic mitoses and contributed this difference to the absence of centrosomes in oocytes. Further, he proposed that the absence of centrosomes in meiosis is crucial to prevent parthenogenesis (Severson et al., 2016). However, we now know that while in most species centrioles are indeed eliminated from oocytes, there are several exceptions as well. In rodents, oocytes and sperm both lack centrioles and thus meiotic as well as the first mitotic divisions are acentrosomal (SZOLLOSI et al., 1972; Manandhar et al., 2005). The size and morphology of meiotic and mitotic divisions are nevertheless strikingly different. Furthermore, in some mollusks, as well as in echinoderms meiotic spindles do contain centrioles(Wu and Palazzo, 1999; Crowder et al., 2015b) (Holland, 1981; Sluder et al., 1993; Nakashima and Kato, 2001)(Borrego-Pinto et al., 2016). Importantly, independent of whether spindles have centrioles or not, meiotic spindles and mitotic spindles are consistently very different from one another, as shown by the sampling of several species across animal phylogeny(Crowder et al., 2015b).

The most prominent difference is that in mitosis spindles feature microtubule asters. Astral microtubules emanating from the centrosomes interact with and establish a mechanical link to the cell cortex. This is required for the orientation of the division plane to contribute to chromosome separation. In contrast, meiotic spindles, consistently across species, have short and less abundant astral microtubules (Crowder et al., 2015b). These short meiotic asters are key to meiotic function: they allow the spindle to localize close to the cortex of the oocyte, and thereby it is a mechanism crucial to reduce the volume of polar bodies. Consistently, if the size of the asters is artificially increased, for example, by stabilization of microtubules by taxol or by other, similar treatments, the result is polar bodies with increased size (Crowder et al., 2015a).

Possibly it is a direct consequence of the reduced number and length of astral microtubules, another long-observed difference between mitotic and meiotic spindles is the 'discontinuity' of the microtubule array at the spindle midzone. We now know that spindle microtubules are nucleated not only at the centrosomes but also within the spindle through the augmin-mediated branching nucleation pathway. Nevertheless, in most mitotic spindles long microtubules extend from each mitotic centrosome to the midzone and beyond, referred to as interpolar microtubules (White & Glotzer, 2012). These microtubules can then cross-link to one another and form antiparallel bundles that stabilize the mitotic spindle. Importantly, after the separation of sister chromatids in anaphase, these antiparallel bundles constitute the central spindle that promotes the initiation of cytokinesis (White & Glotzer, 2012). By contrast, electron tomography studies in *C. elegans* oocytes have found few if any microtubules that would reach from the poles to the midzone or the chromosomes (Srayko et al., 2006). Meiotic spindles appear to be constituted almost exclusively from a short, tiled array of microtubules not only in *C. elegans*, but in *Drosophila* oocytes and *Xenopus* oocyte extracts as well (Burbank et al., 2006; Skold et al., 2005; Yang et al., 2007).

As a consequence, meiotic spindles appear to rely almost exclusively on the shortening of the kinetochore fibers for pulling chromosomes apart in anaphase, referred to as anaphase A (Cheeseman & Desai 2008, Maiato et al. 2004). In mitosis, in parallel to anaphase A, the overlapping interpolar microtubule arrays are pushed apart by kinesin motors leading to the separation of the spindle poles, referred to as anaphase B. Thus, while in mitotic anaphase A and B are typically observed simultaneously, in oocyte meiosis only anaphase A is observed in most species. This again serves the function to minimize the size of the polar body.

Evidence for regulation of meiotic spindle architecture by Mos-MAPK

It has been recognized in several species that Mos-MAPK inhibition results in a 'mitotic-like' spindle morphology. The most prominent feature seen is the appearance of much longer astral microtubules that push the spindle deeper in the cytoplasm and interferes with tight positioning to the cortex. Although this has only been looked at in much fewer species, anaphase in these Mos-MAPK inhibited oocytes appears to result in much 'longer' spindles. This indicates that Anaphase B occurs in Mos-MAPK inhibited oocytes as in embryonic mitoses, but unlike normal meiotic divisions, which only feature Anaphase A. Thus, as for translational regulation, there is an almost one-to-one correlation between Mos-MAPK activity and the switch between the astral "mitotic" spindle morphology featuring Anaphase A and B and the "anastral" meiotic spindle morphology featuring Anaphase A only.

What do we know about the underlying molecular mechanisms? There is evidence that Mos controls a number of microtubule regulators. In particular, in *Xenopus* oocytes extracts it has been shown that Mos-MAPK can phosphorylate MAP2 and MAP4, and in mouse oocytes MISS and DOC1R have been identified as regulators specifically under the control of Mos-MAPK. While these regulators identified so far serve as important hints for the fact that the Mos-MAPK pathway directly controls spindle architecture a comprehensive mechanistic model have not yet emerged for these studies.

The lack of astral microtubules necessitates meiosis-specific mechanisms of spindle assembly

Short asters are critical to reducing the size of the polar body, but at the same time, they are unable to perform their original function in spindle positioning. This necessitates meiosis-specific mechanisms that function independently of astral microtubules. For example, in mammals, the meiotic spindle is translocated to the cortex in an actin-dependent manner (Verlhac et al., 2000; Schuh and Ellenberg, 2007) and in starfish, the chromosomes are translocated by actomyosin contraction to the site of spindle assembly (Burdyniuk et al., 2018).

It is likely that due to the reduced number of interpolar microtubules, the meiotic spindle also requires additional mechanisms to support its mechanical stability, especially in anaphase. Intriguingly, the spindle in mouse oocytes (Azoury et al. 2008, Schuh & Ellenberg 2008) as well as in human, pig, and sheep oocytes (Mogessie & Schuh 2017) is permeated by prominent actin filaments (spindle actin), required for the accurate segregation of chromosomes in both meiotic divisions (Mogessie & Schuh 2017). Notably, actin has been reported in meiotic spindles of a variety of species (Sandquist et al. 2011), including *Xenopus* oocytes (Weber et al. 2004), spermatocytes of insects (Silverman-Gavrila & Forer 2000), and maize sporocytes (Staiger & Cande 1991).

Regulation of polar body extrusion

The geometry of polar body extrusion differs from somatic cell division, i.e. cytokinesis. While in somatic cells principally the spindle midzone defines cleavage furrow, during the polar body formation an extrusion, and out-bulging form in parallel with the closure of the cleavage furrow. So, the polar body bud containing the spindle protrudes from the oocyte cortex and is then closed during polar body cytokinesis. Both of these processes, bulging and closure involve the regulation of the actin cortex. However, as it emerges from recent studies, the regulatory mechanisms are distinct. While closure, the 'pinching off' of the polar body is mediated by the same spindle-induced RhoA module as somatic cytokinesis, bulging out of the polar body appears to rely on another small GTPase regulating the actin cortex, Cdc42.

The 'preparatory step' for polar body formation is called cortical polarization which takes place early in prometaphase I. In this process the cortex at the animal pole undergoes dramatic reorganization manifesting in the decreased density of cortical granules' density (Ducibella et al., 1988) and reorganization of microvilli into the so-called actin cap (Longo and Chen, 1984). While there are again

substantial differences between species, similar a similar process has been observed in diverse species from ascidians to mammals (Sardet et al., 1992; Gard et al., 1995; Kim et al., 2000; Sun et al., 2001). The functions of this specialized cortical cap include shaping the polar body, anchoring the MII spindle, and preventing sperm binding to the animal pole.

In mouse oocytes, the pathway leading to the polarization of the cortex is well understood. The formation of the actin cap coincides with spindle migration, suggesting that the chromosomes mediate cortical polarization (Longo and Chen, 1984; Deng et al., 2007; Yi et al., 2013). Indeed, Ran-GTP produced on chromatin is involved (Deng et al., 2007): where chromosomes are in close proximity to the cortex, Ran-GTP activates two other small GTPases Rac (Brunet and Verlhac, 2011) and Cdc42 (Mogessie et al., 2018; Mei et al., 2022). Rac recruits and activates N-WASP, which in turn activates the Arp2/3 complex to nucleate a branched network of actin filaments (Dehapiot and Halet, 2013; Yi et al., 2013). (Rohatgi et al., 1999). Cdc42 is a plasma membrane-bound GTPase that in addition to Rac is also contributing to N-WASP localization at the polarized cortex (Yi et al., 2011; Dehapiot et al., 2013; Zhang et al., 2017) and therefore is crucial for cortical polarization (Dehapiot and Halet, 2013; Dehapiot et al., 2013). Cdc42 facilitates the formation of the plasma membrane protrusion needed for the polar body by pulling the spindle outwards the cortex. Additionally, Cdc42 and Rac define the inner boundary of the contractile ring by antagonizing the RhoA activity in *Xenopus* (Ma et al., 2006; Zhang et al., 2008) and in echinoderms (Pal et al., 2020).

Besides regulation by Ran-GTP, cortical polarization is also dependent on MAPK. Mos-MAPK mediates the actin cap formation by another Arp2/3 complex activator WAVE2 (Chaigne et al., 2013). In mice, the MAPK inhibition as well as Mos-/- KO results in perturbing the DNA-dependent actin cap formation (Deng et al., 2005, 2007). Although Ran does not affect the global MAPK activity it may restrict the MAPK activity to the chromosomes (Deng et al., 2007). The activity of MAPK and Ran establishes a positive feedback loop: the chromosomes at the cortex induce the cortical polarization with in turn pushes the chromosomes closer to the cortex and promotes actin cap maintenance (Yi et al., 2011, 2013). Since the actin cap and therefore MII spindle anchorage is dependent on Ran, it may explain why in the mouse Ran perturbations are tolerated in MI but not in MII (Dumont et al., 2007) and why in the MAPK perturbants the spindle loses the close spindle attachment to the cortex (Verlhac et al., 2000).

RhoA is a small GTRase that upon activation by guanidine exchange factor Ect2 forms a contractile ring composed of actin motor myosin-2, F-actin, and Formin-nucleated actin bundles (Liu, 2012). Myosins are involved in the spindle movement and potentially in the contractile furrow closure activated by the Cdc42-binding protein MLCK (Schuh and Ellenberg, 2007), which in turn is a substrate of the MAPK (Morrison et al., 1996). This is supported by the fact that in Mos KO or MAPK-inhibited mice, spindle migration is absent (Choi et al., 1996; Verlhac et al., 2000; Phillips et al., 2002). Recently it was shown that MRCK controls the myosin-2 in the actin cap and promotes spindle rotation (Bourdais et al., 2022). Additionally, in starfish, Mos-MAPK regulates Diaphnous formin which is responsible for the cleavage furrow closure (Ucar et al., 2013).

References

Abe, Y. et al. (2010). A single starfish Aurora kinase performs the combined functions of Aurora-A and Aurora-B in human cells. J Cell Sci *123*, 3978–3988.

Arumugam, K. et al. (2009). Enforcing temporal control of maternal mRNA translation during oocyte cell-cycle progression. Embo J *29*, 387–397.

Barkoff, A. et al. (1998). Meiotic maturation in Xenopus requires polyadenylation of multiple mRNAs. Embo J *17*, 3168–3175.

Barros, T.P. et al. (2005). Aurora A activates D-TACC–Msps complexes exclusively at centrosomes to stabilize centrosomal microtubules. J Cell Biology *170*, 1039–1046.

Belloc, E. et al. (2008). Sequential waves of polyadenylation and deadenylation define a translation circuit that drives meiotic progression. Biochem Soc T *36*, 665–670.

Bieber, F.R. et al. (1981). Genetic Studies of an Acardiac Monster: Evidence of Polar Body Twinning in Man. Science *213*, 775–777.

Blengini, C.S. et al. (2021). Aurora kinase A is essential for meiosis in mouse oocytes. Plos Genet *17*, e1009327.

Blengini, C.S., and Schindler, K. (2021). Acentriolar spindle assembly in mammalian female meiosis and the consequences of its perturbations on human reproduction. Biol Reprod *106*, 253–263.

Borrego-Pinto, J. et al. (2016). Distinct mechanisms eliminate mother and daughter centrioles in meiosis of starfish oocytesCentriole elimination in starfish oocytes. J Cell Biology *212*, 815–827.

Bourdais, A. et al. (2022). MRCK controls myosin II activation in the polarized cortex of mouse oocytes and promotes spindle rotation and male pronucleus centration. Biorxiv 2022.09.25.509421.

Breuer, M. et al. (2010). HURP permits MTOC sorting for robust meiotic spindle bipolarity, similar to extra centrosome clustering in cancer cells. J Cell Biol *191*, 1251–1260.

Brunet, S. et al. (2008). Meiotic Regulation of TPX2 Protein Levels Governs Cell Cycle Progression in Mouse Oocytes. Plos One *3*, e3338.

Brunet, S., and Verlhac, M.H. (2011). Positioning to get out of meiosis: the asymmetry of division. Hum Reprod Update *17*, 68–75.

Burdyniuk, M. et al. (2018). F-Actin nucleated on chromosomes coordinates their capture by microtubules in oocyte meiosis. J Cell Biol *217*, 2661–2674.

Cao, L.-R. et al. (2020). Positive Feedback Stimulation of Ccnb1 and Mos mRNA Translation by MAPK Cascade During Mouse Oocyte Maturation. Frontiers Cell Dev Biology *8*, 609430.

Cao, Q., and Richter, J.D. (2002). Dissolution of the maskin–eIF4E complex by cytoplasmic polyadenylation and poly(A)-binding protein controls cyclin B1 mRNA translation and oocyte maturation. Embo J *21*, 3852–3862.

Chaigne, A. et al. (2013). A soft cortex is essential for asymmetric spindle positioning in mouse oocytes. Nat Cell Biol *15*, 958–966.

Charlesworth, A. et al. (2006). Musashi regulates the temporal order of mRNA translation during Xenopus oocyte maturation. Embo J *25*, 2792–2801.

Chassé, H. et al. (2016). Cyclin B Translation Depends on mTOR Activity after Fertilization in Sea Urchin Embryos. Plos One *11*, e0150318.

Choi, T. et al. (1996). Mos/mitogen-activated protein kinase can induce early meiotic phenotypes in the absence of maturation-promoting factor: a novel system for analyzing spindle formation during meiosis I. Proc National Acad Sci *93*, 4730–4735.

Clift, D., and Schuh, M. (2015). A three-step MTOC fragmentation mechanism facilitates bipolar spindle assembly in mouse oocytes. Nat Commun *6*, 7217.

Crowder, M.E. et al. (2015a). Dynactin-dependent cortical dynein and spherical spindle shape correlate temporally with meiotic spindle rotation in Caenorhabditis elegans. Mol Biol Cell *26*, 3030–3046.

Crowder, M.E. et al. (2015b). A Comparative Analysis of Spindle Morphometrics across Metazoans. Curr Biol *25*, 1542–1550.

Cullen, C.F., and Ohkura, H. (2001). Msps protein is localized to acentrosomal poles to ensure bipolarity of Drosophila meiotic spindles. Nat Cell Biol *3*, 637–642.

Dehapiot, B. et al. (2013). Polarized Cdc42 activation promotes polar body protrusion and asymmetric division in mouse oocytes. Dev Biol *377*, 202–212.

Dehapiot, B., and Halet, G. (2013). Ran GTPase promotes oocyte polarization by regulating ERM (Ezrin/Radixin/Moesin) inactivation. Cell Cycle *12*, 1672–1678.

Deng, M. et al. (2005). Role of MAP kinase and myosin light chain kinase in chromosome-induced development of mouse egg polarity. Dev Biol *278*, 358–366.

Deng, M. et al. (2007). The Ran GTPase Mediates Chromatin Signaling to Control Cortical Polarity during Polar Body Extrusion in Mouse Oocytes. Dev Cell *12*, 301–308.

Ding, J. et al. (2011). Aurora kinase-A regulates microtubule organizing center (MTOC) localization, chromosome dynamics, and histone-H3 phosphorylation in mouse oocytes. Mol Reprod Dev *78*, 80–90.

Dorée, M., and Hunt, T. (2002). From Cdc2 to Cdk1: when did the cell cycle kinase join its cyclin partner? J Cell Sci *115*, 2461–2464.

Ducibella, T. et al. (1988). Quantitative studies of changes in cortical granule number and distribution in the mouse oocyte during meiotic maturation. Dev Biol *130*, 184–197.

Dumont, J. et al. (2007). A centriole- and RanGTP-independent spindle assembly pathway in meiosis I of vertebrate oocytes. J Cell Biology *176*, 295–305.

Eyers, P.A. et al. (2003). A Novel Mechanism for Activation of the Protein Kinase Aurora A. Curr Biol *13*, 691–697.

Galas, S. et al. (1993). A nuclear factor required for specific translation of cyclin B may control the timing of first meiotic cleavage in starfish oocytes. Mol Biol Cell *4*, 1295–1306.

Gard, D.L. et al. (1995). F-actin is required for spindle anchoring and rotation in Xenopus oocytes: a re-examination of the effects of cytochalasin B on oocyte maturation. Zygote *3*, 17–26.

Gergely, F. et al. (2000). D-TACC: a novel centrosomal protein required for normal spindle function in the early Drosophila embryo. Embo J *19*, 241–252.

Giet, R. et al. (2002). Drosophila Aurora A kinase is required to localize D-TACC to centrosomes and to regulate astral microtubules. J Cell Biology *156*, 437–451.

Grill, S.W. et al. (2003). The Distribution of Active Force Generators Controls Mitotic Spindle Position. Science *301*, 518–521.

Harada, K. et al. (2003). Metaphase I arrest of starfish oocytes induced via the MAP kinase pathway is released by an increase of intracellular pH. Development *130*, 4581–4586.

Harasimov, K. et al. (2023). Actin-driven chromosome clustering facilitates fast and complete chromosome capture in mammalian oocytes. Nat Cell Biol *25*, 439–452.

Harvey, A.M. et al. (2023). C. elegans XMAP215/ZYG-9 and TACC/TAC-1 act at multiple times during oocyte meiotic spindle assembly and promote both spindle pole coalescence and stability. Plos Genet *19*, e1010363.

Heald, R. et al. (1996). Self-organization of microtubules into bipolar spindles around artificial chromosomes in Xenopus egg extracts. Nature *382*, 420–425.

Hebras, C., and McDougall, A. (2012). Urochordate Ascidians Possess a Single Isoform of Aurora Kinase That Localizes to the Midbody via TPX2 in Eggs and Cleavage Stage Embryos. Plos One *7*, e45431.

Hochegger, H. et al. (2001). New B-type cyclin synthesis is required between meiosis I and II during Xenopus oocyte maturation. Development *128*, 3795–3807.

Holland, N.D. (1981). Electron Microscopic Study of Development in a Sea Cucumber, Stichopus tremulus (Holothuroidea), from Unfertilized Egg through Hatched Blastula. Acta Zool-Stockholm *62*, 89–111.

Holubcová, Z. et al. (2015). Error-prone chromosome-mediated spindle assembly favors chromosome segregation defects in human oocytes. Science *348*, 1143–1147.

Igea, A., and Méndez, R. (2010). Meiosis requires a translational positive loop where CPEB1 ensues its replacement by CPEB4. Embo J *29*, 2182–2193.

Iwabuchi, M. et al. (2000). Residual Cdc2 activity remaining at meiosis I exit is essential for meiotic M–M transition in Xenopus oocyte extracts. Embo J *19*, 4513–4523.

Jansova, D. et al. (2018). Localization of RNA and translation in the mammalian oocyte and embryo. Plos One *13*, e0192544.

Jessus, C. et al. (2020). Managing the Oocyte Meiotic Arrest—Lessons from Frogs and Jellyfish. Cells *9*, 1150.

Keady, B.T. et al. (2007). MAPK interacts with XGef and is required for CPEB activation during meiosis in Xenopus oocytes. J Cell Sci *120*, 1093–1103.

Kettenbach, A.N. et al. (2011). Quantitative Phosphoproteomics Identifies Substrates and Functional Modules of Aurora and Polo-Like Kinase Activities in Mitotic Cells. Sci Signal *4*, rs5.

Kim, J.H., and Richter, J.D. (2006). Opposing Polymerase-Deadenylase Activities Regulate Cytoplasmic Polyadenylation. Mol Cell *24*, 173–183.

Kim, N.-H. et al. (2000). The distribution and requirements of microtubules and microfilaments in bovine oocytes during in vitro maturation. Zygote *8*, 25–32.

Kinoshita, K. et al. (2005). Aurora A phosphorylation of TACC3/maskin is required for centrosome-dependent microtubule assembly in mitosis. J Cell Biology *170*, 1047–1055.

KISHIMOTO, T. (2018). MPF-based meiotic cell cycle control: Half a century of lessons from starfish oocytes. Proc Jpn Acad Ser B *94*, 180–203.

Kolano, A. et al. (2012). Error-prone mammalian female meiosis from silencing the spindle assembly checkpoint without normal interkinetochore tension. Proc National Acad Sci *109*, E1858–E1867.

Kuroda, T. et al. (2004). Analysis of the Roles of Cyclin B1 and Cyclin B2 in Porcine Oocyte Maturation by Inhibiting Synthesis with Antisense RNA Injection. Biol Reprod *70*, 154–159.

Lancaster, O.M. et al. (2013). Mitotic Rounding Alters Cell Geometry to Ensure Efficient Bipolar Spindle Formation. Dev Cell *25*, 270–283.

Ledan, E. et al. (2001). Meiotic Maturation of the Mouse Oocyte Requires an Equilibrium between Cyclin B Synthesis and Degradation. Dev Biol *232*, 400–413.

Lee, M.J. et al. (2001). Msps/XMAP215 interacts with the centrosomal protein D-TACC to regulate microtubule behaviour. Nat Cell Biol *3*, 643–649.

Lénárt, P. et al. (2005). A contractile nuclear actin network drives chromosome congression in oocytes. Nature *436*, 812–818.

Lévesque, J.T., and Sirard, M.-A. (1996). Resumption of Meiosis is Initiated by the Accumulation of Cyclin B in Bovine Oocytes. Biol Reprod *55*, 1427–1436.

Liu, X.J. (2012). Polar body emission. Cytoskeleton *69*, 670–685.

Longo, F.J., and Chen, D.Y. (1984). Development of surface polarity in mouse eggs. Scanning Microscopy 703–716.

Ma, C. et al. (2006). Cdc42 Activation Couples Spindle Positioning to First Polar Body Formation in Oocyte Maturation. Curr Biol *16*, 214–220.

Maddox, A.S. et al. (2012). Polar body cytokinesis. Cytoskeleton *69*, 855–868.

Manandhar, G. et al. (2005). Centrosome Reduction During Gametogenesis and Its Significance1. Biol Reprod *72*, 2–13.

Mei, Q. et al. (2022). Advances in the study of CDC42 in the female reproductive system. J Cell Mol Med *26*, 16–24.

Mendez, R. et al. (2000). Phosphorylation of CPE binding factor by Eg2 regulates translation of c-mos mRNA. Nature *404*, 302–307.

Mendez, R., and Richter, J.D. (2001). Translational control by CPEB: a means to the end. Nat Rev Mol Cell Bio *2*, 521–529.

Minshall, N. et al. (2007). CPEB Interacts with an Ovary-specific eIF4E and 4E-T in Early Xenopus Oocytes*. J Biol Chem *282*, 37389–37401.

Minshull, J. et al. (1991). Xenopus oocyte maturation does not require new cyclin synthesis. J Cell Biology *114*, 767–772.

Mitchison, T.J. (2020). Cell Biology: Size Scaling of Mitotic Spindles. Curr Biol *30*, R1476–R1478.

Mogessie, B. et al. (2018). Assembly and Positioning of the Oocyte Meiotic Spindle. Annu Rev Cell Dev Bi *34*, 381–403.

Morrison, D.L. et al. (1996). Phosphorylation and activation of smooth muscle myosin light chain kinase by MAP kinase and cyclin-dependent kinase-1. Biochem Cell Biol *74*, 549–557.

Nakashima, S., and Kato, K.H. (2001). Centriole behavior during meiosis in oocytes of the sea urchin Hemicentrotus pulcherrimus. Dev Growth Differ *43*, 437–445.

Pal, D. et al. (2020). Rac and Arp2/3-Nucleated Actin Networks Antagonize Rho During Mitotic and Meiotic Cleavages. Frontiers Cell Dev Biology *8*, 591141.

Phillips, K.P. et al. (2002). Inhibition of MEK or cdc2 Kinase Parthenogenetically Activates Mouse Eggs and Yields the Same Phenotypes as Mos−/− Parthenogenotes. Dev Biol *247*, 210–223.

Reyes, J.M., and Ross, P.J. (2016). Cytoplasmic polyadenylation in mammalian oocyte maturation. Wiley Interdiscip Rev Rna *7*, 71–89.

Rohatgi, R. et al. (1999). The Interaction between N-WASP and the Arp2/3 Complex Links Cdc42-Dependent Signals to Actin Assembly. Cell *97*, 221–231.

Sagata, N. et al. (1988). Function of c-mos proto-oncogene product in meiotic maturation in Xenopus oocytes. Nature *335*, 519–525.

Sardet, C. et al. (1992). Polarity of the ascidian egg cortex before fertilization. Development *115*, 221–237.

Sarkissian, M. et al. (2004). Progesterone and insulin stimulation of CPEB-dependent polyadenylation is regulated by Aurora A and glycogen synthase kinase-3. Gene Dev *18*, 48–61.

Saskova, A. et al. (2008). Aurora kinase A controls meiosis I progression in mouse oocytes. Cell Cycle *7*, 2368–2376.

Schmidt, A. et al. (2006). Cytostatic factor: an activity that puts the cell cycle on hold. J Cell Sci *119*, 1213–1218.

Schuh, M., and Ellenberg, J. (2007). Self-Organization of MTOCs Replaces Centrosome Function during Acentrosomal Spindle Assembly in Live Mouse Oocytes. Cell *130*, 484–498.

Severson, A.F. et al. (2016). Chapter Five Oocyte Meiotic Spindle Assembly and Function. Curr Top Dev Biol *116*, 65–98.

Sluder, G. et al. (1993). Centrosome Inheritance in Starfish Zygotes II: Selective Suppression of the Maternal Centrosome during Meiosis. Dev Biol *155*, 58–67.

So, C. et al. (2019). A liquid-like spindle domain promotes acentrosomal spindle assembly in mammalian oocytes. Science *364*, eaat9557.

Solc, P. et al. (2012). Aurora Kinase A Drives MTOC Biogenesis but Does Not Trigger Resumption of Meiosis in Mouse Oocytes Matured In Vivo. Biol Reprod *87*, Article 85, 1-12.

Stebbins-Boaz, B. et al. (1996). CPEB controls the cytoplasmic polyadenylation of cyclin, Cdk2 and c-mos mRNAs and is necessary for oocyte maturation in Xenopus. Embo J *15*, 2582–2592.

Stebbins-Boaz, B. et al. (1999). Maskin Is a CPEB-Associated Factor that Transiently Interacts with eIF-4E. Mol Cell *4*, 1017–1027.

Sun, Q.-Y. et al. (2001). Dynamic Events Are Differently Mediated by Microfilaments, Microtubules, and Mitogen-Activated Protein Kinase During Porcine Oocyte Maturation and Fertilization In Vitro1. Biol Reprod *64*, 879–889.

Swartz, S.Z. et al. (2021). Selective dephosphorylation by PP2A-B55 directs the meiosis I - meiosis II transition in oocytes. Elife *10*, e70588.

SZOLLOSI, D. et al. (1972). Absence of Centrioles in the First and Second Meiotic Spindles of Mouse Oocytes. J Cell Sci *11*, 521–541.

Tsai, M.-Y. et al. (2003). A Ran signalling pathway mediated by the mitotic kinase Aurora A in spindle assembly. Nat Cell Biol *5*, 242–248.

Ucar, H. et al. (2013). The Mos–MAPK pathway regulates Diaphanous-related formin activity to drive cleavage furrow closure during polar body extrusion in starfish oocytes. J Cell Sci *126*, 5153--5165.

Valdez, V.A. et al. (2023). Mechanisms underlying spindle assembly and robustness. Nat Rev Mol Cell Bio 1–20.

Verlhac, M.-H. et al. (2000). Asymmetric division in mouse oocytes: with or without Mos. Curr Biol *10*, 1303–1306.

Weill, L. et al. (2017). Musashi 1 regulates the timing and extent of meiotic mRNA translational activation by promoting the use of specific CPEs. Nat Struct Mol Biol *24*, 672–681.

Willems, E. et al. (2018). The functional diversity of Aurora kinases: a comprehensive review. Cell Div *13*, 7.

Wollman, R. et al. (2005). Efficient Chromosome Capture Requires a Bias in the 'Search-and-Capture' Process during Mitotic-Spindle Assembly. Curr Biol *15*, 828–832.

Wühr, M. et al. (2008). Evidence for an Upper Limit to Mitotic Spindle Length. Curr Biol *18*, 1256–1261.

Wu, X., and Palazzo, R.E. (1999). Differential regulation of maternal vs. paternal centrosomes. Proc National Acad Sci *96*, 1397–1402.

Yi, K. et al. (2011). Dynamic maintenance of asymmetric meiotic spindle position through Arp2/3-complex-driven cytoplasmic streaming in mouse oocytes. Nat Cell Biol *13*, 1252–1258.

Yi, K. et al. (2013). Sequential actin-based pushing forces drive meiosis I chromosome migration and symmetry breaking in oocytes. J Cell Biol *200*, 567–576.

Zhang, J. et al. (2017). Intersectin 2 controls actin cap formation and meiotic division in mouse oocytes through the Cdc42 pathway. Faseb J *31*, 4277–4285.

Zhang, X. et al. (2008). Polar Body Emission Requires a RhoA Contractile Ring and Cdc42-Mediated Membrane Protrusion. Dev Cell *15*, 386–400.

Chapter 2. Phospho-proteomics identifies translation and spindle organization as the main targets of Mos-MAPK in oocyte meiosis

(Article is in preparation for publication)

Ivan Avilov[1], Yehor Horokhovskyi[2], Mingfang Cai[1], Aleksander Orzechowski[1], Luisa Welp[3], Henning Urlaub[3], Juliane Liepe[2] and Peter Lenart[1]

[1]Research Group Cytoskeletal Dynamics in Oocytes, [2]Research Group Quantitative and Systems Biology, and [3]Research Group Bioanalytical Mass Spectrometry, Max Planck Institute for Multidisciplinary Sciences, Am Fassberg 11, 37077, Göttingen, Germany

Correspondence to peter.lenart@mpinat.mpg.de

Abstract

The Mos kinase is a constitutive activator of the ERK/MAPK pathway exclusively expressed during oocyte meiosis in the majority of animals. Mos-MAPK has been shown to drive meiosis-specific cell cycle processes and is involved in cytoskeletal regulation to mediate the highly asymmetric polar body divisions. While a few individual effectors have already been studied, the molecular targets under the control of Mos-MAPK have not yet been identified systematically.

Here, we first confirmed the cellular phenotypes of Mos-MAPK inhibition in starfish oocytes by live-cell microscopy. This identified the first meiotic metaphase as the critical transition when Mos-MAPK is activated to trigger key meiotic events; haploidization and asymmetric division. As starfish oocytes are available in large amounts and develop synchronously, we were able to perform phospho-proteomics analysis of samples specifically at this transition. This revealed a set of protein groups phosphorylated in a Mos-MAPK-dependent manner. A large group of identified proteins is involved in the regulation of translation through the CPE-element binding protein CPEB. We indeed show that timely translation of cyclin B is alone sufficient to drive haploidization in meiosis II, as injection of active Cdk1-Cyclin B protein at the end of meiosis I is able to rescue Mos-MAPK inhibition. A second large group of identified phospho-proteins is regulators of centrosomal microtubule nucleation. By live imaging and high-resolution immunofluorescence, we consistently show that Mos-MAPK primarily functions by reducing the size of microtubule asters in anaphase, to thereby ensure the asymmetry of polar body divisions.

Taken together, we used phospho-proteomics to identify the molecular modules under the control of Mos-MAPK in oocytes. Identification of these core, conserved mechanisms underlying oocyte meiosis is highly relevant for understanding reproductive processes across species, including humans, as well as in the pathological context when Mos is expressed erroneously acting as an oncogene.

Introduction

To produce haploid gametes, chromosome number needs to be reduced by half, to a single set of chromosomes during meiotic divisions. This is achieved by driving two division cycles called meiosis I (MI) and meiosis II (MII) without DNA replication (S-phase) in between. At the molecular level, skipping S-phase between the two meiotic divisions requires that the main mitotic kinase, Cdk1-CyclinB is rapidly reactivated after the first meiotic division so that the cell enters into a second division without intervening interphase. Earlier work in *Xenopus* oocytes showed that reactivation of Cdk1-Cyclin B can be achieved by timely translation of Cyclin B (Hochegger et al., 2001) and/or dephosphorylation of Cdk1 (Iwabuchi et al., 2000) shortly after completion of MI. Reactivation of Cdk1-Cyclin B after MI prevents entry to interphase that is manifested at the cellular level in the absence of nuclear reformation.

The second key meiotic function, specific to the female gamete, is to restrict the number of fertilization-competent gametes to only one, in order to preserve all nutrients for a single large egg cell, required to support embryo development. This necessitates that the other daughter cells produced by meiotic divisions are unviable to avoid gamete competition and potential blastomere mixing (Otsuki et al., 2012). This is achieved by an extremely asymmetric division of the oocyte, producing tiny, non-viable polar bodies and a single egg cell (Severson et al., 2016).

Thirdly, oocyte meiosis is synchronized with fertilization and other events of reproduction by two cell cycle arrest points (Jessus et al., 2020). The first one controls meiosis entry (a.k.a. meiotic maturation) making sure that meiotic divisions, i.e. the actual haploidization takes place just before fertilization. Therefore, fully grown oocytes universally arrest at prophase I which is released by the maturation hormone. The second arrest point is called 'CSF arrest' (cytostatic factor arrest), and it functions to directly link the meiotic progression of the oocyte with the actual event of fertilization or spawning (i.e. the release of the oocyte from the ovary). In vertebrates, the CSF arrest is at metaphase II, but species show a wide diversity adapted to their variable reproductive strategies with some species arresting at MI, or in the G1-phase after meiosis.

These unique features of oocyte meiosis are essential for producing a haploid egg. Strikingly, after fertilization in the same egg cytoplasm mitotic divisions take place with alternating S- and M-phases. What are the molecular mechanisms that 'switch' between these two functionally fundamentally distinct forms of division: meiosis before and mitotic divisions after fertilization?

The Mos kinase has been long recognized as an excellent candidate. Mos is a constitutive activator of the ERK/MAPK cascade that function specifically and exclusively during oocyte meiosis and is degraded after fertilization (Dupré et al., 2011). In somatic cells, the ERK pathway is activated by extracellular signals (e.g. growth factors) and is a key pathway controlling proliferation. Therefore, ectopic expression of Mos in somatic cells results in the oncogenic transformation that originally led to its identification as the transforming gene of the Moloney murine sarcoma virus (Oskarsson et al., 1980). When Mos is expressed physiologically in oocytes (also referred to as cellular or c-Mos, as opposed to the viral v-Mos), it plays important role in the regulation of oocyte meiosis. These functions appear to be mediated by the downstream effector $p90^{RSK}$, although there are exceptions to the rule, for example, in mouse oocytes $p90^{RSK}$ does not seem to be involved in Mos-MAPK signaling (Dumont et al., 2005).

The Mos protein was first characterized in *Xenopus* oocytes (Sagata et al., 1988), followed by mice (Colledge et al., 1994; Hashimoto et al., 1994), other deuterostome species including tunicates (Sensui et al., 2012), starfish (Tachibana et al., 2000). Mos and its conserved functions have since been demonstrated also in the non-bilaterian jellyfish *Clytia hemisphaerica* that clearly evidences its ancestral origin (Amiel et al., 2009). However, in protostomes, Mos seems to have lost its importance as *Drosophila*

Mos mutants display normal oocyte development (Ivanovska et al., 2004), and in *C. elegans* the Mos gene appears to be secondarily lost (Dupré et al., 2011).

When Mos was first characterized in *Xenopus* oocytes, it was found that translation of the Mos protein is required for meiosis entry (Sagata et al., 1988). However, as it turned out later, this particular function of Mos is rather restricted to a relatively small number of species that strictly depend on the translation of new proteins for hormone-induced meiotic entry. Once Mos had been studied in other species, additional and more conserved functions emerged (Dupré et al., 2011). First, Mos plays a major role in preventing S-phase between the two meiotic divisions, a function key to the reduction of the genomic content. In *Xenopus*, upon inhibition of Mos-MAPK oocytes exit MI, reform the nucleus, and initiate S-phase (Sagata et al., 1988; Tachibana et al., 2000; Phillips et al., 2002)). In starfish, inhibition of Mos-MAPK activity completely abolishes the second meiotic division, so that MI is followed by the first mitotic cycle (Tachibana et al., 2000). In mouse oocytes, studies show somewhat variable results, but it is clear that a substantial portion of the Mos knockout or Mos-MAPK inhibited oocytes reform a nucleus after MI (Araki et al., 1996; Phillips et al., 2002) or at least show an interphase-like morphology (Verlhac et al., 1996). Whether oocytes then undergo S-phase is not clear, and may be prevented because at this stage mouse oocytes seem to lack essential constituents of the replication machinery. Together these data suggest that across species Mos-MAPK is involved in the reactivation of Cdk1-Cyclin B at the end of MI, thereby driving the second meiotic division while skipping S-phase. The molecular mechanisms by which Mos-MAPK facilitates Cdk1-Cyclin B reactivation remain poorly understood.

The second main function of Mos-MAPK is to render the meiotic divisions highly asymmetric. Studies in mice, jellyfish, and other species show that Mos-MAPK inhibition converts meiotic spindle to a mitotic-like morphology (Choi et al., 1996; Verlhac et al., 1996; Bodart et al., 2002; Amiel et al., 2009). Upon inhibition of Mos-MAPK, both the first and the second meiotic spindles display long aster-like microtubules, and these long microtubules appear to push spindle, which normally would tightly localize to the cortex, deeper in the cytoplasm (Choi et al., 1996; Verlhac et al., 1996; Amiel et al., 2009). The reverse effect has also been observed in tunicates: mitotic embryos ectopically expressing Mos showed meiotic spindle morphology (Dumollard et al., 2017). Furthermore, in mitosis of somatic cells Mos overexpression also resulted in meiotic-like spindles with less abundant astral microtubules and spindles positioned off-center (Fukasawa and Woude, 1995). In mouse oocytes, substantial efforts have been made to identify the molecular mechanisms underlying Mos-mediated these changes in spindle morphology that led to the identification of important candidates including the microtubule regulators MISS and DOC1R (Lefebvre et al., 2002; Terret et al., 2003). However, a comprehensive mechanistic model of how Mos-MAPK regulates spindle morphology is still lacking.

Additionally, Mos is also required to establish the CSF arrest and thereby synchronize oocyte meiosis with fertilization (Jessus et al., 2020). Indeed one of the most prominent and universal effects of Mos-MAPK inhibition is the loss of CSF arrest and subsequent parthenogenic activation of oocytes (Colledge et al., 1994; Hashimoto et al., 1994). In the best-characterized case of *Xenopus* oocytes, the function of Mos-MAPK in CSF arrest is to maintain Cdk1-Cyclin B activity at high levels, thereby keeping oocytes in metaphase until fertilization triggers the degradation of Mos (Haccard and Jessus, 2006). In molecular terms, this function shows similarity to Mos' other role in preventing the S-phase between MI and MII, both requiring the production of extra Cdk1-Cyclin B activity. However, Mos appears to additionally act on Erp1/Emi2 to prevent Cyclin B degradation by the APC/C (Wu and Kornbluth, 2008). In other species, while the involvement of Mos-MAPK in CSF-type arrests is clear, the underlying molecular mechanisms are less well understood.

Taken together, the atypical activation of the ERK/MAPK pathway by Mos mediates several essential meiotic functions conserved across animal species, however, the underlying molecular

mechanisms remain incompletely understood. Here, we aim at identifying the molecular modules under the control of Mos-MAPK by combining phospho-proteomics and live imaging in a unique model system, the oocytes of the starfish, *Patiria miniata*. Starfish oocytes are suited for high-resolution live imaging of meiosis to characterize cellular phenotypes, and at the same time available in large quantities and proceed through meiosis with high synchrony to allow proteomics experiments. Furthermore, Mos-MAPK has already been extensively characterized in starfish. These studies clearly demonstrate that Mos-MAPK controls several of the functions in starfish that have been shown to depend on Mos-MAPK activity in other species. These include the reactivation of Cdk1-Cyclin B at the end of meiosis I to drive meiosis II (Iwabuchi et al., 2000; Hochegger et al., 2001), and it has been shown that the CSF-like arrest that in starfish occurs at the G1 phase, is also dependent on Mos-MAPK (Mori et al., 2006). It has also been shown that Mos-MAPK controls spindle morphology and affects the asymmetry of the division (Ucar et al., 2013), however, the mechanisms remain incompletely understood. These studies also established that the small-molecule inhibitor U0126, a selective inhibitor of Mos' downstream kinase MEK1 (Favata et al., 1998) can completely abolish Mos-dependent activation of the MAPK pathway during meiotic divisions (Mori et al., 2006; Ucar et al., 2013). The effects of U0126 treatment closely mirrored the inhibition of Mos-MAPK by other means, such as anti-Mos morpholino injection (Tachibana et al., 2000), or injecting an inhibitory antibody against the downstream effector p90Rsk (Mori et al., 2006).

Results

Mos-MAPK activity drives the second meiotic division

We first imaged live starfish oocytes by high-resolution confocal microscopy to complement the previous, detailed biochemical characterization of Mos-MAPK's functions during meiosis (Tachibana et al., 2000). To this end, we labeled chromatin and microtubules to monitor the effects of U0126 treatment on cellular events during the two meiotic and subsequent mitotic divisions (Fig 1A).

U0126-treated and DMSO-treated control oocytes progressed normally through the initial steps of meiotic maturation: after the addition of the maturation hormone, NEBD commenced in 20-25 min. Thereafter chromosomes congress to the animal pole, indicating that actin- and microtubule-driven mechanisms of chromosome transport (Burdyniuk et al., 2018) are independent of MAPK activity (Fig. 1A). The first meiotic spindle then formed and aligned all chromosomes to the metaphase plate both in treated and untreated oocytes (Fig. 1A). The time from NEBD to metaphase I showed no significant difference (Fig. 1B). These observations are well consistent with biochemical assays that detected MAPK activity first at the time of metaphase I (Tachibana et al., 2000).

After metaphase I, U0126-treated oocytes showed a strikingly different behavior compared to DMSO-treated controls. Control oocytes, after extrusion of the first polar body, rapidly progress into the second meiotic division and form the metaphase II spindle within ~40 minutes (Fig. 1B). During this transition between the first and second meiotic divisions chromosomes remain condensed and the nuclear envelope does not re-form (Fig. 1A). By contrast, U0126-treated oocytes exit M-phase after meiosis I evidenced by gradual decondensation of chromatin and reformation of the nucleus (Fig. 1D), further confirmed by immunostaining the nuclear envelope marker, lamin B (Fig. 1D). These pronuclei that formed in U0126-treated oocytes ~1 hour after metaphase I showed similar morphology to pronuclei in control oocytes that form after the completion of the two meiotic divisions (Fig. 1D). Together, cellular phenotypes are consistent with previous BrdU-labeling experiments and biochemical assays showing that Mos-MAPK-inhibited oocytes decondense chromatin, reform the nucleus and enter S-phase after metaphase I (Tachibana et al., 2000).

U0126-treated oocytes did however eventually enter a second division, and then begin parthenogenetic embryo development without fertilization, consistent with abolished CSF arrest already documented in starfish (Mori et al., 2006). While by simple counting this may be considered the second meiotic division, by its timing and morphology it clearly corresponds to the first mitotic division: it occurs at the time of the first mitotic division in untreated, fertilized oocytes (Fig. 1C), and the spindle is large and features prominent astral microtubules typical to mitotic spindles (Fig. 1A).

To reinforce observations made by live imaging, we performed a morphometric analysis of metaphase spindles stained by immunofluorescence (Fig. 2A). In metaphase I, U0126-treated and untreated control spindles have a width and length (excluding centrosomal asters) statistically not different from one another (Fig. 2B). However, when the centrosomal asters are also considered, there is a clear difference between U0126-treated and untreated oocytes already at metaphase I: the diameter of the centrosomal area increased from ~3 μm to almost 5 μm (Fig. 1C). In control oocytes, metaphase I is followed by metaphase II. The metaphase II spindle showed a similar morphology to metaphase I except for an approximately twice-smaller centrosomal area.

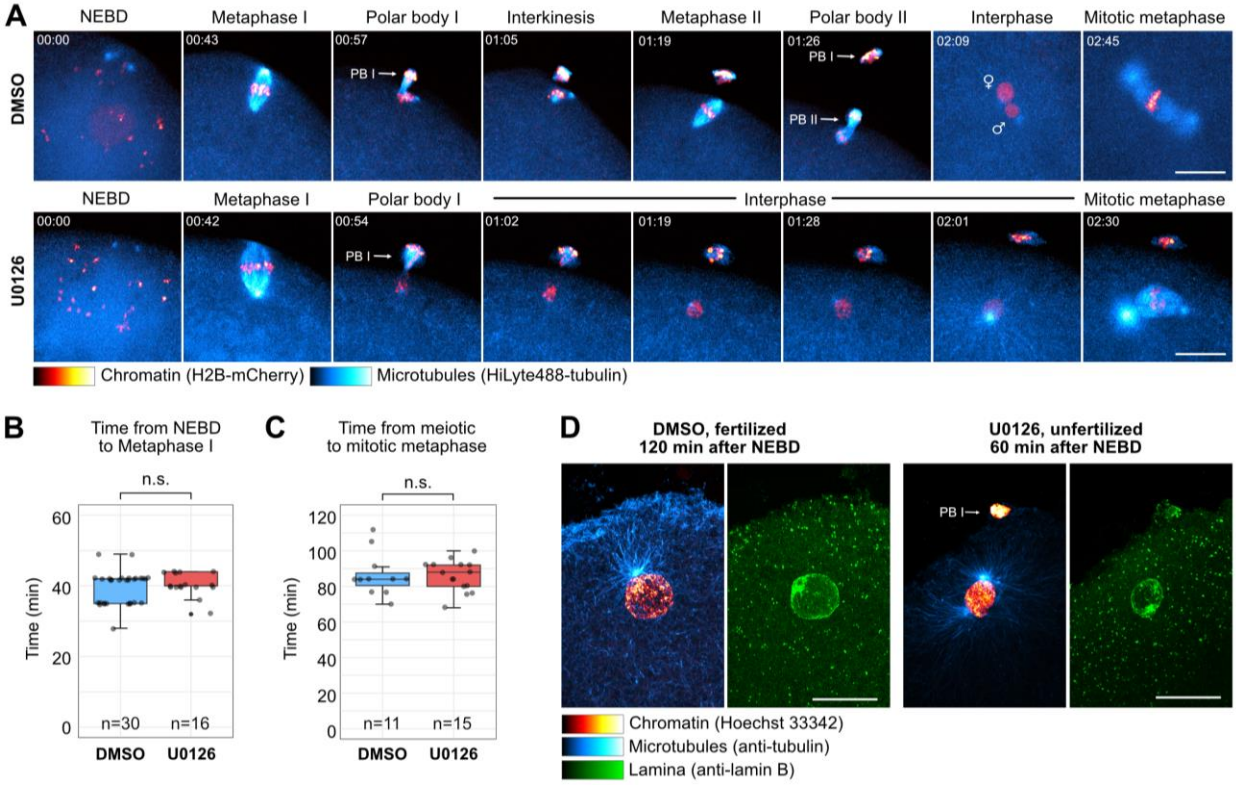

Figure 1. Inhibition of Mos-MAPK activity abolishes the second meiotic division and causes oocytes to progress directly into parthenogenic embryo development without fertilization

(A) Selected frames from a time-lapse recording of oocytes expressing H2B-mCherry (red) and injected with HiLyte488-tubulin (blue) to label chromosomes and microtubules, respectively. Oocytes were imaged through meiosis and then fertilized after meiosis I directly while imaging on a spinning disk confocal microscope. Before inducing maturation, oocytes were treated either with 20 µM U0126 or an equal amount of DMSO. Maximum intensity projections are shown, scale bars are 20 µm, and time is given as mm:ss. Arrows indicate the polar bodies. Venus and Mars signs indicate female and male pronuclei respectively.

(B) Boxplot showing the time from nuclear envelope breakdown (NEBD) to metaphase I quantified on recordings similar to shown in (A). Statistical comparison was done using the Mann-Whitney test.

(C) Boxplot showing the time from meiotic metaphase I to the first mitotic metaphase quantified on recordings similar to those shown in (A). Statistical comparison was done using the Mann-Whitney test.

(D) Immunofluorescence images of oocytes stained for microtubules (anti-tubulin, blue), chromatin (Hoechst 33342, red), and the lamina (anti-lamin B, green). Oocytes were treated with 20 µM U0126 or an equal amount of DMSO and then fixed 60 and 120 minutes after inducing maturation, respectively. Samples were imaged on a spinning disk microscope. Maximum intensity projections are shown, scale bars are 20 µm.

This is likely explained by the fact that in meiosis I starfish oocytes still have duplicated centrioles at the spindle poles, while in meiosis II only single centrioles are present (Borrego-Pinto et al., 2016a). Spindle morphology in the second division in U0126-treated oocytes is strikingly different from normal meiotic metaphase II. In all measured parameters spindle morphology is distinct from meiotic spindles and is statistically indistinguishable from mitotic morphology (Fig. 1C). In particular, spindle length increases from ~6 µm to ~10 µm, and the diameter of the centrosomal area approximately doubles from ~3 µm to ~6 µm between meiotic and mitotic metaphase, with the second metaphase in U0126-treated oocytes exactly matching mitotic values (Fig 1C).

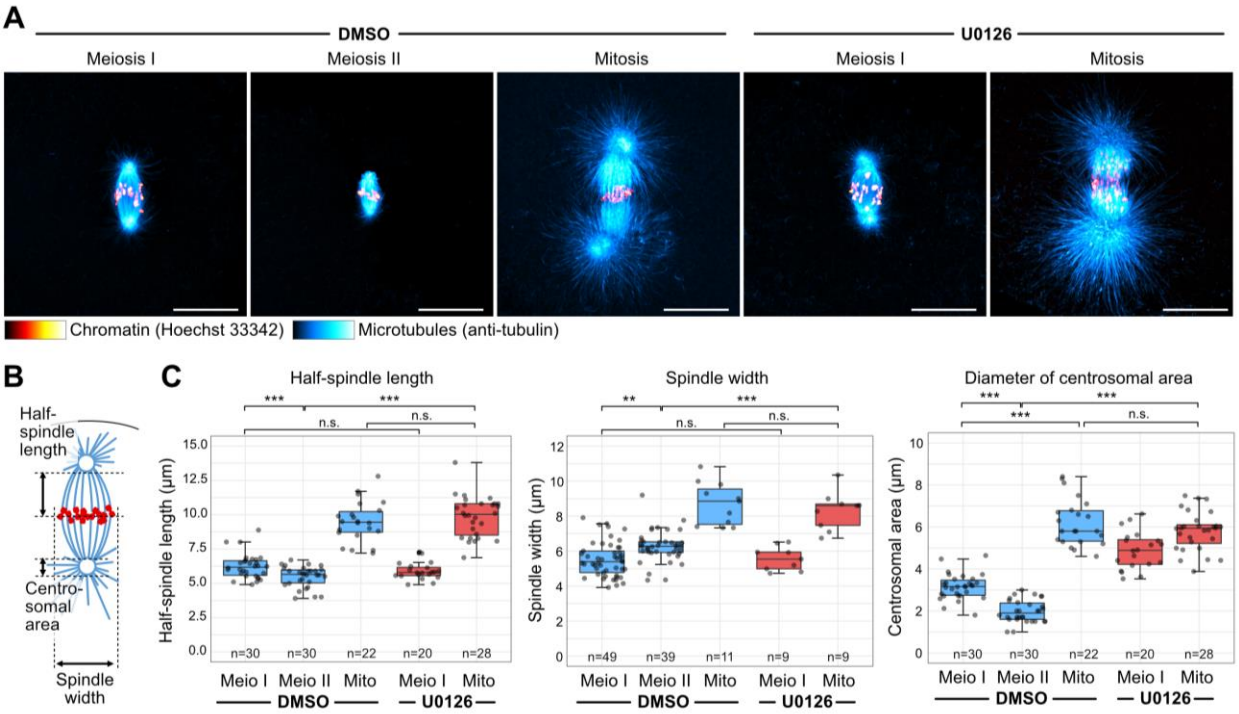

Figure 2. Changes in spindle morphology upon inhibition of Mos-MAPK

(A) Immunofluorescence images of oocytes stained for microtubules (anti-tubulin antibody, blue) and chromatin (Hoechst 33342, red) at the indicated stages and treated with 20 µM U0126 or an equal amount of DMSO. Imaging was done on a spinning disk confocal microscope. Maximum intensity projections are shown, scale bars are 20 µm. **(B)** Schematics of the meiotic spindle illustrating the carried-out measurements. Microtubules are blue and chromatin is red.

(C) Boxplot showing 3D measurements performed on images similar to those shown in (A) and as illustrated in (B). **P<0.05, ***p<0.0001. Statistical analysis was done using a two-tailed T-test.

Additionally, in unperturbed mitosis of embryos, we observed the formation of F-actin patches located near the spindle midzone both in fixed and phalloidin-stained samples (Fig. 3), and in live embryos expressing the F-actin marker UtrCH (not shown). These F-actin structures are not observed in meiosis. However, U0126 treatment caused a mitotic-like actin localization observed already in the first meiotic spindle (Fig. 3), further evidencing that Mos-MAPK inhibition renders meiotic spindles mitotic-like.

Taken together, the timing of the divisions, as well as the cellular morphology of pronuclei and metaphase spindles, indicate that U0126-treated oocytes proceed directly from meiosis I to parthenogenetic development without undergoing meiosis II. That is, in the absence of Mos-MAPK activity, the first and largely normal meiotic division is followed by interphase and S-phase and then the first mitotic division. These observations are fully consistent with previous biochemical assays demonstrating that Mos-MAPK activity is required to drive meiosis II ensuring haploidization of the female gamete (Tachibana et al., 2000).

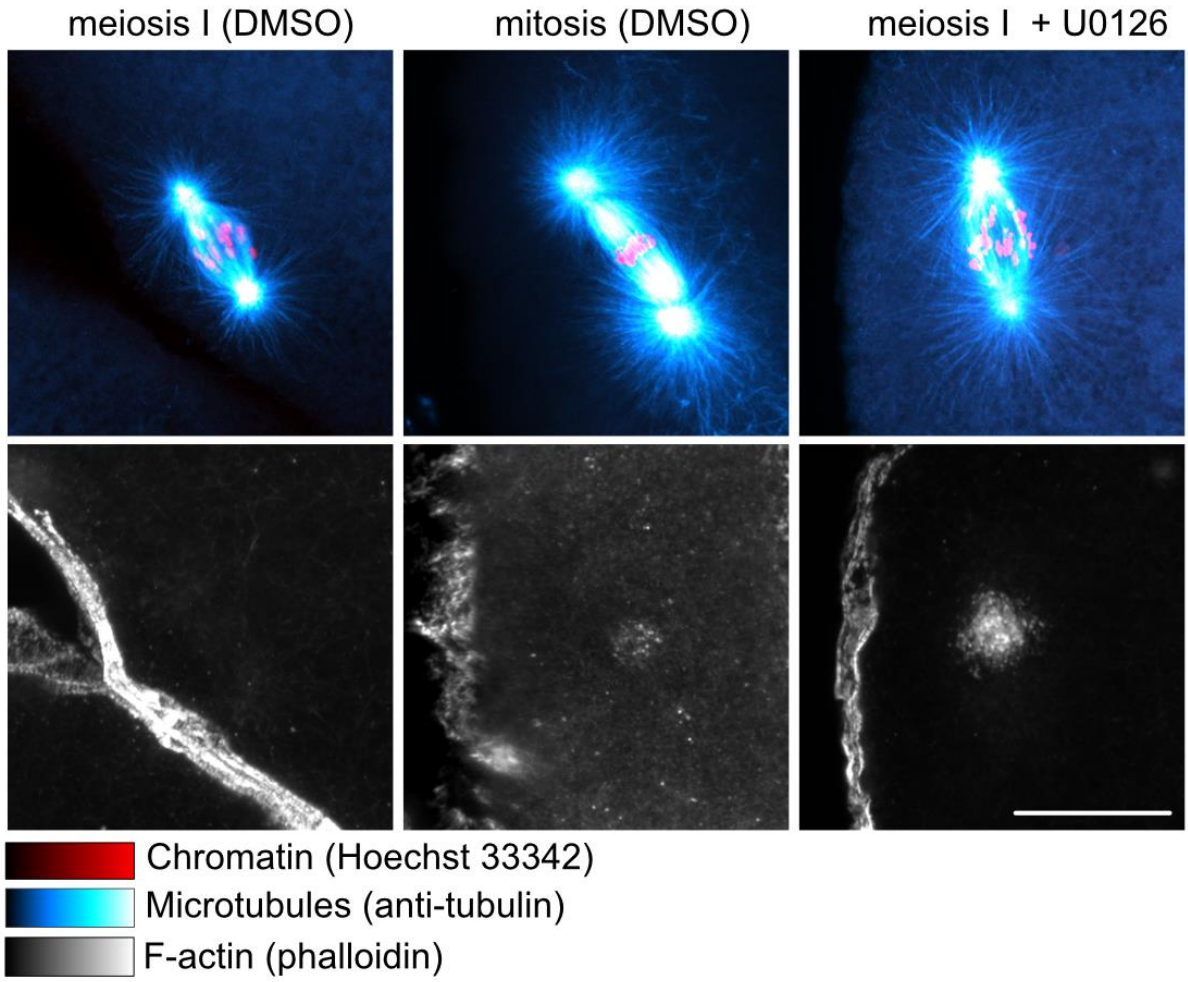

Figure 3. Spindles in Mos-MAPK-inhibited oocytes display mitotic-like F-actin patches

Immunofluorescence images of oocytes stained for microtubules (anti-tubulin antibody, blue), chromatin (Hoechst 33342, red), and with phalloidin to visualize actin filaments (grays) at the indicated stages, and treated with 20 μM U0126 or equal amount of DMSO. Airyscan confocal imaging. Maximum intensity projections are shown, scale bar is 20 μm.

Phosphoproteomic analysis of Mos-MAPK inhibition in oocytes at metaphase I

Our data and consistent previous observations clearly demonstrate that Mos-MAPK activity drives the second meiotic division. In this process, there appears to be a critical bifurcation point at metaphase I: if Mos activates the MAPK pathway, then the oocyte proceeds to meiosis II without undergoing an S-phase. If the Mos-MAPK pathway is inhibited, the oocytes skip meiosis II entirely and proceed into an interphase, S-phase, and a subsequent mitotic division followed by parthenogenetic embryo development. This transition occurs at metaphase I, further supported by the fact that before metaphase I Mos is inactive in starfish oocytes (Tachibana et al., 2000).

Therefore, to identify the downstream targets of the Mos-dependent MAPK pathway at this critical transition, we chose to perform a phospho-proteomic analysis of oocytes at metaphase I. Oocytes were collected from three starfish animals, each treated with U0126 or an equal amount of the DMSO solvent, concomitant with inducing meiotic maturation. Taking advantage of the highly synchronous progression of meiosis in starfish oocytes, we could easily prepare extracts and rapidly froze samples at metaphase I (Fig 4A). The stage and synchrony we confirmed by fixing and Hoechst-staining a small

portion of the sample. In the samples used for further analysis, 92-96% of the oocytes displayed chromosomes aligned on a metaphase plate.

Samples were then processed, enriched for phospho-peptides, and analyzed by multiplexed quantitative tandem mass tag (TMT) mass spectrometry (Fig. 4A). Since starfish animals are collected in the wild, we expected significant diversity between our biological replicates. In addition, the *Patiria miniata* proteome is not extensively characterized and annotated. Therefore, we merged the Echinobase v2 proteome with the newer NCBI annotation and derived a non-redundant protein database, and performed a functional annotation to transfer KEGG identifiers and gene ontology (GO) terms (Fig. 4A, Supplemental file 1).

In total, we quantified 9 035 protein groups, of which 4716 contained phospho-peptides (Fig. 4B). These numbers were comparable to previously published phosphoproteomic analysis of starfish oocytes (Swartz et al., 2021). Our deferential expression analysis (DEA) showed no significant changes in the proteome level. This is also consistent with the findings of Swartz and coworkers, who showed that protein levels remain largely constant throughout meiotic divisions (Swartz et al., 2021).

We then used ratios between phosphorylated peptides to their total protein intensities in U0126 *versus* DMSO treated samples (12374 unique phospho-peptides, Fig. 4B). This resulted in 185 unique phospho-peptides that passed the significance threshold. Despite sampling genetically diverse individuals, unsupervised clustering of differentially phosphorylated peptides clearly separated U0126-treated samples from DMSO controls evidencing an effect much above biological variability (Fig. 5A).

Next, to gain an initial and unbiased view of the data, we ran a few automated analyses. Firstly, we performed an over-representation analysis to test which biological processes were associated with proteins that underwent differential phosphorylation. This revealed the enrichment of gene ontology (GO) terms related to processes of cell cycle and cytoskeletal regulation (Fig. 5A).

Secondly, we used a prediction tool to identify putative human protein kinases responsible for phosphorylation changes induced by U0126 treatment in starfish oocytes (Johnson et al., 2023). This analysis showed a striking enrichment of kinases related to the MAPK-pathway: the top hits are the AGC family of kinases, which include $p90^{RSK}$, the main downstream effector kinase of Mos-MAPK (Fig. 5B). Expectedly, the STE family, kinases of the MAPK pathway are also identified. We further detected a significant enrichment of the CAMK family, which may be explained by the fact that RSK kinases contain two distinct kinase domains, the second of which belongs to the CAMK family. Additionally, some of the other kinases involved in actin regulation (ROCK, MYLK) were also identified within the AGC and CAMK families. Intriguingly, we observed a significant enrichment of the otherwise unrelated family Aurora kinases (Fig 5B).

We then manually curated the list of phosphoproteins with significantly changed phosphorylation statuses. This confirmed several hits related to cytoskeletal processes and cell cycle regulation. Additionally, we identified a large number of translational regulators, including several of the top hits with the highest enrichment and significance (Fig. 5C). Furthermore, we found changes in the phosphorylation of MAPK pathway components, and identified proteins involved in DNA replication and repair, chromatin maintenance, transcription, and RNA processing. Finally, we also identified some proteins involved in ubiquitin-mediated protein degradation, general metabolism as well as vesicular trafficking, and several novel, yet unannotated proteins (Supplemental file 2).

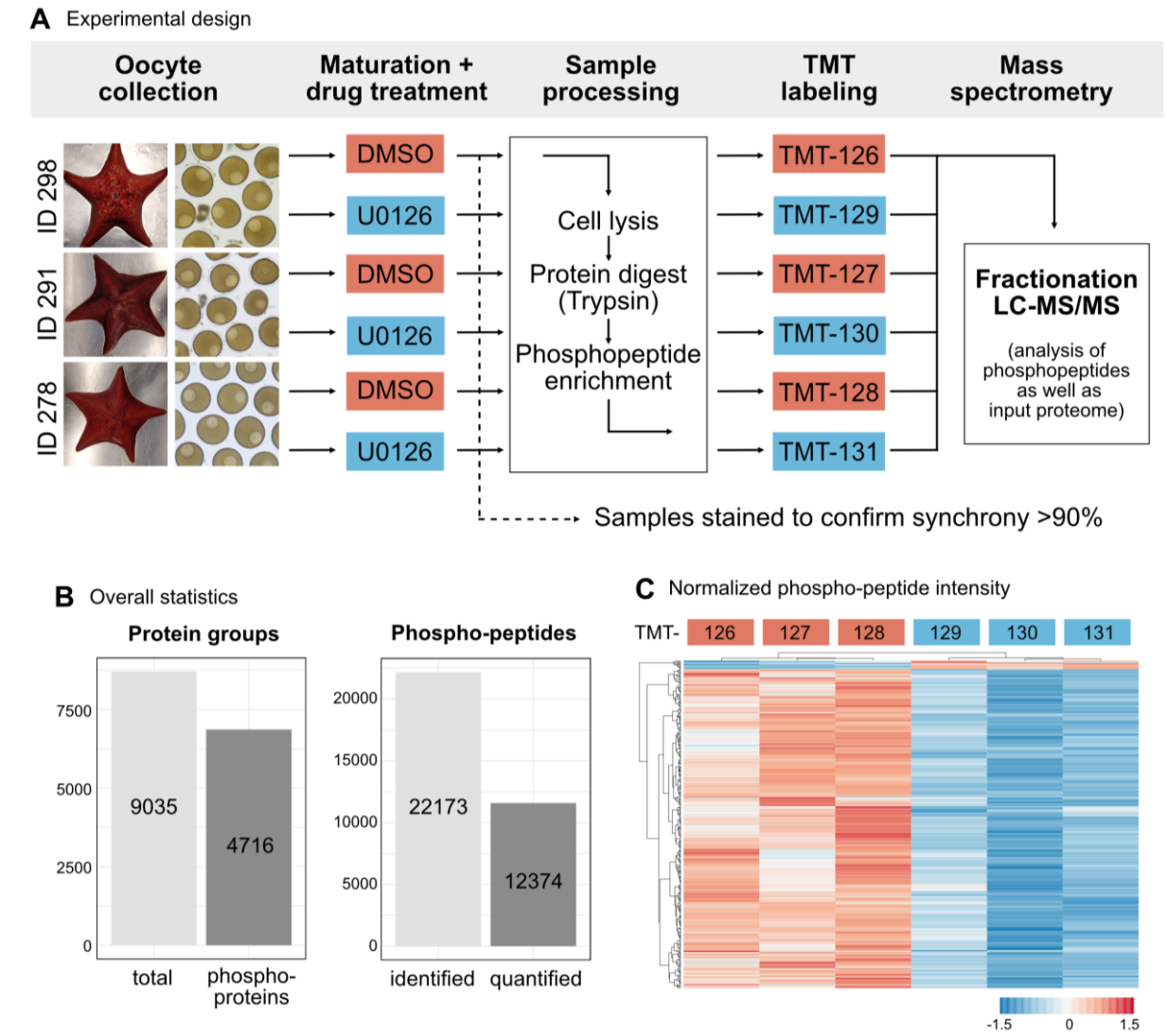

Figure 4. Phospho-proteomics of oocytes at metaphase I reveals consistent effects of Mos-MAPK inhibition across biological replicates.

(A) Outline of the phospho-proteomics experiment. Mos-MAPK-inhibited (blue) and control (red) oocytes were collected at metaphase I in three biological replicates. Phospho-peptides were enriched prior to TMT labeling. Enriched and non-enriched samples were analyzed by MS2. Metaphase I occurred in >90% of the oocytes as confirmed by immunofluorescence.

(B) Overall statistics representing protein groups and phospho-peptides identified and quantified.

(C) Unsupervised clustering of differentially phosphorylated peptides (rows) vs TMT channels (columns) confirms the effect of treatment above variability of biological replicates. Red: control, blue: Mos-MAPK inhibition. Heatmap is normalized according to Log2 fold-changes scaled to the mean of 0 and standard deviation of 1.

In summary, our phosphoproteomic analysis of U0126-treated oocytes revealed no change in protein levels and identified a set of 271 unique phospho-peptides, which changed significantly and consistently across biological replicates upon U0126 treatment. Automated and manual analyses used to validate the dataset were in excellent agreement with expectations based on previously published data as well as our microscopic observations: translation, cell cycle, and cytoskeletal regulation were identified as the main processes affected, and kinase profiling found the MAPK-pathway and $p90^{RSK}$ to be the major effector kinases.

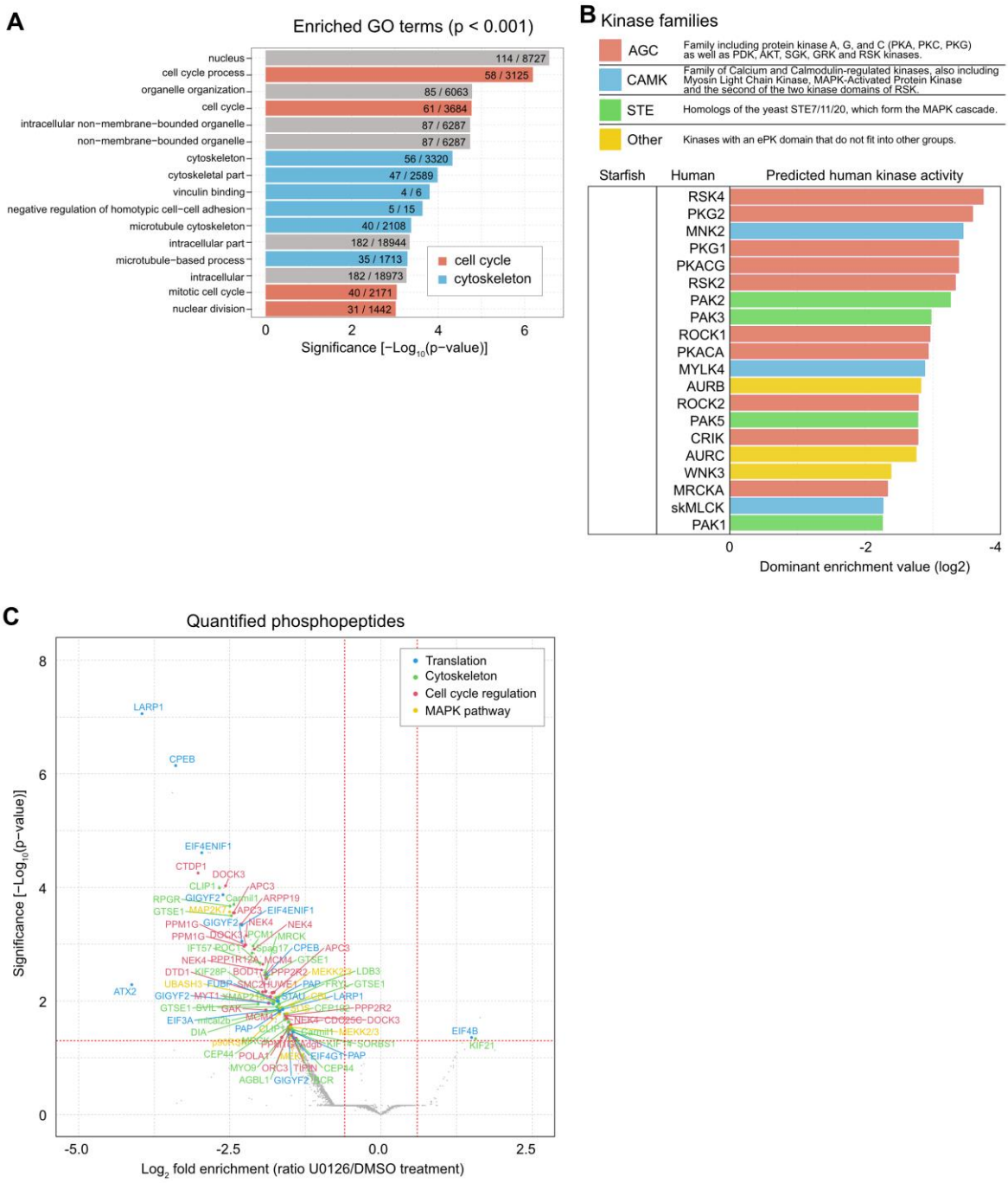

Figure 5. Phospho-proteomics of oocytes at metaphase I reveal cell cycle regulation, cytoskeleton and translation as three main processes regulated by Mos-MAPK activity

(A) Gene ontology enrichment analysis of differentially phosphorylated proteins identified cell cycle regulation and cytoskeleton as the main processes regulated by Mos-MAPK activity.

(B) Prediction for human effector kinases that enriched in the sample.

(C) Volcano plot of the quantified phospho-peptides. The majority of phospho-peptides were manually classified into four categories: Translation, Cytoskeleton, Cell cycle regulation, and MAPK pathway. The rest of the phospho-peptides including those from unidentified proteins are marked in grey.

Phosphoproteomics identifies functional modules regulated by the Mos-MAPK pathway

Next, we used the manually curated hitlist of phospho-peptides significantly changed by U0126 treatment to identify functional modules, i.e. molecular complexes that may mediate the cellular processes regulated by Mos-MAPK activity.

Firstly, we detected dephosphorylation of MEK and the downstream effector p90^{RSK} (Table 1 and Fig. 6), confirming the inhibition of the MAPK pathway (Mori et al., 2006). Secondly, U0126 treatment causes oocytes to exit after meiosis I rather than entering the second meiotic division. Consistently, we detected changes indicating the inactivation of Cdk1-Cyclin B. This includes dephosphorylation of the main activator and inhibitor of Cdk1-Cyclin B, the Cdc25 phosphatase, and the Myt1 kinase, respectively (Table 1 and Fig. 6). We also detect dephosphorylation of the APC/C subunit Cdc27 (APC3) responsible for degradation of Cyclin B. Furthermore, Arpp19 and PP2A are also dephosphorylated. PP2A is known to antagonize Cdk1-Cyclin B and has recently been identified as an important regulator of the meiotic cell cycle in starfish oocytes (Swartz et al., 2021). We also observe several additional hits indicative of an overall signature of M-phase exit such as regulators of DNA replication (Supplemental file 2). Together, these changes confirm that U0126-treatment inhibits the Mos-MAPK pathway leading to the inactivation of Cdk1-Cyclin B, and thus exit from M-phase after meiosis I.

In addition to cell cycle signaling, translational regulation emerged from our analyses as the most prominent functional module affected by the inhibition of Mos-MAPK. We identified changes in the phosphorylation status of several components of the cap-dependent translation initiation complex (eIF3A, eIF4B, eIF4G) along with PPM1G, a phosphatase regulator of 4E-BP1 (Liu et al., 2013) (Table 1 and Fig. 6). Among the top hits is LARP1, a translational regulator of mRNAs characterized by a 5' terminal oligopyrimidine (5'TOP) motif typically associated with the mTOR pathway (Berman et al., 2021). LARP1 binds the 5'TOP motif and is thought to play a role in circularizing the transcript by interaction with the PolyA-binding protein (PABP) at the 3' end. Possibly some of the most relevant, and indeed highest scoring hits are the CPE-element binding protein, CPEB, and the eIF4E transporter, eIF4ENIF1. These proteins form a complex together with Maskin/TACC3 to inhibit translation with eIF4ENIF1 bound to the 5'-cap and CPEB bound to the CPE-element in the 3'-UTR (Fig. 6) (Mendez and Richter, 2001; Minshall et al., 2007). However, upon phosphorylation, the inhibitory complex dissociates and CPEB recruits the PolyA polymerase PAP to activate translation (Mendez and Richter, 2001). Together, the changes induced by U0126 treatment are fully in support of a model, in which the Mos-MAPK pathway activates translation in meiosis by phosphorylation of CPEB and other translational regulators.

Table 1. Functional molecular modules consistently dephosphorylated on multiple subunits upon inhibition of Mos-MAPK

The modules were manually curated from the significant hit list (185 entries) of the phospho-proteomics profiling of the oocytes in control or Mos-MAPK-inhibited oocytes at metaphase I. All entries are available in Supplementary file 2. P-value adjusted for multiple hypothesis testing. Log2 fold change in phospho-peptide abundance upon Mos-MAPK inhibition is indicated.

	Name	KEGG	Protein IDs	Peptide	MS scan IDs	p-adj	Enrichment
MAPK module	MEK1	K04369	XP_038079443.1, PMI_017007	NLTLPVKPDDSAPSNAVNNSS*ASMAAIAK	51401	0.0444	-1.5136
	p90RSK	K04373	XP_038049299.1, PMI_022459	T*PKDSPGLPPSASAHQLFR	44589	0.0165	-1.6801
cdk1-Cyclin B module	PPP2R2	K04354	XP_038070796.1, PMI_020469	KRPLSTSDGT*AK	22877	0.0180	-1.5714
	PPP2R2	K04354	XP_038070796.1, PMI_020469	RPLS*TSDGTAKK	23882	0.0040	-1.8997
	MYT1	K06633	PMI_008112	AVSFRQSEPSVLQS*PHYNEK	41151	0.0109	-1.8548
	APC3	K03350	PMI_002534, XP_038047876.1, PMI_014580	LFS*NNSVKENATK	45583	0.0003	-2.4236
	APC3	K03350	PMI_002534, XP_038047876.1, PMI_014580	LFS*NNS*VK	49005, 45078	0.0003	-2.4422
	CDC25C	K05866	XP_038070722.1	NRS*ETIMWEACNDKENVDIQNK	42276	0.0262	-1.4918
	ARPP19		XP_038072705.1, PMI_013584	KQS*TEISK	23112	0.0004	-2.3112
Translational activation module	LARP1	K18757	PMI_014589	EGRES*VDSPR	8801, 7715	0.0000	-3.9525
	CPEB	K02602	XP_038045408.1, PMI_005839, PMI_001490	HTS*NNPGRPEK	10213	0.0000	-3.3840
	CPEB	K02602	XP_038045408.1, PMI_005839, PMI_001490	YPS*QEIQQDYEK	37277	0.0035	-1.8924
	EIF4ENIF1	K18728	PMI_009884	KS*EPDGESGEKEEEGGDK	21052, 19560	0.0000	-2.9642
	EIF3A	K03254	PMI_009181	S*AGIKDEEDEPR	22666	0.0140	-1.6728
	EIF4B	K03258	XP_038044282.1	SNEDDSAFHKEEPLSPTSPTAPKS*PK	36461	0.0440	1.5003
	EIF4G1	K03260	XP_038075416.1	VIQRVS*QTIK	36609	0.0444	-1.4466
	PAP	K14376	XP_038074837.1, PMI_002048	LPS*GELPDMSSPMPK	53218, 49713, 47545	0.0111	-1.7180
	PPM1G	K17499	PMI_005456, PMI_016115	KAS*ESTPTDDDDSKR	16212, 19904, 17237	0.0011	-2.2632
	ATX2	K23625	PMI_011421, XP_038075475.1, PMI_025445	DGTRGHS*PQHASVQR	6500	0.0165	-4.1221
Microtubule module	CLIP1	K10421	XP_038055294.1, PMI_010288	KTS*TSTVNSETSQR	14508	0.0001	-2.6735
	CLIP1	K10421	XP_038055294.1, PMI_010288	S*VDLTGNKPSLTNK	42275	0.0232	-1.5252
	XMAP215	K16803	XP_038047612.1, PMI_009212	SNRLS*QGSMSSEPVNGSAEQER	22932	0.0107	-1.7741
	GTSE1	K10129	XP_038054192.1	KES*DESQGSDSQESK	15744	0.0003	-2.4737
	GTSE1	K10129	XP_038054192.1	LPSTPST*PVHQDKK	33139, 34006	0.0038	-1.8905
	GTSE1	K10129	XP_038054192.1	LLSSDQS*ATKPVGR	38688	0.0113	-2.0316
	POC1	K16482	XP_038054221.1, PMI_022968, PMI_011690	S*TGADINAHSEPK	21180	0.0022	-2.0017
	PCM1	K16537	XP_038056285.1, XP_038056290.1	LLS*VQQQLR	46891	0.0011	-2.1149
	CEP44	K16761	XP_038055484.1	HAS*GSLVR	15956	0.0211	-1.5896
	CEP44	K16761	XP_038055484.1	RVS*VSVNELR	34019	0.0482	-1.3946
	CEP192	K16725	XP_038068323.1	RPS*FGTGHIKT*PEGR	27259	0.0172	-1.5904
	KIF21	K10395	XP_038053367.1, XP_038053368.1	LHSHSDRENES*ADEKEDAAEK	18719	0.0460	1.5649
	KIF14	K17915	PMI_006555, XP_038045418.1	IDS*PMT*PLKR	40449	0.0344	-1.4586
	FRYL		XP_038055332.1, PMI_004592, PMI_010187	RS*S*SGGTLEK	17295	0.0113	-1.6849
Cortical contraction module	MYPT1	K06270	XP_038073240.1, XP_038073245.1	TGS*ASTDTSSTSVR	12906	0.0023	-1.9539
	MRCK	K16307	XP_038071518.1	RGGGS*VGAENNEVK	17206	0.0032	-1.9099
	MRCK	K16307	XP_038071518.1	RLES*EKNTLSHR	21479	0.0278	-1.5109
	mDia2	K16688	XP_038063096.1, PMI_026018, PMI_028305	LQSRPS*VEEEEAHQEYER	26257	0.0146	-1.6930
	MYO9	K10360	XP_038073351.1, PMI_008384	KQS*DPQQAAEALGLPSDKPGK	42738	0.0337	-1.5479
	BCR	K08878	XP_038059104.1	LS*TPDVEILNVR	53153	0.0480	-1.4272

Another large group of phospho-peptides that showed a change upon U0126 treatment are regulators of the cytoskeleton. We noted that a substantial subset of those proteins is involved in regulating centrosomal microtubule nucleation (Table 1 and Fig. 6). We found components with roles in centrosome maturation, such as the recruitment of the pericentriolar material to centrioles (CEP192, CEP44, and POC1), the main pericentriolar material constituent, PCM1, as well as the protein furry (FRY)-like, thought to be important for centrosome integrity early in cell division (Ikeda et al., 2012; Conduit et al., 2015). Secondly, we found several proteins that play a role in nucleating and stabilizing astral microtubules including the general microtubule plus tip binding proteins XMAP215/chTOG and CLIP1 (Slep and Vale, 2007), and GTSE1, a plus tip binding protein that specifically regulates the stability of astral microtubules (Bendre et al., 2016). Furthermore, we identified several members of the kinesin superfamily that regulate anaphase. A kinesin-4 family member (identified as KIF4/21/27) may be involved in anaphase in interaction with PRC1 at the central spindle (Bieling et al., 2010), and similarly, the kinesin-3 KIF14 may be required for anaphase in interaction with citron kinase (Gruneberg et al., 2006). Interestingly, a meiosis-specific paralog of KIF14, NabKin was reported to specifically regulate polar body cytokinesis in *Xenopus* oocytes (Samwer et al., 2013).

Besides microtubules, we also identified several proteins that regulate the actin cytoskeleton (Table 1 and Fig. 6). In particular, regulators of the small GTPases Cdc42, Rac1, and RhoA as well as their downstream effectors have been detected among phospho-peptides significantly changed upon U0126 treatment. This includes the BCR which is a GTPase-activating protein for Cdc42 as well as the activator

of RhoA, MYO9. Importantly, we detected a significant dephosphorylation of mDia2 downstream of RhoA, which confirms earlier findings showing mDia2 to be a downstream target of Mos-MAPK in starfish (Ucar et al., 2013). Additionally, we found a significant effect on the Cdc42 binding protein MRSK, which recently have been shown to drive the initial, meiosis-specific step of polar body cytokinesis (Bourdais et al., 2022). We also find Rac1 among the dephosphorylated proteins that may be involved in Arp2/3-dependent actin nucleation and act as an antagonist of RhoA during polar body cytokinesis (Halet and Carroll, 2007; Pal et al., 2020).

Taken together, a substantial set of cytoskeletal regulators appear to be controlled by Mos-MAPK activity likely to play key roles in the meiosis-specific, extremely asymmetric divisions that produce the polar bodies.

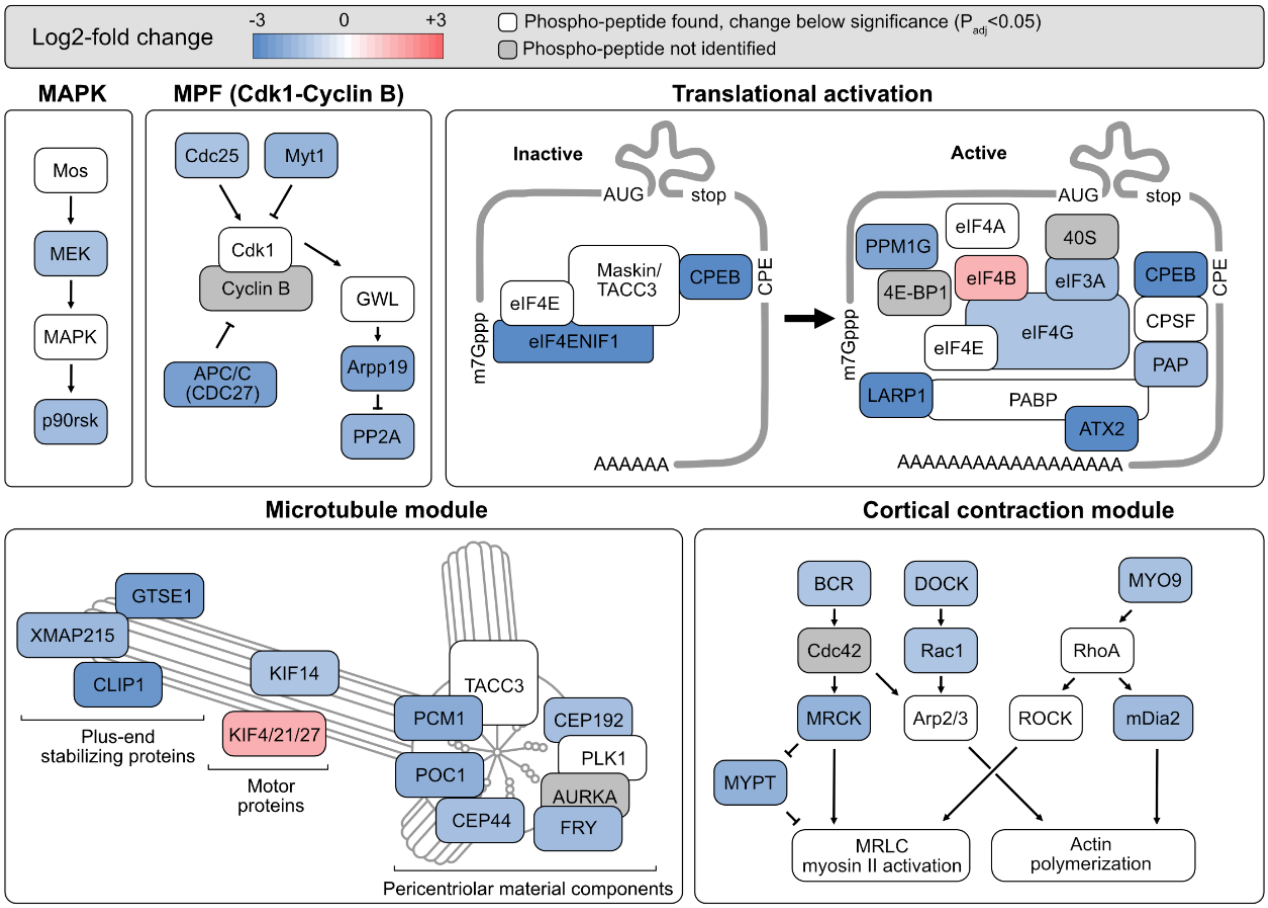

Figure 6. Phospho-proteomics identifies functional modules consistently dephosphorylated on multiple subunits upon inhibition of Mos-MAPK activity

The modules were manually curated from the significant hit list (185 entries) of the phospho-proteomics profiling of the oocytes in control or Mos-MAPK-inhibited oocytes at metaphase I. All entries are listed in Table 1. P-value adjusted for multiple hypothesis testing. Log2 fold change in phospho-peptide abundance upon Mos-MAPK inhibition is indicated.

Translation of Cyclin B is sufficient to drive the second meiotic division

Our phosphoproteomics data combined with the above experiments suggest that Mos-MAPK inhibition results in CPEB dephosphorylation, which in turn may inhibit CPE-dependent translation. Earlier studies in *Xenopus* oocytes proposed that timely translation of Cyclin B may be the key mechanism to reactivate Cdk1-Cyclin B at the end of meiosis I and thereby drive meiosis II (Hochegger et al., 2001). Thus, we wanted to test whether Mos-MAPK may drive meiosis II by regulation of Cyclin B translation.

Therefore, we first blocked Cyclin B translation by injection of an anti-Cyclin B morpholino. Injected oocytes were able to complete the first meiotic division with normal timing and displaying normal spindle morphology (Fig. 7A, B). This observation is expected as starfish oocytes contain cdk1-cyclin B protein (a.k.a. pre-MPF) sufficient to drive meiosis I (Hara et al., 2012). After meiosis I, morpholino-injected oocytes entered interphase, formed nuclei, and stopped the further meiotic progression, unlike control oocytes, which entered meiosis II (Fig. 7A).

These observations are further supported by the cell-cycle-dependent formation of phase-separated droplets of histone H1-Alexa647, which we used here to label chromosomes. These condensates have been observed to form in the interphase and dissolve in M-phase (Shakya et al., 2020). In control oocytes, histone H1 condensates are observed for a brief period between the two meiotic divisions, and again at the G1 stage at the end of meiosis (Fig. 7A). In Cyclin B morpholino-injected oocytes, the histone H1 condensates appeared and persisted following meiosis I, confirming the sustained arrest in interphase (Fig. 7A). Complete inhibition of translation by Emetine displayed effects very similar to Cyclin B morpholino injection: formation of the first meiotic spindle with normal morphology followed by re-formation of the nucleus and sustained interphase arrest (Fig. 7C). This again reinforces the hypothesis that Cyclin B translation alone may be sufficient to drive the second meiotic division.

Next, we wanted to test whether additional Cdk1-Cyclin B is sufficient to drive the meiosis I to II transition. To this end, we injected active Cdk1-Cyclin B protein complex (Veld et al., 2021) directly after metaphase I into oocytes treated with U0126. In control oocytes U0126 treatment prevented transition to meiosis II, instead of the nucleus formation, followed by parthenogenetic mitotic divisions (Fig 7D). Strikingly, injection of Cdk1-Cyclin B complex shortly after metaphase I reverted the U0126 phenotype: as in normal meiosis, a second metaphase spindle formed directly, without the formation of a nucleus (Fig 7D). Likely due to the excess of Cdk1-Cyclin B injected, oocytes then remained arrested at metaphase II in a 'CSF-like' state.

Taken together, while it is not surprising that Cdk1-Cyclin B activity is required to drive division, our data specifically demonstrates that additional Cdk1-Cyclin B protein is alone sufficient to drive a second meiotic division, if introduced shortly after meiosis I. We also show that Cyclin B morpholino and general translation inhibition have strikingly similar effects to Mos-MAPK inhibition in preventing meiosis II. This together suggests, that a key function of Mos-MAPK activity is to induce translation of extra Cyclin B at the meiosis I to II transition, thereby driving the second meiotic division.

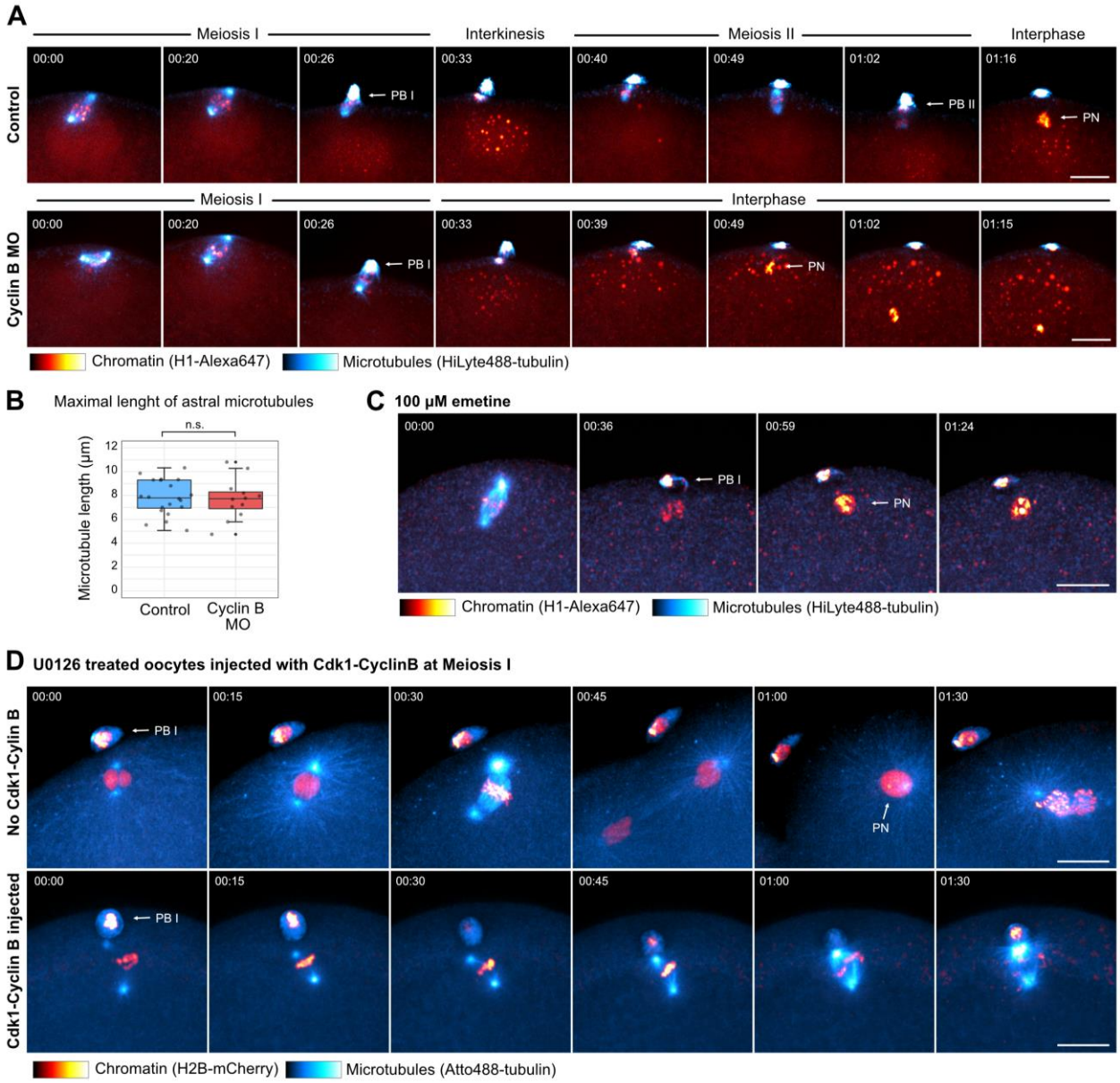

Figure 7. Translation of Cyclin B is sufficient to drive the second meiotic division

(A) Selected frames from a time-lapse recording of oocytes injected with H1-Alexa647 (red) and HiLyte488-tubulin (blue) to label chromosomes and microtubules, respectively. Oocytes were imaged through meiosis on a spinning disk confocal microscope. Before inducing maturation, oocytes were injected with either a morpholino targeting Cyclin B or water as control. Maximum intensity projections are shown, scale bars are 20 µm, and time is given as mm:ss. PB I and II denote the first and second polar bodies, respectively; PN is the pronucleus.

(B) Boxplot showing a comparison of the maximal length of microtubules at metaphase I between control oocytes and oocytes injected with Cyclin B morpholino. Statistical comparison was done using a two-tailed T-test.

(C) Selected frames from a time-lapse recording of an oocyte injected with H1-Alexa647 (red) and HiLyte488-tubulin (blue) to label chromosomes and microtubules, respectively. The oocyte was imaged through meiosis on a spinning disk confocal microscope. Before inducing maturation, the oocyte was treated with 100 µM Emetine to block translation. Maximum intensity projections are shown, the scale bar is 20 µm, and time is given as mm:ss. PB I denotes the first polar body, and PN is the pronucleus.

(D) Selected frames from a time-lapse recording of oocytes expressing H2B-mCherry (red) and injected with HiLyte488-tubulin (blue) to label chromosomes and microtubules, respectively. Oocytes were imaged through meiosis on a spinning disk confocal microscope. Before inducing maturation, oocytes were treated with 20 µM U0126. Then oocytes were either left unmanipulated or they were injected with active Cdk1-Cyclin B protein immediately following extrusion of the first polar body. Maximum intensity projections are shown, scale bars are 20 µm, and time is given as mm:ss. PB I denotes the first polar body, and PN is the pronucleus.

Mos-MAPK regulates the size of centrosomal asters of meiosis I spindle

That Mos-MAPK activity affects the asymmetry of meiotic divisions has been recognized early on and since then confirmed in multiple species (Dupré et al., 2011). However, one caveat is that, as we show above, Mos-MAPK inhibition also affects the timing of divisions. This complicates somewhat the interpretation of studies that relied solely on samples fixed at specific time points. Therefore, we carefully correlated live recordings with fixed samples clearly evidenced that Mos-MAPK inhibition changes in spindle morphology already in meiosis I (Fig 1A, Fig 2A, C). By contrast, inhibition of Cyclin B translation by morpholino injection (Fig 7A, B) or general translation inhibition by Emetine (Fig. 7C) did not affect meiosis I spindle morphology. These observations indicate that Mos' effect on spindle morphology is independent of its role in the translational regulation of Cdk1-Cyclin B activity.

To analyze the effects on spindle organization in more detail, we recorded the first meiotic division at high spatial and temporal resolution in oocytes injected with EB3-mClover3 to label microtubule plus tips. We quantified the maximal length of the astral microtubules and the distance between the spindle poles at prophase, metaphase, anaphase, and telophase in DMSO- and U0126-treated oocytes. These analyses confirmed our previous observation of enlarged centrosomal areas in the U0126-treated metaphase I spindle, displaying longer astral microtubules and slightly increased pole-to-pole distance (Fig 8A-C). Strikingly, as cells progressed into anaphase, the difference between control and U0126-treated spindles dramatically increased. In control spindles astral microtubules and pole distance shortened. In stark contrast, in U0126-treated oocytes asters and pole distance continued to grow as spindles progressed into anaphase and telophase (Fig. 8A-C). As visualized in Fig 8A-C, there is a striking correlation between the size of the asters and pole distances, suggesting that the two processes may be functionally linked. Also consistent with the increased spindle and aster size, the size of the first polar body increased to approx. twice in diameter in Mos-MAPK inhibited oocytes as compared to control (Fig. 8E). As evident on live recordings, cytokinesis of these enlarged polar bodies frequently fails, and only 80% of Mos-MAPK inhibited oocytes could successfully complete polar body extrusion (Fig. 8F).

To complement the live-cell data, we also performed immunofluorescence stainings of spindles at the same stages of meiosis I and recorded high-resolution 3D datasets (Fig. 9). These data were fully consistent with live recordings revealing the same striking difference in microtubule aster size and pole distance between control and Mos-MAPK inhibited oocytes (Fig, 8A).

Our data clearly demonstrate that Mos-MAPK regulates spindle morphology. We thus wanted to explore whether Mos and downstream components of the pathway (MEK1, $p38^{MAPK}$, and $p90^{RSK}$) may localize to the spindle to directly regulate its organization. Therefore, we expressed fluorescent protein fusions Mos-MAPK pathway components from injected mRNAs in oocytes. Unfortunately, we were unable to confidently detect a specific spindle localization of any of the components tested (Fig. 10A). One complication is that in starfish oocytes the spindle area is devoid of yolk vesicles, and therefore any soluble protein appears approx. twice brighter in the spindle area as compared to the surrounding, yolk-filled cytoplasm (Terasaki, 2006).

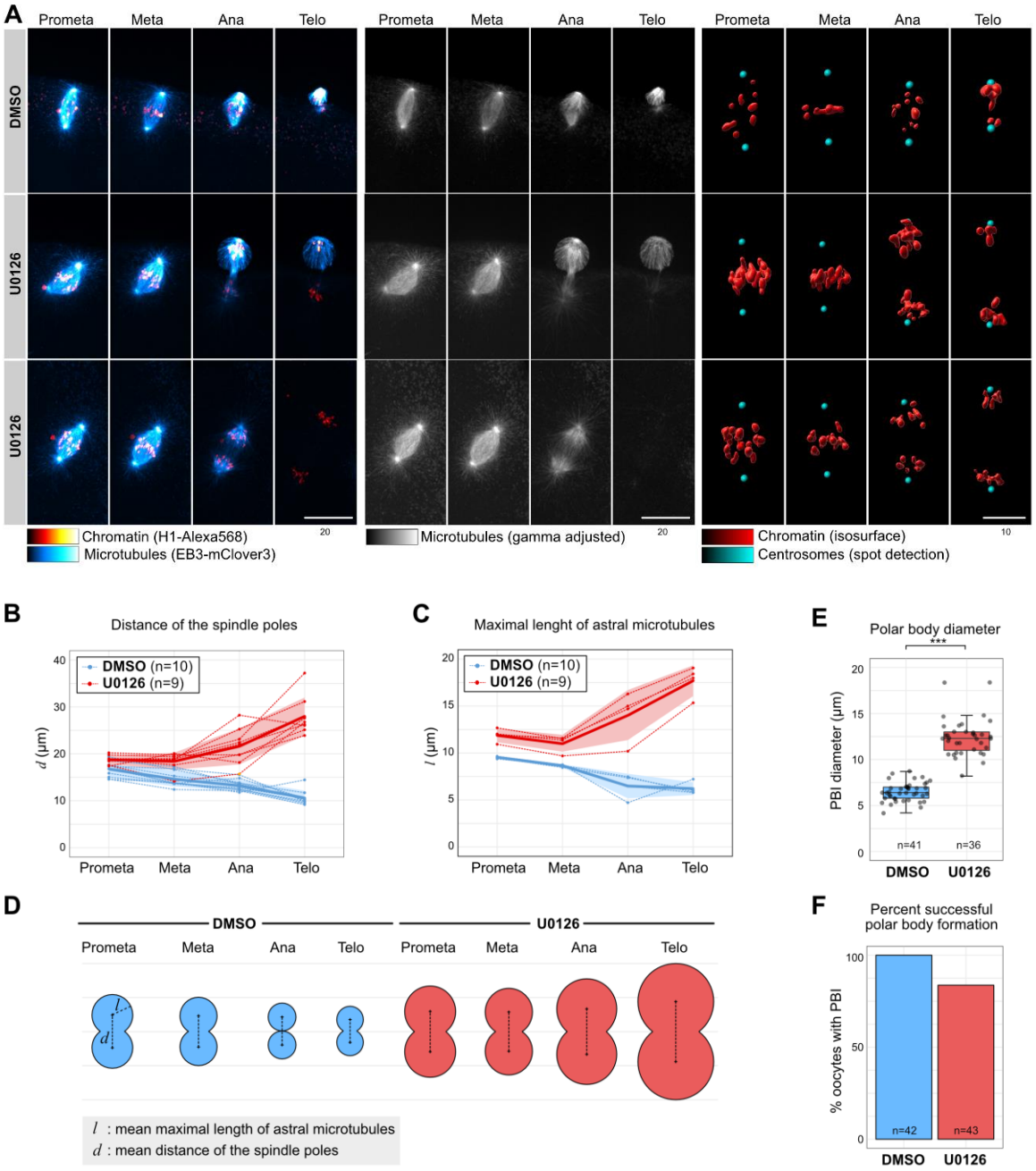

Figure 8. Mos-MAPK reduces aster size in meiosis and prevents spindle elongation in anaphase B, together ensuring minimal polar body size.

(A) Selected frames from a time-lapse recording of the microtubule spindle in an oocyte undergoing meiosis I on a spinning disk confocal microscope. Chromosomes are labeled with H1-Alexa568 (red) and microtubule plus tips by EB3-mClover3 protein (blue). Before inducing maturation, the oocyte was treated with either 20 µM U0126 or an equal amount of DMSO. (left) overlay of the two fluorescent channels; (middle) the EB3-mClover3 channel is shown with adjusted gamma; (right) 3D rendering of the centrosome (blue) and chromosomes (red). Maximum intensity projections are shown, and scale bars are shown in µm.
(B) 3D distances of the spindle poles at different stages of meiosis I.
(C) The maximal length of astral microtubules quantified at different stages of meiosis I.
(D) Illustration of correlated changes in aster size and pole distance. Mean values shown on (B) and (C) are plotted on schematics of the spindle.
(E) Boxplot showing quantification of polar body sizes ***p<0.0001. Statistical comparison was done using a two-tailed T-test.
(F) Bar chart showing the rate of polar body formation. Polar bodies were counted by live imaging in H1-Alexa568-injected oocytes after meiosis completion.

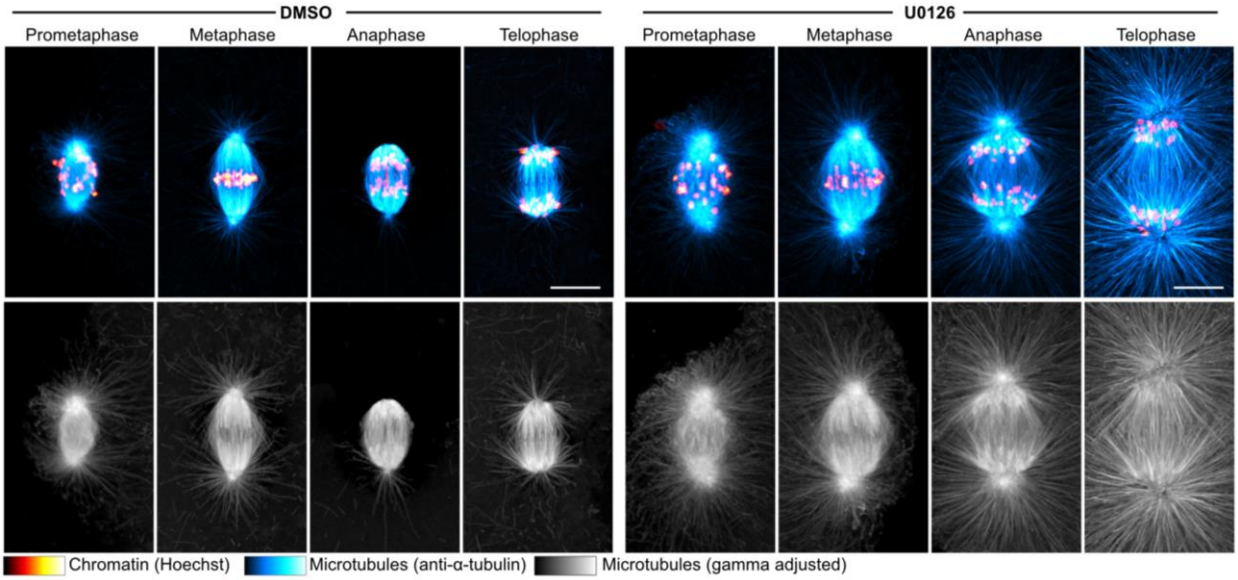

Figure 9. From metaphase onward Mos-MAPK increasingly reduces centrosomal microtubule nucleation, thereby preventing pole separation in anaphase B and the formation of large telophase asters in meiosis.

Immunofluorescence images of oocytes stained for microtubules (anti-tubulin, blue), and chromatin (Hoechst 33342, red). Oocytes were treated with 20 µM U0126 or an equal amount of DMSO, and then fixed at the stages indicated. Imaging was done using spinning disk confocal microscopy. Maximum intensity projections are shown, scale bar is 20 µm. Lower panels show the tubulin channel separately and with adjusted gamma (0.5).

We observed a similar unspecific cytoplasmic localization of downstream Mos-MAPK targets tested, including CPEB and Maskin/TACC3 (Fig. 10B). This was somewhat surprising, as previous studies have demonstrated the localization of both CPEB and Maskin/TACC3 to the meiotic spindle in *Xenopus* oocytes (Albee and Wiese, 2008; Eliscovich et al., 2008). Therefore, as a positive control, we localized the single starfish Aurora kinase mediating the combined functions of vertebrate Aurora A and B (Abe et al., 2010). In mouse and *Xenopus* oocytes TACC3 and Aurora A interact and reciprocally regulate each other's localization (Burgess et al., 2015; So et al., 2019), therefore we wanted to test whether at least Aurora shows a spindle localization. Aurora-mCherry expressed in starfish oocytes from injected mRNA showed the expected localization pattern to kinetochores, centrioles, and spindle microtubules in meiosis I (Fig. 10C). The localization pattern was essentially the same in mitosis, and Aurora localization was not affected by U0126 treatment. These data together indicate that while Aurora localizes to the spindle, Mos-MAPK components and its effectors either do not localize to the spindle or we were unable to detect localization due to technical limitations of the experimental system. Strikingly, the inhibition of Aurora with two different small-molecule inhibitors, VX680 (Doggrell, 2004) and Hesperadin (Hauf et al., 2003) completely abolished spindle assembly in starfish oocytes (Fig. 10D). While this drastic effect of Aurora inhibition is an interesting result on its own, it, unfortunately, precluded us to dissect the possible cross-regulation between TACC3 and Aurora localization.

Taken together, our live cell and immunofluorescence data consistently show that Mos-MAPK specifically downregulates centrosomal microtubule nucleation most prominently in ana- and telophase and thereby critically contributes to minimizing polar body size. If Mos-MAPK is inhibited, astral microtubules push the spindle deeper into the cytoplasm which results in substantially larger polar bodies. Mos-MAPK components do not seem to show direct spindle localization to execute these functions.

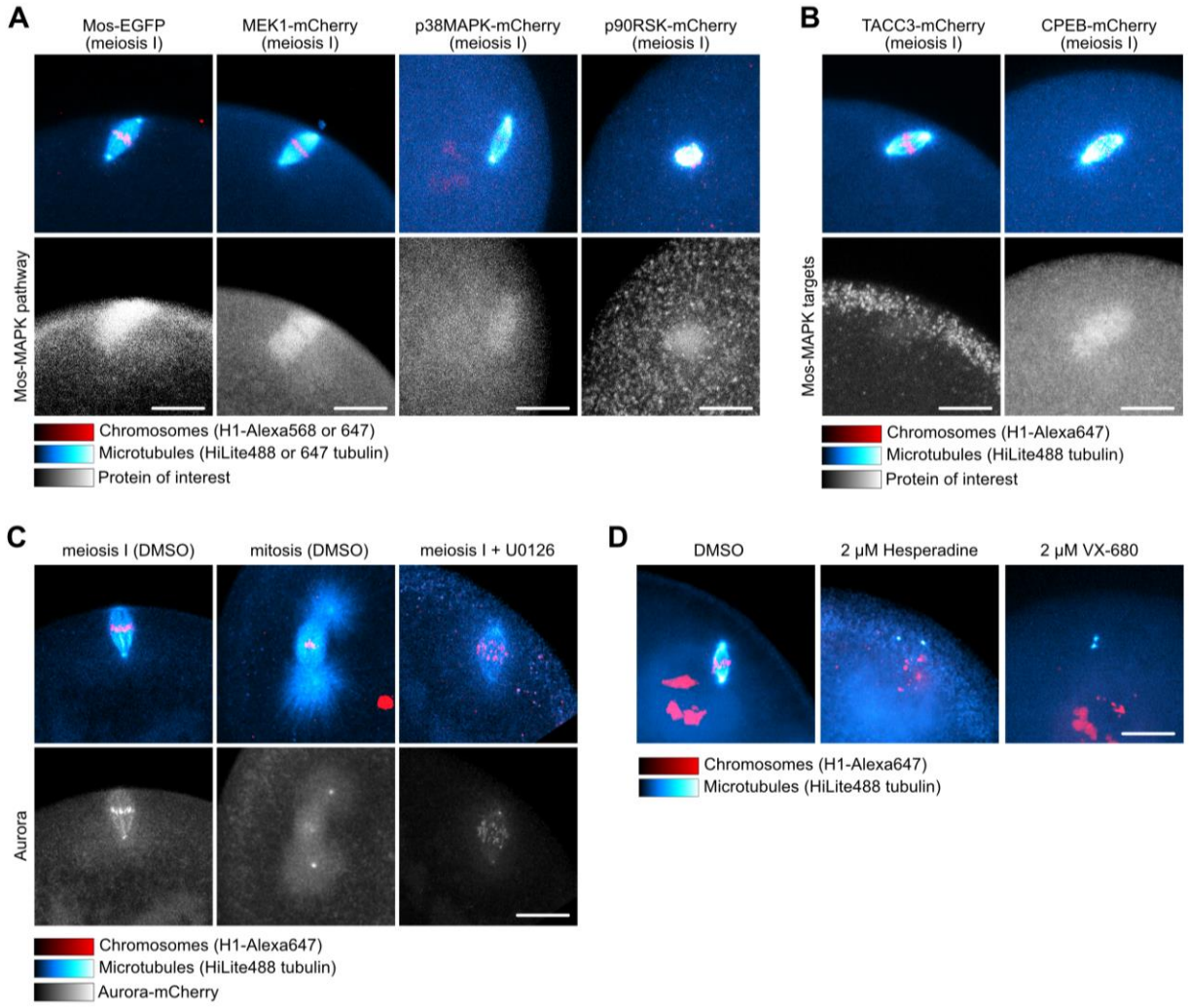

Figure 10. Localization of Mos-MAPK pathway components as well as its downstream targets

(A) Mos-MAPK pathway components display unspecific localization, the bright area results from exclusion of yolk vesicles by the spindle (see text for details). Live oocytes were injected with H1-Alexa647 (red) and HiLyte488-tubulin (blue) to label chromosomes and microtubules, respectively. For Mos-EGFP chromosomes and microtubules were labeled with H1-Alexa568 (red) and HiLyte647-tubulin (blue). Imaging was done by laser scanning confocal microscopy. Maximum intensity projections are shown, scale bars are 20 µm.

(B) CPEB and TACC3 display unspecific localization. Live oocytes were injected with H1-Alexa647 (red) and HiLyte488-tubulin (blue) to label chromosomes and microtubules, respectively. Imaging was done using a laser scanning confocal microscope. Maximum intensity projections are shown, scale bars are 20 µm.

(C) The **s**ingle starfish Aurora is localized at kinetochores and spindle poles in meiosis and mitosis as well as in Mos-MAPK-inhibited meiotic oocytes. Live oocytes were injected with H1-Alexa647 (red) and HiLyte488-tubulin (blue) to label chromosomes and microtubules, respectively. Oocytes were treated with 20 µM U0126 or an equal amount of DMSO. Imaging was done on a laser scanning confocal microscope. The red bright spot in "mitosis DMSO" is an injection artifact. Maximum intensity projections are shown, and scale bars are 20 µm.

(D) Aurora inhibition with Hesperadin and VX-680 results in abortive spindle formation. Live oocytes were injected with H1-Alexa647 (red) and HiLyte488-tubulin (blue) to label chromosomes and microtubules, respectively. Imaging was done on a spinning disk confocal microscope. Oocyte imaged at the same time post-NEBD – 36 min. Maximum intensity projections are shown, scale bars are 20 µm.

Discussion

Mos-MAPK as a critical 'switch' toward the meiotic division program

Activation of the ERK/MAPK pathway by Mos is a conserved feature of meiotic divisions of oocytes across the animal species, controlling a number of key meiotic functions. However, the downstream molecular targets of Mos-MAPK that underlie these functions are mostly unknown. Here, we took advantage of the transparent starfish oocytes available in large numbers to address this question by correlating cellular phenotypes monitored by live-cell microscopy with changes in the phospho-proteome analyzed by mass spectrometry.

First, our live-cell characterization of Mos-MAPK-inhibited oocytes confirmed previous observations in starfish (Tachibana et al., 2000), and identified the metaphase of meiosis I as the critical bifurcation point. Mos-MAPK is activated at this point to mediate the highly asymmetric polar body divisions and triggers the reactivation of Cdk1-Cyclin B to drive the second meiotic division without an intervening S-phase. If Mos-MAPK is inhibited by U0126, the first meiotic division is less asymmetric and oocytes exit after meiosis I and enter interphase, re-form the nucleus, initiate S-phase, and start parthenogenic embryo development.

Phospho-proteomic profiling of Mos-MAPK-inhibited oocytes in metaphase I, on the one hand, showed a clear signature of meiotic exit as compared to controls, again fully consistent with earlier biochemical data (Tachibana et al., 2000). On the other hand, phospho-proteomics clearly identified multiple subunits of conserved molecular modules regulating translation and cytoskeletal regulation.

Mos-MAPK mediates haploidization by triggering Cyclin B translation to drive meiosis II

Firstly, we identified the molecular module regulating the CPE-mediated translation of stored mRNAs. Together, our data strongly support the model, in which Mos-MAPK phosphorylates CPEB leading to the disassembly of the inhibitory complex formed by CPEB, Maskin/TACC3, and eIF4ENIF1. (Of note, while no Maskin/TACC3 phospho-peptides passed the significance threshold, we detected many phospho-peptides below significance (Supplemental file 2). This then leads to the recruitment of the machinery responsible for polyadenylation of the mRNA and subsequent translation initiation. Overall, our hitlist included more than two-thirds of the known subunits of the polyadenylation and translation initiation complexes. Interestingly, our tip hits also included LARP1, a regulator specific to mRNAs with a 5' terminal oligopyrimidine (5'TOP). This motif is known to associate with the mTOR pathway (Berman et al., 2021), and it is intriguing to find that this mechanism may play a role in meiotic regulation.

Translation of which mRNAs may be regulated by Mos-MAPK? A recent phospho-proteomic survey of starfish oocyte meiosis showed that only a very limited number of proteins show a change in protein levels, and there is very little change even when translation is completely inhibited (Swartz et al., 2021). Indeed, there are very few proteins that show changes in protein levels such as CPEB and some of its regulators and, prominently, Cyclin B (Swartz et al., 2021). We further show that prevention of Cyclin B translation by morpholino injection results in a strikingly similar phenotype to Mos-MAPK inhibition causing oocytes to exit meiosis after meiosis I. The same phenotype is observed after translation inhibition by emetine. Together, this strongly supports the model, whereby Mos-MAPK regulates the translation of Cyclin B. This additional Cyclin B translated at the end of meiosis would then drive the reactivation of Cdk1-Cyclin B to drive oocytes into the second meiotic division and prevent entry into the interphase and eventually S-phase.

This model is consistent with findings in several other species. The CPEB inhibitory complex was shown to regulate the translation of Cyclin B and is required for MI-to-MII transition in *Xenopus* oocytes

(Hochegger et al., 2001; Arumugam et al., 2009). Additionally, in recent reports, Mos- MAPK was shown to facilitate Cyclin B translation by stimulating CPEB degradation in mouse oocytes (Cao et al., 2020).

Mos-MAPK facilitates asymmetric division by reducing the size of centrosomal microtubule asters

Another molecular module we identified in our phospho-proteomics experiment is the regulators of the microtubule cytoskeleton. The identified proteins fall into three categories: (i) constituents of the centrosome, in particular the pericentriolar material (PCM), (ii) regulators of microtubule growth localized at the plus-tips of microtubules, and (iii) kinesin motor proteins. While these proteins are not part of single 'machinery' as is the case for translational regulation, they have a common function in organizing centrosomal microtubule arrays. Notably, our hitlist is very specific in that we did not identify any regulators of the other major pathways in spindle organization, such as those that depend directly on chromatin or are activated by chromatin-produced RanGTP (e.g. TPX2, HURP, or NuMA).

The cellular phenotypes we characterized here in detail by high-resolution microscopy, are in excellent agreement with the expected functions of the identified phospho-proteins. Inhibition of Mos-MAPK renders meiosis I spindle more 'mitotic' with larger centrosomal asters and longer astral microtubules. Strikingly, our live and fixed cell data revealed that compared to the relatively mild difference in prometa- and metaphase, Mos-MAPK inhibition has a much more dramatic effect during anaphase and telophase. There is a much larger difference in centrosome size and the length of astral microtubules at these later stages of division. A critical consequence is that while in normal meiosis I chromosomes separate mostly by shortening of the kinetochore fibers (anaphase A), in Mos-MAPK inhibited oocytes anaphase A and anaphase B, the separation of the spindle poles are observed in parallel – as it is typical for mitotic divisions. Intriguingly, our live and fixed cell data reveals a tight correlation between the maximal length of astral microtubules and pole-to-pole distance, suggesting that the two processes may be linked (Fig. 8 and 9). The explanation for this can be that centrosomal microtubules grow in all directions, away from the spindle as astral microtubules, and into the spindle as long interpolar microtubules (Fig. 8 and 9). These interpolar microtubules are essential to form the overlapping microtubule bundles at the spindle midzone that are then pushed apart in anaphase B by the PRC1/kinesin-4 module (Bieling et al., 2010). In normal meiosis, with Mos-MAPK active, these interpolar microtubules are apparently almost completely absent resulting in the division with Anaphase A without separation of spindle poles.

Mos-MAPK thus functions to minimize polar body size in two ways: (i) by reducing aster size it allows the spindle to localize tightly to the cortex; (ii) by preventing anaphase B, it limits the distance between the cortex and the spindle midzone. Thereby Mos-MAPK basically switches off two important mitotic functions: spindle positioning and orientation by astral microtubules, and anaphase B which functions in mitosis to move chromosome masses away from the cleavage furrow (Fig. 11).

We studied here starfish oocytes, which have the unusual feature of retaining centrioles in meiotic divisions (Sluder et al., 1993). This might make the above results somewhat more pronounced in comparison to other species with acentrosomal meiotic spindles. However, it is now clear from studies in multiple species that acentrosomal microtubule organizing centers (aMTOCs) functionally replace centriolar centrosomes, and these structures indeed contain most if not all of the proteins we have identified (Mogessie et al., 2018). Long and extended microtubule asters have indeed been observed upon inhibition of Mos-MAPK in nearly all species investigated so far including *Xenopus*, mouse, and *Clytia* oocytes (Verlhac et al., 1996; Bodart et al., 2005; Amiel et al., 2009). Notably, in previous studies on fixed cells, the focus of observation has automatically been the relatively longer prometaphase and metaphase stages. We however showed that the effect of Mos-MAPK inhibition is most prominent in the later stages of division. Therefore, it will be interesting to investigate these later stages in other species.

Indeed, spindle elongation in anaphase has already been observed in live recordings of Mos knockout oocytes in mice (Verlhac et al., 2000).

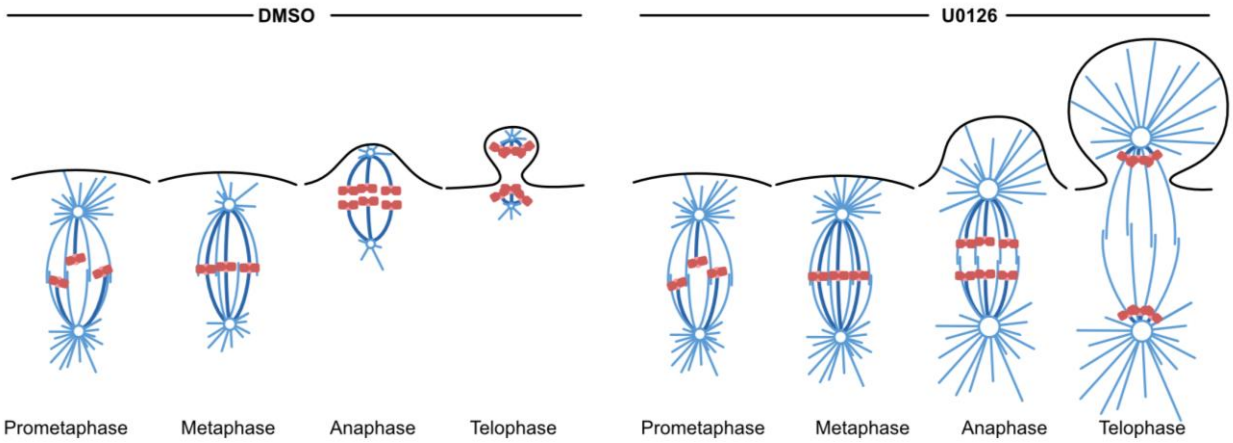

Figure 11. Mos-MAPK downregulates centrosomal microtubule nucleation and prevents anaphase B

Mos-MAPK specifically downregulates pericentriolar material proteins, reduces the growth as well as the amount of astral and interpolar microtubules, and prevents Anaphase B. This allows close attachment of the meiotic spindle to the oocyte cortex in order to complete the division as compactly as possible, resulting in an extremely asymmetric cell division, the extrusion of the polar body.

Materials and Methods

Oocyte collection, drug treatments, and microinjection

Bat stars (*Patiria miniata*) were obtained in the springtime from Southern California (South Coast Bio-Marine LLC, Monterey Abalone Company, or Marinus Scientific Inc). They were kept at 16 ˚C for the rest of the year in seawater aquariums at MPI-NAT's animal facility. Ovaries and testis were isolated as described previously (Wessel et al., 2010) Oocytes were isolated and used immediately or stored for 1-2 days in seawater at 14 ˚C, for some experiments ovaries were stored for 2-3 days in seawater at 14 ˚C and oocytes were isolated thereafter (Wessel et al., 2010).

mRNAs and other fluorescent markers were injected using Kiehart chambers and a horizontally mounted needle as described previously (Jaffe and Terasaki, 2004; Borrego-Pinto et al., 2016b), with the modification that instead of mercury-filled needles, simple back-loaded capillaries were used in combination with a FemtoJet (Eppendorf) injector. mRNA was injected the day before to allow protein expression, whereas fluorescently labeled protein markers were injected just a few hours prior to imaging.

Meiosis was induced by the addition of 1-methyladenine (1-MA, Acros Organics) at 10 μM final concentration. NEBD started typically 20–25 min after 1-MA addition. U0126 (Sigma) was administered together with 1-MA at 20 μM. VX-680 (Sigma) and Hesperidin (Sigma) were added at 20 μM 1h before administration of 1-MA. Emetine (Sigma) was added at 100 μM conc. 30 min before administration of 1-MA. All drugs were dissolved in molecular biology grade DMSO. The same DMSO stock was used for mock treatment in drug experiments. For fertilization, freshly isolated sperm was added prior to the emission of the first polar for the oocyte in Petri dishes at 1:750000 dilution, and for the injected oocytes in Kiehart chambers at 1:20000 dilution. Every experiment was repeated at least three times, with oocytes taken from at least two different animals.

Live imaging

Chromosomes were labeled by either injecting mRNA encoding human H2B-mCherry or H1 protein purified from calf thymus (Sigma) labeled with AlexaFluor 568 or 647 as described previously (Bun et al., 2018). Microtubules were labeled either by injection of HiLyte488- or HiLyte647-tubulin purified from the porcine brain (Cytoskeleton), or recombinant human EB3-mClover protein (a generous gift from So (Nick) Chun, Department of Meiosis, MPI-NAT, Göttingen, Germany). Anti-cyclin B morpholino TAACCAATGCGAGTTCCGAGGAG (Gene Tools), was injected at 500 mM immediately before 1-MA stimulation according to (Swartz et al., 2021).

Active Cdk1-Cyclin B complex was prepared according to (Veld et al., 2021). In order to get rid of the glycerol complex was purified throw a 10K MWCO protein concentrator (Pierce) and dissolved in PBS with 200 mM sucrose. The activity of the complex was confirmed by its ability to cause maturation in starfish oocytes (Kishimoto, 2015). Cdk1-Cyclin B was injected into the U0126-treated oocytes directly after the first polar body extrusion. Dynamics of labeled tubulin-HiLyte488 and H2B-mCherry were observed in U0126-treated and control oocytes in parallel in the same injection chamber.

The mRNA expression vectors with Mos, MEK1, MAPK, RSK, TACC3, CPEB, and Aurora were generated by cloning the cDNA of the respective genes into the pGEMHE backbone with mCherry on C-terminus as described previously (Borrego-Pinto et al., 2016b) with modifications. First, the starfish homologs of the target genes were searched in our house-made starfish transcriptome (more details below). Secondly, cDNA reverse transcription was done by Maxima Reverse Transcriptase kit (Thermo). Thirdly, cloning was done according to the Gibson assembly protocol (Gibson et al., 2010) with a house-made Gibson assembly kit (a generous gift from Dirk Görlich, Department of Cellular Logistics, MPI-NAT,

Göttingen, Germany), and the primer design was done with the SnapGene (Dotmatics). Finally, the cloned pGEMHE vectors were expressed in E. coli and purified with GeneJET Plasmid Midiprep Kit (Thermo). Capped mRNAs with poly-A tail were synthesized from linearized pGEMHE vectors using the HiScribe™ T7 ARCA mRNA Kit (NEB). The mRNA was purified by Monarch RNA Cleanup Kit (NEB). Purified mRNAs were stored at 2-6 µg/µl and prior to injection with Femtojet diluted to 100-500 ng/ µl.

Starfish oocytes were imaged directly in the injection chambers. Live-cell images were acquired either on a Visitron Systems (Puchheim, Germany) spinning disk confocal microscope or on a Zeiss LSM780 (Jena, Germany) laser scanning confocal microscope. The spinning disk system is based on a Nikon Ti2 microscope body and a Yokogawa W1 scanhead complemented by a custom laser unit, homogenizer unit, and electronics unit by Visitron Systems and two Prime BSI cameras (Teledyne Photometrics). For live imaging experiments, a CFI SR Plan Apo IR 60x 1.27 NA water immersion objective was used. On the laser scanning system, we used a C-Apochromat 40 1.20 NA water immersion objective lens. For live-cell imaging experiments, at least 3–5 oocytes were recorded per session. Long imaging throughout meiosis and mitosis was done on a spinning disk system with the following imaging parameters: exposure time 200 ms, pixel size 110 nm, 11-15 z-slices with 3 or 4 µm step size, time intervals 3-5 min. Short imaging of the specific stages of egg development done on a spinning disk system with the following imaging parameters: exposure time 100 ms, pixel size 110 nm, 70 z-slices with 200-300 nm step size, time intervals 3-5 min. On the laser scanning microscope, settings were: imaging area 100 µm × 100 µm, pixel size 200 nm, 15 z-slices with 2 µm step size, pinhole set to 2 AU, time intervals 3-5 min. mClover3 and tubulin-HiLyte488 were excited with a 488 nm laser and detected at 490 - 561 nm. mCherry and Alexa 568 were excited with a 561 nm laser and detected at 561 - 630 nm. Alexa 568 was excited with a 633 nm laser and detected at 633 - 700 nm. Images of the control and experimental groups were acquired under identical imaging conditions on the same microscope.

Images were processed in ImageJ/FIJI (Schindelin et al., 2012), if not stated otherwise the live images underwent mean filtering (intensity set to 2), maximal Z-projection of the imaging volume of 10 µm (Short imaging) and 15 µm (Long imaging) and displayed with automatic contrast adjustments. The maximal length of microtubules is estimated by measuring the distance of aster tips to the centriole both labeled with EB3-mClover in ImageJ/FIJI (Schindelin et al., 2012) in the maximal Z-projected imaging volume of 10 µm. Results were plotted and statistical analyses were performed either by using Excel (Microsoft) or R.

Immunostaining

Oocytes were fixed at the desired times in a PFA/GA fixative (100 mM HEPES [pH 7.0], 50 mM EGTA, 10 mM MgSO4, 0.5% Triton-X100, 400 mM Sucrose, 2% formaldehyde, 0.2% glutaraldehyde) modified from (Strickland et al., 2004). Subsequently, samples were permeabilized and blocked in blocking buffer (PBS+0.1% Triton-X100 plus 3% BSA and the Image-IT reagent (ThermoFisher Scientific). Antibody staining was done for 24 h in a blocking buffer at room temperature with the primary antibody premixed with secondary nanobodies. Microtubules were labeled with Anti-α-Tubulin Mouse mAb (clone DM1A) (Sigma), and lamin was labeled with a custom-made Rabbit polyclonal antibody (Wesolowska et al., 2020) primarily labeled with Alexa 488 NHS ester (Thermo Fisher Scientific) according to manufacturer instructions. Secondary staining was done by anti-mouse secondary nanobodies with Atto-488 (NanoTag) or Donkey Fab Anti-Mouse IgG Ax594 (Jackson). F-actin was labeled with Abberior STAR RED phalloidin (Abberior), and DNA was labeled with the Hoechst 33342 (Thermo Fisher Scientific). Oocytes were mounted with the antifade agent ProLongGlass (Thermo Fisher Scientific) under a coverslip pressed quite firmly onto tiny pillars of grease or double-sided tape (Scotch).

Fixed oocytes were imaged on the same microscope systems as used for live imaging with modifications. The imaging settings were an exposure time of 200 ms, pixel size of 110 nm, and 70 z-slices with 200 or 600 nm step size. On the laser scanning system, we used a Zeiss LSM880 AiryScan microscope using a C-Apochromat 40 x 1.20 NA water immersion objective lens. On the laser scanning microscope, settings were: imaging area 100 µm × 100 µm, pixel size 40 nm, 80 z-slices with 200 nm step size, pinhole set to 1AU. Fluorophore excitation and detection were done the same as for live imaging. Images of the control and experimental groups were acquired under identical imaging conditions on the same microscope.

Quantification of half-spindle length, spindle width, and diameter of centrosomal areas was done in Imaris (Oxford instruments) in 3D volume. Images were processed and deconvolved using the Huygens software (Scientific Volume Imaging) with either confocal, AiryScan, or spinning disk settings as appropriate. Non-deconvolved images were processed in ImageJ/FIJI (Schindelin et al., 2012), images underwent mean filtering (intensity set to 1), maximal Z-projection of the imaging volume of 10 µm and displayed with automatic contrast adjustments. Gamma adjustments were done in Imaris (Oxford instruments).

Sample preparation for mass spectrometry

We collected three biological replicates of starfish oocytes at the metaphase I stage, by treating oocytes with 1MA. The synchronicity of oocytes was confirmed by staining a small portion of the collected oocytes with Hoechst 33342. For the samples used for further analysis, we observed a metaphase plate in 92-96% of the oocytes by confocal microscopy. 20 µl of starfish oocytes lysed on ice in SDS lysis buffer (4% [w/v] SDS, 150 mM Hepes-KOH pH 7.0, 2 mM DTT, 10 mM EDTA, 250 mM sucrose), buffer contained Complete Roche inhibitors Mini (Roche) that diluted according to manufacturer instructions. The mechanical cell disruption was done by centrifuging the oocyte suspension through 40 µm plastic mesh at 7000 g. Samples were diluted to a final 0.1% SDS and 1 mM MgCl2 was added. Proteins were reduced with 5 mM dithiothreitol (DTT) for 30 min at 37°C, 300 rpm, and alkylated with 10 mM iodoacetamide (IAA) for 30 min at 25°C, 300 rpm, in the dark. The reaction was quenched with 10 mM DTT for 5 min at 25°C, 300 rpm.

Sample cleanup was performed by applying a single-pot, solid-phase-enhanced sample preparation protocol by (Hughes et al., 2019). Briefly, carboxylate-modified magnetic beads (Cytiva; 65152105050350, 45152105050250, mixed 1:1) were added at a 1:10 protein-to-bead mass ratio and an equal volume of 100% [v/v] acetonitrile (ACN) was added. Beads were washed twice with 80% [v/v] EtOH and once with 100% [v/v] ACN. Proteins were digested in 50 mM TEAB containing trypsin (Promega, V5111) at a 1:20 enzyme-to-protein ratio ON at 37 °C, 1000 rpm. Peptides were removed from the magnetic beads and aliquots were taken for whole proteome analysis. Residual samples were subjected to phosphopeptide enrichment according to the EasyPhos protocol (Humphrey et al., 2015). Briefly, peptide mixtures were adjusted to final 228 mM KCl, 3.9 mM KH_2PO_4, 38% [v/v] ACN, 4.5% [v/v] trifluoroacetic acid (TFA), mixed and cleared by centrifugation. TiO_2 beads (GL Sciences, 5010-21315, 10 µm) in 80% ACN, 6% TFA were added at a beads-to-protein ratio of 10:1. Peptides were incubated with beads for 20 min at 40°C, 1000 rpm. Beads were resuspended and washed in 60% [v/v] ACN, 1% [v/v] TFA four times. Finally, beads were resuspended in 80% [v/v] ACN, 0.5% [v/v] acetic acid and transferred to empty columns (Harvard Apparatus, 74-3840). Phosphopeptides were eluted in two steps with 40% [v/v] ACN, 15% [v/v] NH_4OH. TMTsixplex™ (Thermo Scientific, 90061) labelling was performed according to manufacturers instructions. Whole proteome and phosphopeptide-enriched samples were labelled separately and combined in separate samples. Both were further cleaned using C18 MicroSpin columns (Harvard Apparatus, 74-4601) according to manufacturer's instructions. Samples were dissolved in 10 mM NH_4OH pH 10, 5% [v/v] ACN and peptides were loaded onto an

Xbridge C18 column (Waters, 186003128) using an Agilent 1100 series chromatography system. The column was operated at a flow rate of 60 µl/min with a buffer system of buffer A, 10 mM NH_4OH pH 10; and buffer B, 10 mM NH_4OH pH10, 80% [v/v] ACN. The column was equilibrated with 5% B and separation was performed over 64 min using the following gradient: 5% B (0-7 min), 8-30% B (8-42 min), 30-50% B (43-50 min), 90-95% B (51-56 min), 5% B (57-64 min). For phosphopeptides, the first 6 min were collected as flow-through (FT), followed by 48 x 1 min fractions, which were reduced to 23 fractions by concatenated pooling. The remaining fractions were discarded. For the whole proteome sample, 54 x 1 min fractions were collected and combined to 19 final fractions. The remaining fractions were discarded. Fractionated whole proteome and phosphopeptide samples were dried in a speed vac concentrator and subjected to LC-MS/MS analysis.

LC-MS/MS analysis

Whole proteome and phosphopeptide samples were dissolved in 2% [v/v] ACN 0.1% [v/v] TFA and injected onto a C18 PepMap100-trapping column (0.3 x 5 mm, 5 µm, Thermo Scientific) connected to an in-house packed C18 analytical column (75 µm x 300 mm; Reprosil-Pur 120C18-AQ, 1.9 µm, Dr Maisch GmbH). Columns were equilibrated using 8% buffer A (0.1% [v/v] formic acid (FA)), 2% buffer B (80% [v/v] ACN, 0.1% [v/v] FA) (phosphopeptides), or 95% buffer A, 5% buffer B (whole proteome peptides). Liquid chromatography was performed using an UltiMate-3000 RSLC nanosystem (Thermo Scientific). Phosphopeptides were analysed for 88 min using a linear gradient (10% to 30% buffer B (80% [v/v] ACN, 0.1% [v/v] FA in 60 min) followed by a linear increase to 40% buffer B over 10 min and a 5 min washing step at 90% of buffer B. Whole proteome peptides were analysed for 88 min, and a buffer B gradient of 10% to 45% over 60 min was applied followed by a linear increase to 60% buffer B over 10 min and washing at 90% buffer B for 5 min. Eluting peptides were analysed on an Orbitrap Exploris 480 instrument (Thermo Scientific). For the analysis of phosphopeptides, the following MS settings were used: MS1 scan range, 350–1600 *m/z*; MS1 resolution, 120,000 FWHM; AGC target MS1, 3E6; maximum injection time MS1, 50 ms; isolation window, 1.6 *m/z*; collision energy, 34%; charge states, 2+ to 6+; dynamic exclusion, 25 s; MS2 resolution, 30,000, AGC target MS2, 1e5; maximum injection time MS2, 64 ms. For the analysis of whole proteome peptides, the following MS settings were used: MS1 scan range, 350–1600 *m/z*; MS1 resolution, 60,000 FWHM; AGC target MS1, 3E6; maximum injection time MS1, 50 ms; isolation window, 0.8 *m/z*; collision energy, 34%; charge states, 2+ to 6+; dynamic exclusion, 25 s; MS2 resolution, 15,000, AGC target MS2, 5e4; maximum injection time MS2, 54 ms.

Reference proteome annotation

Two available different sources of genomic information were integrated together: Echinobase v2 (echinobase.org) (Kudtarkar and Cameron, 2017)and NCBI annotation (RefSeq ID 23626818) for Patiria Miniata. First, protein sequencers from both sources clustered together to identify representative sequences using mmseqs2 [Linclust] easy-clust workflow with a sequence similarity threshold of 0.95 (-c flag).

Transcript sequences for Echinobase v2 were derived from the genome sequence and transcriptome annotation in gff format with gffread [gffread] software with -M and -K flags in order to discard duplicated transcripts and transcripts fully contained in other longer sequences.

Transcript sequences were extracted extract the from both transcriptomes that correspond to proteins marked as representative sequences by mmseqs2 using a custom R script.

A set of protein-coding transcripts with reduced redundancy was annotated via TRAPID web interface [TRAPID] using EggNOG 4.5.1 database (Bucchini et al., 2021). KEGG ontology gene names were used as a main annotation; in case of their absence NCBI names were used, and in when neither of the above was available – Echinobase v2 identifiers were kept. Gene ontology and KEGG ontology identifiers

were downloaded and formatted into a GMT format file to be used as functional annotation sets for over-representation analysis.

Differential protein expression analysis

MS raw files were processed using MaxQuant version 1.6.17.0 (Cox and Mann, 2008) with default settings except for: fixed modification, carbamidomethylation (C); variable modifications, oxidation (M), acetylation (N-term), phosphorylation (S,T,Y) (only for phosphopeptide data); enzyme, trypsin/P digestion. MS2 (TMTsixplex™) was selected as quantification type.

A "proteinGroups" table with corrected reporter ion intensities from MaxQuant was used for differential expression. After removing contaminants and decoys, proteins with Q-value of detection <= 0.01 and with at least 1 unique peptide were kept for further analysis. We made a choice of requiring only 1 unique peptide in order to evaluate the differential expression of MOS kinase, that would had been filtered out otherwise.

Reporter ion intensities were log2-transformed and linear models were fit using least squares method from limma R library (Ritchie et al., 2015). P-valiues were estimated with empirical Bayes method and multiple hypothesis testing correction was done with Benjamini and Hochberg method [padj BH]. A significance cutoff of 0.05 adjusted p-value was used.

Differential phospho-proteomics analysis

MaxQuant output tables were filtered to remove decoys and contaminants. All peptides with posterior error probability (PEP) <= 0.01 were kept. Protein groups did not undergo additional filtering by Q-value or number of unique peptides, in order to preserve the most proteins possible for downstream normalization of phospho-peptide intensities. Missing values in corrected TMT reporter intensities of all total protein in "proteinGroups" table were imputed conservatively, with minimal reporter intensity per channel.

Ratios of phospho-peptide intensities from "modificationSpecificPeptides" table to the corrected intensities of their parent proteins were log2-transformed and used for subsequent differential expression with limma [limma]. Overall, 76% of phospho-peptides had a corresponding total protein intensity necessary for normalization. A linear model testing for the difference between means of phospho-peptide ratios in treatment and control groups were fit with least-square approach and p-values were estimated with empirical Bayes approach. Multiple hypothesis correction was done with Benjamini and Hochberg for false discovery rate (FDR) estimation [padj_BH]. In addition, q-values were used to inform the significance cutoff choice [qvalue] which was set to adjusted p-value (BH) of 0.07.

Functional enrichment of differential phosphorylation analysis

Gene list functional enrichment was performed using g:Profiler tool g:GOSt [g:Profiler]. Three sets of gene names corresponding to up-regulated, down-regulated and all significant hits were enriched using a default "g_SCS" correction method and a significance threshold of 0.05. A functional annotation from TRAPID was uploaded to the web-server of g:Profiler and used as an organism specific reference (organism "gp__EGla_34PO_4UY").

Heatmap of differential phosphorylation

Normalized ratios of significantly up- and down- regulated phospho-peptides were scaled to the mean of 0 and standard deviation of 1. In order to cluster the results by magnitude of differential expression and functional annotation, each peptide was checked for originating from a protein belonging to the following functional terms: "cytoskeleton", "microtubule cytoskeleton", "spindle", "cell cycle", "regulation of protein kinase activity", "dephosphorylation" and a matrix with binary indicators (1 for match, 0 for mismatch) was bound to columns to the scaled phospho-peptide intensity matrix. Euclidean distance between peptides in this matrix underwent hierarchical clustering with "ward.D2" method (Murtagh and Legendre, 2014). to minimize the squared variance within clusters. Heatmap was plotted

using “pheatmap”[pheatmap] R package with default settings and row order from the abovementioned clustering.

Prediction of effector human kinases

MaxQuant "evidence" table was used to extract the `Phospho (STY) Probabilities` for each peptide-spectrum match (PSM). A mean probability per amino acid across all PSMs with the same peptide sequence was computed and the maximal value per peptide sequence was used to estimate the most likely position of phosphorylation. All the peptides tested for differential expression, including insignificant hits were converted to the asterisk format, where the phosphorylated amino acid is marked with an asterisk (*) after the phospho-acceptor (S, T, Y). Peptide sequences, log-fold changes and p.values of differential expression were submitted for kinase prediction at phosphosite.org (Hornbeck et al., 2015) kinaseLibraryAction functional enrichment analysis based on differential expression. P-value threshold of 0.05 was used to discriminate between foreground and the background sets.

Acknowledgements

We thank all members of the Lenart laboratory at MPI-NAT for protocols, reagents and support, in particular Jasmin Jakobi and Antonio Politi. We thank MPI-NAT’s Animal Facility, specifically Sascha Krause and Ulrike Teichmann. We would like to thank So (Nick) Chun and Melina Schuh for providing the recombinant EB3-mClover3 protein, Pim J Huis In't Veld and Andrea Musacchio for Cdk1-Cyclin B complex and Dirk Goerlich for Gibson assembly kit. I.A. is member and has been partially funded by the IMPRS Molecular Biology Programme. The laboratory is funded by the Max Planck Society.

Competing interests

The authors declare no competing financial interests.

References

Abe, Y. et al. (2010). A single starfish Aurora kinase performs the combined functions of Aurora-A and Aurora-B in human cells. J Cell Sci *123*, 3978–3988.

Albee, A.J., and Wiese, C. (2008). Xenopus TACC3/Maskin Is Not Required for Microtubule Stability but Is Required for Anchoring Microtubules at the Centrosome. Mol Biol Cell *19*, 3347–3356.

Amiel, A. et al. (2009). Conserved Functions for Mos in Eumetazoan Oocyte Maturation Revealed by Studies in a Cnidarian. Curr Biology Cb *19*, 305--311.

Araki, K. et al. (1996). Meiotic Abnormalities of c-mos Knockout Mouse Oocytes: Activation after First Meiosis or Entrance into Third Meiotic Metaphase. Biol Reprod *55*, 1315–1324.

Arumugam, K. et al. (2009). Enforcing temporal control of maternal mRNA translation during oocyte cell-cycle progression. Embo J *29*, 387–397.

Bendre, S. et al. (2016). GTSE1 tunes microtubule stability for chromosome alignment and segregation by inhibiting the microtubule depolymerase MCAK. J Cell Biol *215*, 631–647.

Berman, A.J. et al. (2021). Controversies around the function of LARP1. Rna Biol *18*, 207–217.

Bieling, P. et al. (2010). A Minimal Midzone Protein Module Controls Formation and Length of Antiparallel Microtubule Overlaps. Cell *142*, 420–432.

Bodart, J.-F.L. et al. (2002). Characterization of MPF and MAPK Activities during Meiotic Maturation of Xenopus tropicalis Oocytes. Dev Biol *245*, 348–361.

Bodart, J.-F.L. et al. (2005). Differential roles of p39Mos–Xp42Mpk1 cascade proteins on Raf1 phosphorylation and spindle morphogenesis in Xenopus oocytes. Dev Biol *283*, 373–383.

Borrego-Pinto, J. et al. (2016a). Distinct mechanisms eliminate mother and daughter centrioles in meiosis of starfish oocytesCentriole elimination in starfish oocytes. J Cell Biology *212*, 815–827.

Borrego-Pinto, J. et al. (2016b). Oogenesis, Methods and Protocols. Methods Mol Biology *1457*, 145–166.

Bourdais, A. et al. (2022). MRCK controls myosin II activation in the polarized cortex of mouse oocytes and promotes spindle rotation and male pronucleus centration. Biorxiv 2022.09.25.509421.

Bucchini, F. et al. (2021). TRAPID 2.0: a web application for taxonomic and functional analysis of de novo transcriptomes. Nucleic Acids Res *49*, gkab565-.

Bun, P. et al. (2018). A disassembly-driven mechanism explains F-actin-mediated chromosome transport in starfish oocytes. Elife *7*, e31469.

Burdyniuk, M. et al. (2018). F-Actin nucleated on chromosomes coordinates their capture by microtubules in oocyte meiosis. J Cell Biol *217*, 2661–2674.

Burgess, S.G. et al. (2015). Aurora-A-Dependent Control of TACC3 Influences the Rate of Mitotic Spindle Assembly. Plos Genet *11*, e1005345.

Cao, L.-R. et al. (2020). Positive Feedback Stimulation of Ccnb1 and Mos mRNA Translation by MAPK Cascade During Mouse Oocyte Maturation. Frontiers Cell Dev Biology *8*, 609430.

Choi, T. et al. (1996). Mos/mitogen-activated protein kinase can induce early meiotic phenotypes in the absence of maturation-promoting factor: a novel system for analyzing spindle formation during meiosis I. Proc National Acad Sci *93*, 4730–4735.

Colledge, W.H. et al. (1994). Disruption of c-mos causes parthenogenetic development of unfertilized mouse eggs. Nature *370*, 65--68.

Conduit, P.T. et al. (2015). Centrosome function and assembly in animal cells. Nat Rev Mol Cell Bio *16*, 611–624.

Cox, J., and Mann, M. (2008). MaxQuant enables high peptide identification rates, individualized p.p.b.-range mass accuracies and proteome-wide protein quantification. Nat Biotechnol *26*, 1367–1372.

Doggrell, S.A. (2004). Dawn of Aurora kinase inhibitors as anticancer drugs. Expert Opin Inv Drug *13*, 1199–1201.

Dumollard, R. et al. (2017). Ascidians: An Emerging Marine Model for Drug Discovery and Screening. Curr Top Med Chem *17*, 2056–2066.

Dumont, J. et al. (2005). p90Rsk is not involved in cytostatic factor arrest in mouse oocytes. J Cell Biology *169*, 227–231.

Dupré, A. et al. (2011). Mos in the Oocyte: How to Use MAPK Independently of Growth Factors and Transcription to Control Meiotic Divisions. J Signal Transduct *2011*, 350412.

Eliscovich, C. et al. (2008). Spindle-localized CPE-mediated translation controls meiotic chromosome segregation. Nat Cell Biol *10*, 858–865.

Favata, M.F. et al. (1998). Identification of a Novel Inhibitor of Mitogen-activated Protein Kinase Kinase*. J Biol Chem *273*, 18623–18632.

Fukasawa, K., and Woude, G.F.V. (1995). Mos overexpression in Swiss 3T3 cells induces meiotic-like alterations of the mitotic spindle. Proc National Acad Sci *92*, 3430–3434.

Gibson, D.G. et al. (2010). Chemical synthesis of the mouse mitochondrial genome. Nat Methods *7*, 901–903.

Gruneberg, U. et al. (2006). KIF14 and citron kinase act together to promote efficient cytokinesis. J Cell Biology *172*, 363–372.

Haccard, O., and Jessus, C. (2006). Redundant pathways for Cdc2 activation in Xenopus oocyte: either cyclin B or Mos synthesis. Embo Rep *7*, 321–325.

Halet, G., and Carroll, J. (2007). Rac Activity Is Polarized and Regulates Meiotic Spindle Stability and Anchoring in Mammalian Oocytes. Dev Cell *12*, 309–317.

Hara, M. et al. (2012). Greatwall kinase and cyclin B-Cdk1 are both critical constituents of M-phase-promoting factor. Nat Commun *3*, 1059.

Hashimoto, N. et al. (1994). Parthenogenetic activation of oocytes in c-mos-deficient mice. Nature *370*, 68--71.

Hauf, S. et al. (2003). The small molecule Hesperadin reveals a role for Aurora B in correcting kinetochore–microtubule attachment and in maintaining the spindle assembly checkpoint. J Cell Biology *161*, 281–294.

Hochegger, H. et al. (2001). New B-type cyclin synthesis is required between meiosis I and II during Xenopus oocyte maturation. Development *128*, 3795–3807.

Hornbeck, P.V. et al. (2015). PhosphoSitePlus, 2014: mutations, PTMs and recalibrations. Nucleic Acids Res *43*, D512–D520.

Hughes, C.S. et al. (2019). Single-pot, solid-phase-enhanced sample preparation for proteomics experiments. Nat Protoc *14*, 68–85.

Humphrey, S.J. et al. (2015). High-throughput phosphoproteomics reveals in vivo insulin signaling dynamics. Nat Biotechnol *33*, 990–995.

Ikeda, M. et al. (2012). Furry Protein Promotes Aurora A-mediated Polo-like Kinase 1 Activation*. J Biol Chem *287*, 27670–27681.

Ivanovska, I. et al. (2004). The Drosophila MOS Ortholog Is Not Essential for Meiosis. Curr Biol *14*, 75–80.

Iwabuchi, M. et al. (2000). Residual Cdc2 activity remaining at meiosis I exit is essential for meiotic M–M transition in Xenopus oocyte extracts. Embo J *19*, 4513–4523.

Jaffe, L.A., and Terasaki, M. (2004). Quantitative Microinjection of Oocytes, Eggs, and Embryos. Methods Cell Biol *74*, 219–242.

Jessus, C. et al. (2020). Managing the Oocyte Meiotic Arrest—Lessons from Frogs and Jellyfish. Cells *9*, 1150.

Johnson, J.L. et al. (2023). An atlas of substrate specificities for the human serine/threonine kinome. Nature *613*, 759–766.

Kishimoto, T. (2015). Entry into mitosis: a solution to the decades-long enigma of MPF. Chromosoma *124*, 417–428.

Kudtarkar, P., and Cameron, R.A. (2017). Echinobase: an expanding resource for echinoderm genomic information. Database J Biological Databases Curation *2017*, bax074.

Lefebvre, C. et al. (2002). Meiotic spindle stability depends on MAPK-interacting and spindle-stabilizing protein (MISS), a new MAPK substrate. J Cell Biology *157*, 603–613.

Liu, J. et al. (2013). Protein Phosphatase PPM1G Regulates Protein Translation and Cell Growth by Dephosphorylating 4E Binding Protein 1 (4E-BP1)*. J Biol Chem *288*, 23225–23233.

Mendez, R., and Richter, J.D. (2001). Translational control by CPEB: a means to the end. Nat Rev Mol Cell Bio *2*, 521–529.

Minshall, N. et al. (2007). CPEB Interacts with an Ovary-specific eIF4E and 4E-T in Early Xenopus Oocytes*. J Biol Chem *282*, 37389–37401.

Mogessie, B. et al. (2018). Assembly and Positioning of the Oocyte Meiotic Spindle. Annu Rev Cell Dev Bi *34*, 381–403.

Mori, M. et al. (2006). p90Rsk is required for G1 phase arrest in unfertilized starfish eggs. Development *133*, 1823--1830.

Murtagh, F., and Legendre, P. (2014). Ward's Hierarchical Agglomerative Clustering Method: Which Algorithms Implement Ward's Criterion? J Classif *31*, 274–295.

Oskarsson, M. et al. (1980). Properties of a Normal Mouse Cell DNA Sequence (sarc) Homologous to the src Sequence of Moloney Sarcoma Virus. Science *207*, 1222–1224.

Otsuki, J. et al. (2012). Symmetrical division of mouse oocytes during meiotic maturation can lead to the development of twin embryos that amalgamate to form a chimeric hermaphrodite. Hum Reprod *27*, 380–387.

Pal, D. et al. (2020). Rac and Arp2/3-Nucleated Actin Networks Antagonize Rho During Mitotic and Meiotic Cleavages. Frontiers Cell Dev Biology *8*, 591141.

Phillips, K.P. et al. (2002). Inhibition of MEK or cdc2 Kinase Parthenogenetically Activates Mouse Eggs and Yields the Same Phenotypes as Mos−/− Parthenogenotes. Dev Biol *247*, 210–223.

Ritchie, M.E. et al. (2015). limma powers differential expression analyses for RNA-sequencing and microarray studies. Nucleic Acids Res *43*, e47–e47.

Sagata, N. et al. (1988). Function of c-mos proto-oncogene product in meiotic maturation in Xenopus oocytes. Nature *335*, 519–525.

Samwer, M. et al. (2013). The nuclear F-actin interactome of Xenopus oocytes reveals an actin-bundling kinesin that is essential for meiotic cytokinesis. Embo J *32*, 1886–1902.

Schindelin, J. et al. (2012). Fiji: an open-source platform for biological-image analysis. Nat Methods *9*, 676–682.

Sensui, N. et al. (2012). Role of Mos/MEK/ERK cascade and Cdk1 in Ca2+ oscillations in fertilized ascidian eggs. Dev Biol *367*, 208–215.

Severson, A.F. et al. (2016). Chapter Five Oocyte Meiotic Spindle Assembly and Function. Curr Top Dev Biol *116*, 65–98.

Shakya, A. et al. (2020). Liquid-Liquid Phase Separation of Histone Proteins in Cells: Role in Chromatin Organization. Biophys J *118*, 753–764.

Slep, K.C., and Vale, R.D. (2007). Structural Basis of Microtubule Plus End Tracking by XMAP215, CLIP-170, and EB1. Mol Cell *27*, 976–991.

Sluder, G. et al. (1993). Centrosome Inheritance in Starfish Zygotes II: Selective Suppression of the Maternal Centrosome during Meiosis. Dev Biol *155*, 58–67.

So, C. et al. (2019). A liquid-like spindle domain promotes acentrosomal spindle assembly in mammalian oocytes. Science *364*, eaat9557.

Strickland, L. et al. (2004). Light Microscopy of Echinoderm Embryos. Methods Cell Biol *74*, 371–409.

Swartz, S.Z. et al. (2021). Selective dephosphorylation by PP2A-B55 directs the meiosis I - meiosis II transition in oocytes. Elife *10*, e70588.

Tachibana, K. et al. (2000). c-Mos forces the mitotic cell cycle to undergo meiosis II to produce haploid gametes. Proc National Acad Sci *97*, 14301--14306.

Terasaki, M. (2006). Quantification of fluorescence in thick specimens, with an application to cyclin B—GFP expression in starfish oocytes. Biol Cell *98*, 245–252.

Terret, M.E. et al. (2003). DOC1R: a MAP kinase substrate that control microtubule organization of metaphase II mouse oocytes. Development *130*, 5169–5177.

Ucar, H. et al. (2013). The Mos–MAPK pathway regulates Diaphanous-related formin activity to drive cleavage furrow closure during polar body extrusion in starfish oocytes. J Cell Sci *126*, 5153--5165.

Veld, P.J.H. in 't et al. (2021). Reconstitution and use of highly active human CDK1:Cyclin-B:CKS1 complexes. Protein Sci.

Verlhac, M.H. et al. (1996). Mos is required for MAP kinase activation and is involved in microtubule organization during meiotic maturation in the mouse. Development *122*, 815–822.

Verlhac, M.-H. et al. (2000). Asymmetric division in mouse oocytes: with or without Mos. Curr Biol *10*, 1303–1306.

Wesolowska, N. et al. (2020). Actin assembly ruptures the nuclear envelope by prying the lamina away from nuclear pores and nuclear membranes in starfish oocytes. Elife *9*, e49774.

Wessel, G.M. et al. (2010). Use of Sea Stars to Study Basic Reproductive Processes. Syst Biol Reprod Mec *56*, 236–245.

Wu, J.Q., and Kornbluth, S. (2008). Across the meiotic divide – CSF activity in the post-Emi2/XErp1 era. J Cell Sci *121*, 3509–3514.

Chapter 3. Actin assembly ruptures the nuclear envelope by prying the lamina away from nuclear pores and nuclear membranes in starfish oocytes

Published online in eLife 2020;9:e49774. DOI: https://doi.org/10.7554/eLife.49774

eLIFE elifesciences.org

RESEARCH ARTICLE

Actin assembly ruptures the nuclear envelope by prying the lamina away from nuclear pores and nuclear membranes in starfish oocytes

Natalia Wesolowska[1], Ivan Avilov[2], Pedro Machado[3†], Celina Geiss[1], Hiroshi Kondo[1‡], Masashi Mori[1§], Peter Lenart[1,2]*

[1]Cell Biology and Biophysics Unit, European Molecular Biology Laboratory (EMBL), Heidelberg, Germany; [2]Max Planck Institute for Biophysical Chemistry, Göttingen, Germany; [3]Electron Microscopy Core Facility, European Molecular Biology Laboratory (EMBL), Heidelberg, Germany

Abstract The nucleus of oocytes (germinal vesicle) is unusually large and its nuclear envelope (NE) is densely packed with nuclear pore complexes (NPCs) that are stockpiled for embryonic development. We showed that breakdown of this specialized NE is mediated by an Arp2/3-nucleated F-actin 'shell' in starfish oocytes, in contrast to microtubule-driven tearing in mammalian fibroblasts. Here, we address the mechanism of F-actin-driven NE rupture by correlated live-cell, super-resolution and electron microscopy. We show that actin is nucleated within the lamina, sprouting filopodia-like spikes towards the nuclear membranes. These F-actin spikes protrude pore-free nuclear membranes, whereas the adjoining stretches of membrane accumulate NPCs that are associated with the still-intact lamina. Packed NPCs sort into a distinct membrane network, while breaks appear in ER-like, pore-free regions. We reveal a new function for actin-mediated membrane shaping in nuclear rupture that is likely to have implications in other contexts, such as nuclear rupture observed in cancer cells.

***For correspondence:** plenart@mpibpc.mpg.de

Present address: †Centre for Ultrastructural Imaging, King's College London, London, United Kingdom; ‡The Francis Crick Institute, London, United Kingdom; §RIKEN Center for Developmental Biology, Kobe, Japan

Competing interests: The authors declare that no competing interests exist.

Funding: See page 18

Received: 28 June 2019
Accepted: 24 January 2020
Published: 28 January 2020

Reviewing editor: R Dyche Mullins, University of California, San Francisco, United States

Introduction

The nuclear envelope (NE), composed of inner and outer nuclear membranes, is a specialized sub-compartment of the endoplasmic reticulum (ER) that separates the nucleus and the cytoplasm in eukaryotic cells. The inner and outer NE is fused at nuclear pore complexes (NPCs) to mediate nucleo-cytoplasmic transport. This complex NE membrane structure is mechanically supported by a network of intermediate filaments, the lamina, which lines the nucleoplasmic side (***Burke and Ellenberg, 2002***).

Across species and cell types a considerable diversity of nuclear structure allows adaptation to physiological function. For example, the composition of the lamina is adapted to provide the high mechanical stability that is necessary in muscle cells, or sufficient flexibility in immune cells, which need to squeeze through confined spaces (***Thiam et al., 2016***). Oocytes have a very specialized nuclear architecture with an exceptionally large nucleus, also known as the germinal vesicle, which stores nuclear components that are necessary to support early embryonic development. The oocyte NE is densely packed with NPCs that serve as a stockpile of these complexes (rendering oocytes a popular model in which to study NPCs), and the lamina is thick so that it is able to provide mechanical support for this very large structure (***Goldberg and Allen, 1995***).

The NE must be dismantled at the onset of every cell division to give microtubules access to chromosomes, and then reassembled at the end of division once the chromosomes are segregated.

Depending on the species and nuclear architecture, there is a broad diversity in disassembly mechanisms. In *Drosophila* and *Caenorhabditis elegans* embryos, the NE and the lamina remains partially intact during cell division, whereas in vertebrates and deuterostomes (including the echinoderm starfish), the complex NE structure is fully disassembled during division. In somatic mammalian cells, NE disassembly involves the complete dismantling of the NPCs, depolymerization of the lamina, and reabsorption of the nuclear membranes into the ER (**Hetzer, 2010**; **Ungricht and Kutay, 2017**).

In all species in which nuclear envelope breakdown (NEBD) has been investigated in detail, including somatic cells and oocytes from various species, NEBD begins with a partial permeabilization of the NE resulting from phosphorylation-driven disassembly of the NPCs and other NE components (**Dultz et al., 2008**; **Mühlhäusser and Kutay, 2007**; **Terasaki et al., 2001**; **Lénárt et al., 2003**; **Martino et al., 2017**; **Linder et al., 2017**). This allows proteins, and smaller dextrans up to ~70 kDa, to leak in or out of the nucleus (**Lénárt et al., 2003**). Furthermore, it is likely that the mechanical properties of the NE are affected, that is the NE is weakened and destabilized as a result of the phosphorylation of lamins and lamina-associated proteins (**Ungricht and Kutay, 2017**). Importantly, however, during this first phase of NEBD, the overall structure of the NE (as observed by electron microscopy (EM)) is still intact and the compartmentalization of large protein complexes (e.g. ribosomes and microtubules) is maintained (**Terasaki et al., 2001**; **Lénárt et al., 2003**).

In all of the species and cell types investigated to date, the slow, phosphorylation-driven weakening of the NE is followed by a sudden rupture of the NE leading to rapid and complete mixing of cyto- and nucleoplasm. As this dramatic change is easily visible, even by transmitted light microscopy, this second step is commonly identified as 'NEBD,' marking the transition between the prophase and the prometaphase of cell division. Observations from several cell types suggest that this sudden rupture requires mechanical force generated by the cytoskeleton. In cultured mammalian cells, microtubules tear the NE in a dynein-dependent process (**Beaudouin et al., 2002**; **Salina et al., 2002**). By contrast, we have shown recently that in the large oocyte nucleus, the actin cytoskeleton rather than the microtubule cytoskeleton is required for NE rupture. A transient F-actin 'shell' is polymerized by the Arp2/3 complex on the inner surface of the NE and membranes undergo complete rupture within two minutes of its formation (**Mori et al., 2014**). The rapid and dramatic reorganization of the NE during NEBD that is mediated by cytoskeletal forces, involving either microtubule-driven rupture in somatic cells or the F-actin shell in oocytes, has not been well understood.

Here, we use a combination of live-cell and super-resolution light microscopy, together with correlated electron microscopy, to capture these sudden changes in NE organization. We find that the F-actin shell is nucleated within the still-intact lamina and projects filopodia-like spikes into the nuclear membranes. The resulting nuclear membrane protrusions are free of NPCs, but are juxtaposed by NPC-dense clusters. Subsequently, these NPC-dense conglomerates invaginate and sort into the NPC-rich membrane network, while breaks appear on the pore-free regions.

Results

F-actin assembly causes reorganization of the nuclear membranes leading to rupture

We have shown previously that NE rupture, characterized by a wave-like entry of large cytoplasmic molecules into the nucleus, is mediated by a transient F-actin shell on the inner side of the NE, which is nucleated by the Arp2/3 complex (**Mori et al., 2014**). The F-actin shell first appears as an equatorial band of foci when the NE is still intact and impermeable to large dextrans (**Figure 1A**, 0 s). Approximately 30–45 s later, as the F-actin foci grow and intensify, merging to form a continuous F-actin shell, the first breaks on the NE appear, allowing a large 500 kDa dextran to flood into the nucleus (**Figure 1A**, 45 s). The shell then spreads towards the poles before a wave of membrane rupture takes place after a delay of ~30 s (**Figure 1A**, 90 s).

It became obvious to us that we needed to address what happens in the 30–45 s period between the start of actin assembly and NE rupture, as this appears to be a critical moment in F-actin-driven NE rupture. Our previous live-cell imaging assays lacked sufficient resolution to tackle the question (**Mori et al., 2014**), therefore we established brighter, recombinant-protein-based probes and used

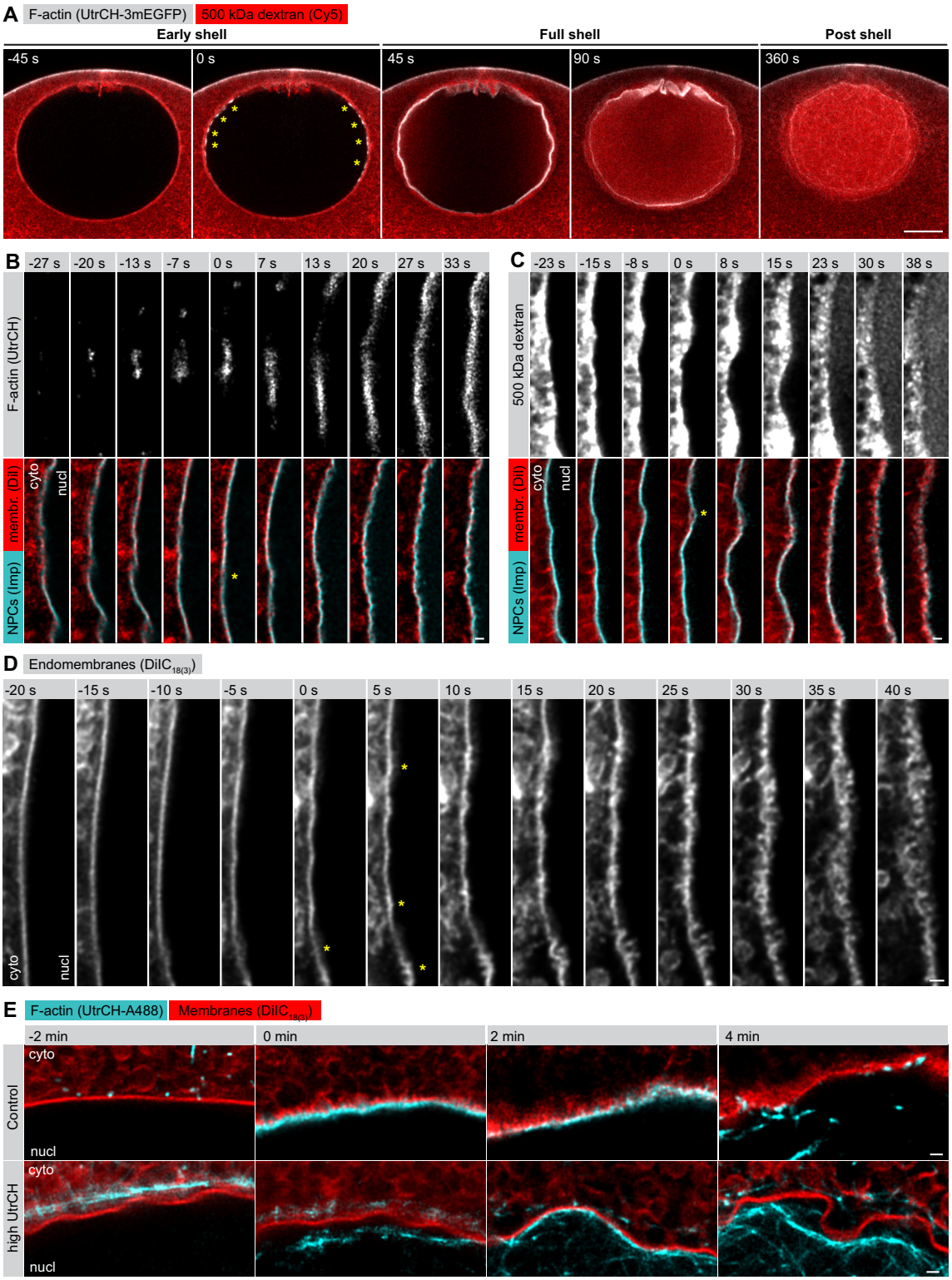

Figure 1. F-actin-driven membrane reorganization precedes NE rupture. (**A**) Live imaging of UtrCH-3mEGFP (white) and Cy5-labeled Dextran-500 kDa (red) in a starfish oocyte undergoing NEBD. Selected single confocal sections are shown from a time series. scale bar: 20 µm. Yellow asterisks mark F-actin foci. (**B**) Live imaging of a section of the rupturing NE in an oocyte injected with recombinant AlexaFluor488-labeled UtrCH, AlexaFluor647-labeled importin-β (45-462) (Imp), and $DiIC_{18(3)}$ (DiI). Selected frames are shown from a deconvolved AiryScan time series. Scale bar: 1 µm. Yellow

Figure 1 continued on next page

Figure 1 continued

asterisks mark the first visible sites of membrane reorganization. (**C**) As in panel (**B**) except that the oocyte was injected with a 500 kDa dextran instead of UtrCH. (**D**) Similar to panel (**B**) except that the oocyte was injected with $DiIC_{18(3)}$ alone and imaged at the highest possible frame rate and resolution. (**E**) In an experiment similar to that shown in panel (**B**), oocytes were injected with either low (~1 μM) or a very high amount (~20 μM) of UtrCH-AlexaFluor488 and equal amounts of $DiIC_{18(3)}$. At high concentrations, UtrCH depletes the available actin monomers by stabilizing cytoplasmic F-actin networks, and thereby efficiently prevents Arp2/3-driven assembly and NE rupture.

the AiryScan technology combined with deconvolution to visualize changes in NE reorganization at the sub-micrometer scale.

When we looked at the process with our new approach, we saw that as the first F-actin foci began to assemble, the NE still appeared smooth and continuous, as visualized by a membrane probe ($DiIC_{18(3)}$) and a marker of NPCs (a fragment of importin-β) (***Figure 1B***, −13 s). 10–15 s later, we observed the first spike-like membrane protrusions towards the cytoplasm, which then rapidly escalated into a complex, convoluted and fragmented membrane structure (***Figure 1B–D***). Intriguingly, during this process NPCs appeared to separate partially from the membrane towards the nucleoplasmic side. Dextran entry did not coincide with the formation of the initial membrane spikes, it occurred 20–30 s later, when membrane reorganization had progressed to a rather advanced stage (***Figure 1C***).

This membrane reorganization is dependent on actin assembly. If the F-actin shell is inhibited by injecting a large amount of the actin-binding UtrCH domain to deplete available actin monomers, the NE membrane stays smooth and continuous (***Figure 1E***). Even in this case, the nucleus does collapse and the NE ruffles and folds as a result of the progressing partial NE disassembly. However, unlike in control oocytes, these large and folded membrane fragments remain intact long after NEBD, as we showed in earlier work (***Mori et al., 2014***).

Thus, we concluded that, in starfish oocytes, actin assembly mediates a reorganization of nuclear membranes that leads to NE rupture.

Lamina remains intact during NE rupture

We next turned to immunofluorescence to visualize the endogenous NE components at an even higher resolution in order to reveal fine details of the F-actin-mediated NE rearrangements. We developed an antibody against the only identified starfish lamin protein, which together with the pan-NPC antibody mAb414 enabled us to visualize endogenous NE components together with phalloidin-stained F-actin. However, the F-actin shell is very transient, polymerizing and depolymerizing within 2 min, so the development of a reliable temporal reference for fixed-cell assays was also necessary. Fortunately, the F-actin shell emerges in a highly reproducible spatial pattern, which enabled us to time the fixed samples by correlating them with morphologies observed live (compare ***Figures 1A*** and ***2A***).

With this assay in hand, we first wanted to clarify whether the F-actin shell destabilizes the NE by tearing the lamin network, as this mechanism has been reported for microtubule-driven NE rupture in somatic cells (***Beaudouin et al., 2002***; ***Salina et al., 2002***). We have addressed this question in starfish oocytes before, but in this earlier work, we exogenously overexpressed a GFP fusion of human lamin B, which could have had different disassembly kinetics (***Lénárt et al., 2003***). To visualize the endogenous lamina directly this time, we analyzed samples stained with the starfish anti-lamin antibody at different stages of NE rupture. This confirmed our previous observations that the endogenous lamin network remains continuous even minutes after NE rupture, although it folds and ruffles as the nucleus collapses during NEBD (***Figure 2B***). In addition, imaging portions of the lamina *en face* by stimulated emission depletion (STED) microscopy suggests that the lamin mesh gradually coarsens during the process of NEBD (***Figure 2B***).

We conclude that the rupture of the NE does not proceed by F-actin-induced tearing or rapid disassembly of the lamina, which remains a continuous network throughout NEBD.

The F-actin shell assembles within the lamina sprouting spikes that separate nuclear membranes

In order to localize the F-actin shell relative to NE components, we next co-localized the lamina or the nuclear membranes (as marked by NPCs) at the time of shell formation, with the F-actin shell

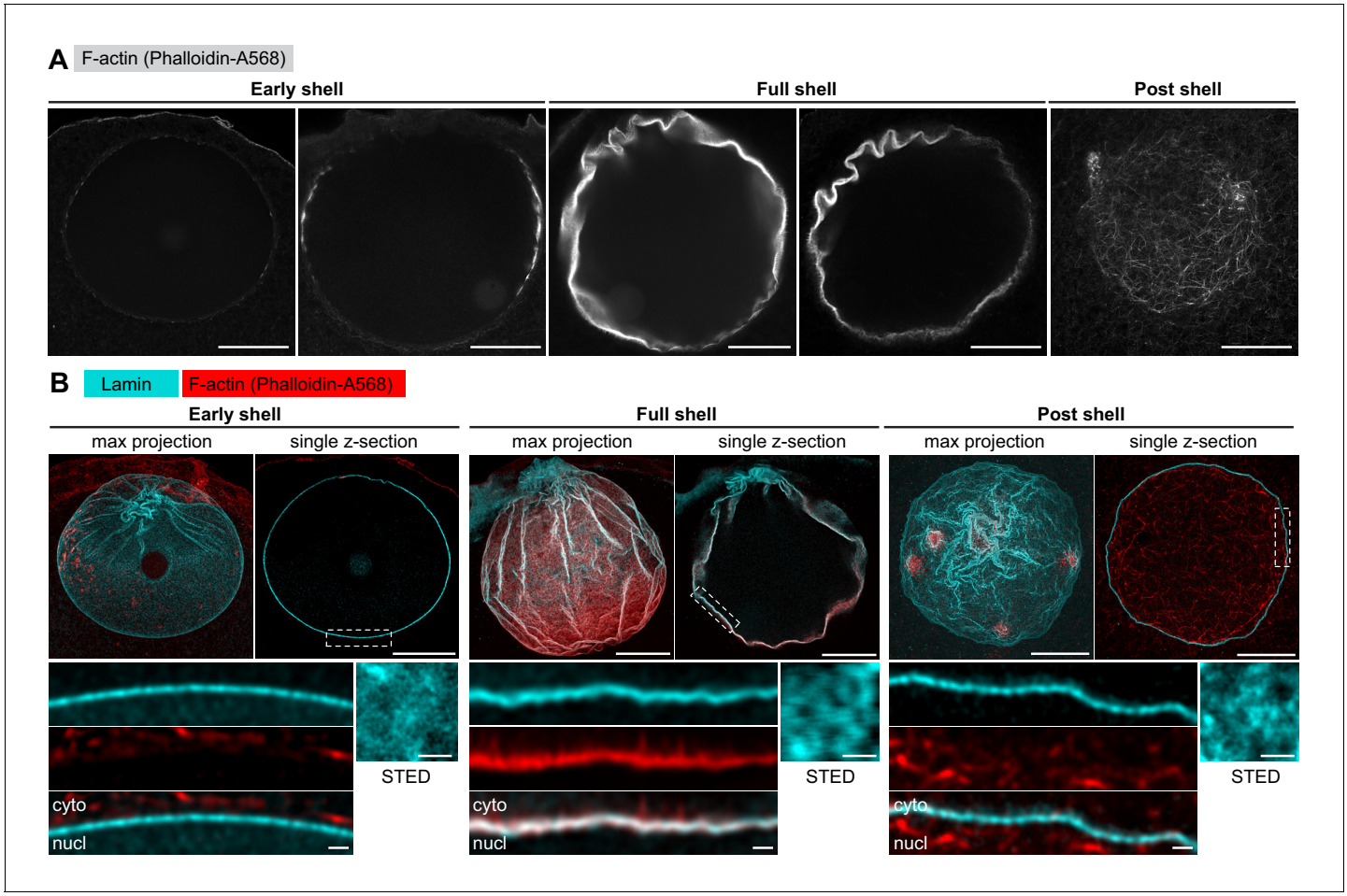

Figure 2. The lamina remains intact during NE rupture. (**A**) Fixed samples with F-actin labeled by phalloidin-AlexaFluor568. Individual confocal sections are shown and ordered to match the live time series shown in ***Figure 1A***. Scale bar: 20 μm. (**B**) Immunostained starfish oocytes with anti-lamin antibody shown in cyan and phalloidin-AlexaFluor568 in red. The images show three time-points: early shell, full shell and post shell. Each panel shows a maximum projection of the whole z-stack (left), a single selected optical section across the equatorial plane (right), and a close-up of the area in the single section highlighted with dashed rectangle (bottom). The small insets on the bottom right show *en face* views of the lamina in oocytes stained with the anti-lamin antibody and imaged by stimulated emission depletion (STED) microscopy at the corresponding stages. Scale bars: 20 μm (top), 5 μm (bottom left) and 0.5 μm (bottom right).

stained by phalloidin. We observed that although the lamina co-localized with phalloidin, the NPC staining formed a separate layer of fragmented appearance up to 500 nm 'above' the F-actin shell (***Figure 3A,B***). Thus, the still-intact lamina appears to serve as the scaffold upon which the F-actin shell assembles, whereas the nuclear membranes appear to fragment and separate away from the lamina and the F-actin shell.

We confirmed these observations by STED imaging of the lamina and NPCs (note that these samples were co-stained with phalloidin for staging, but it was not possible to image the third color on this particular STED setup). Before NE rupture, the NPC and lamina stainings overlapped at the approx. 50 nm resolution afforded by STED, which is consistent with the known ultrastructure of the NE (***Figure 3C***, pre-NEBD) (***Burke and Ellenberg, 2002***). In stark contrast, at the shell stage, we were able to visualize NPC-stained NE fragments 'floating' above the intact lamina (***Figure 3C***, post-NEBD). This separation of lamina and membranes is dependent on the F-actin shell, because this process did not occur when we prevented F-actin shell formation by inhibiting Arp2/3 using the small molecule inhibitor CK-666 (***Figure 3C***, post-NEBD + CK-666). Consistent with the live imaging described above, the NE appears ruffled due to collapse of nuclear volume even if the F-actin shell is inhibited.

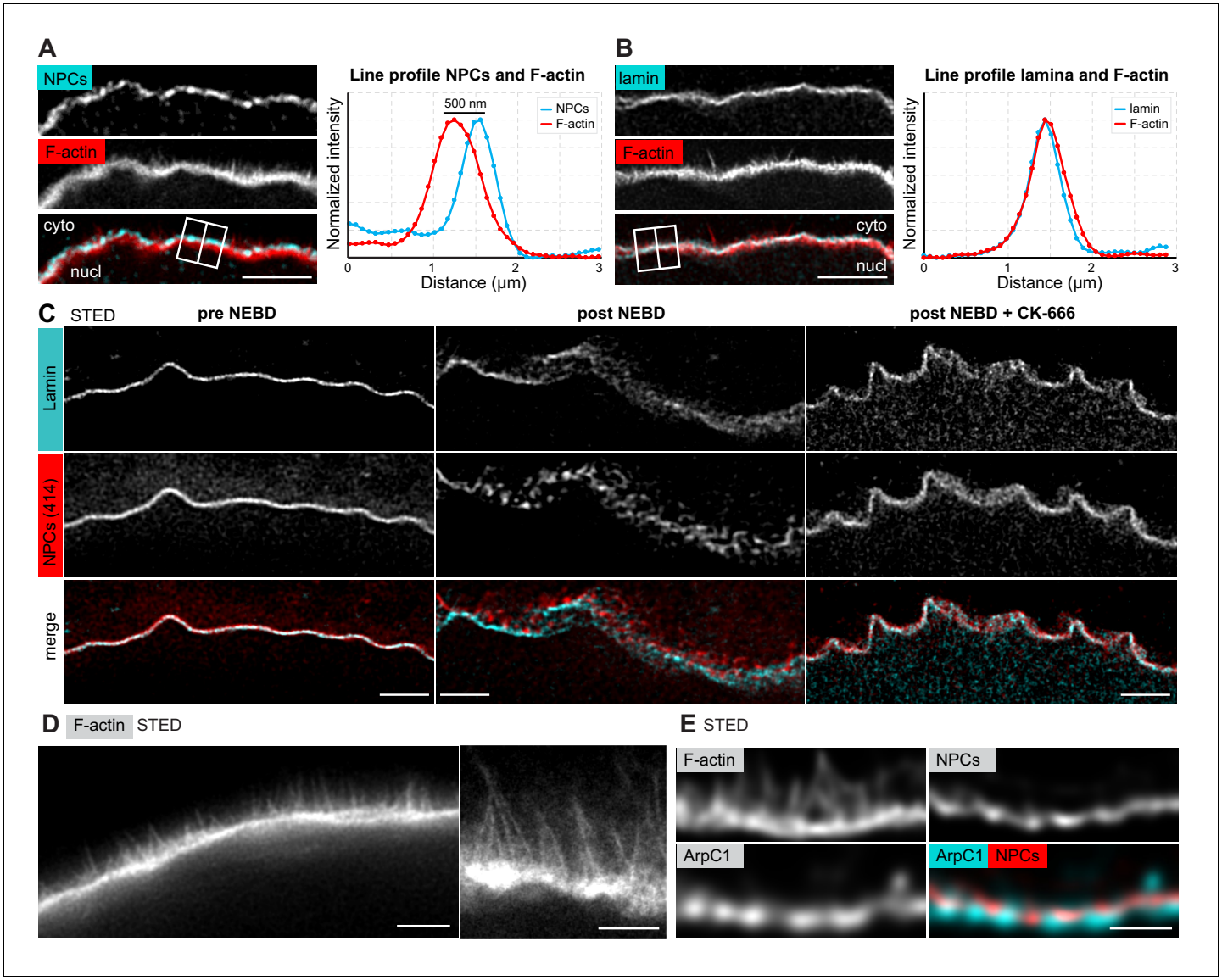

Figure 3. The F-actin shell separates the lamina and the nuclear membranes during NEBD. (**A**) Left: portion of the NE undergoing rupture immunostained with mAb414 for NPCs (cyan) and phalloidin-AlexaFluor568 for F-actin (red). A crop of a portion of NE from a confocal Z-section is shown. Scale bar: 2 µm. Right: plot of a line profile over the region marked with a white rectangle; normalized intensities of both channels are shown. (**B**) Same as panel (**A**) but stained with anti-lamin antibody and phalloidin-AlexaFluor568. (**C**) Portions of the NE stained with anti-lamin antibody (cyan) and mAb414 (red) and imaged by STED. Left, before NEBD; middle, after NEBD; right, after NEBD but first treated with CK-666 to inhibit the formation of the F-actin shell. Scale bars: 2 µm. (**D**) Phalloidin-Abberior Star RED staining of the F-actin shell imaged by STED microscopy. Scale bars: 5 µm (left) and 2 µm (right). (**E**) F-actin shell stained with mAb414 to label NPCs, an anti-ArpC1 antibody to label the Arp2/3 complex, and Phalloidin-Abberior Star RED to label F-actin, imaged by STED microscopy. Scale bar: 2 µm.

STED imaging of samples that were optimally fixed for phalloidin staining revealed filopodia-like F-actin spikes of 0.5–2 µm in length, spaced at ~0.1 µm, and extending from the base of the F-actin shell towards the nuclear membranes (***Figure 3D***). Furthermore, using a starfish-specific anti-ArpC1 antibody, we localized the Arp2/3 complex at the base of the F-actin shell just beneath the NE, whereas the F-actin spikes extending from the base were not labeled by ArpC1 (***Figure 3E***).

Taken together, our data show that the F-actin shell is nucleated by the Arp2/3 complex localized in the lamina and extends filopodia-like spikes, which separate the nuclear membranes away from the lamina.

Correlative EM captures intermediates of NE rupture

Unfortunately, although live imaging showed dramatic rearrangement of membranes, we were unable to visualize fine membrane structures in immunofluorescent samples directly, because preserving F-actin in fixed oocytes requires the addition of detergents to the fixative. The oocyte NE is, however, densely packed with NPCs, so NPC staining does provide a good proxy for the nuclear membrane, as shown above. Nonetheless, during NE rupture, this organization may change. Therefore, to clarify the F-actin mediated rearrangements of nuclear membranes, we decided to target the early stages of the F-actin shell formation using electron microscopy (EM). In this time-window of approximately 30 s, when the actin shell has just partially propagated, we expected to observe intermediate steps of NE rupture, with parts of the NE already ruptured while other regions are still intact (see ***Figure 1A***).

For this purpose, we developed a correlative electron microscopy protocol using high-pressure freezing and freeze substitution, which resulted in excellent preservation of the cellular structures (***Burdyniuk et al., 2018***). Correlation to light microscopy was achieved by using fluorescently labeled dextrans, which are directly visible on EM sections, as indicators of NEBD progression (***Figure 4A,B***): the small, 25-kDa dextran enters the nucleus during the first phase of NEBD through the disassembling NPCs, whereas the large, 160-kDa dextran only enters when the NE is ruptured (***Lénárt et al., 2003***). Thus, the stage when the 25-kDa dextran almost completely fills the nucleus but the large, 160-kDa dextran is still excluded identifies the time-window of F-actin shell formation and NE rupture.

We then performed automated large field-of-view montage transmission EM imaging of the whole nuclear cross-section to assess the state of the NE. An overview is shown in ***Figure 4C***, this and two additional montages are available at high resolution as Supplemental Data (***Figure 4—figure supplements 1–3***). The montage illustrates the key advantage of the system, which allows the progression of NE rupture to be observed spatially ordered on a single section of the large oocyte nucleus. The arrangement of the rupture site is fully consistent with the live and fixed light microscopy data: NE rupture initiates near the 'equator' of the nucleus and spreads as a wave towards the poles (***Figure 4D***).

We carefully examined these large montages and observed a set of frequently recurring characteristic membrane configurations. We assigned them to one of four categories and gave each a symbol to mark their incidence (***Figure 4C***). Numbers under each category quantify the occurrence of each feature within the section, and numbers in parentheses represent similar quantifications in two other sections shown in ***Figure 4—figure supplements 2*** and ***3***, illustrating that these are structures that occur frequently at the time of NE rupture.

Taken together, using our correlative light and electron microscopy approach, we were able to capture oocytes in the process of NE rupture.

F-actin spikes protrude pore-free nuclear membranes

The large dataset (***Figure 4—figure supplements 1–3***), the high frequency of events observed and, importantly, the spatial arrangement from the equatorial rupture site towards the still-intact poles allowed us to reconstruct the steps of NE rupture and to correlate these to observations made in live and fixed cells.

First, as consistent with earlier observations, the NE is smooth, continuous and is tightly packed with NPCs with a regular spacing of ~200 nm in immature oocytes, as well as in oocytes just before NE rupture and even in the intact polar regions of the NE undergoing rupture (see ***Figure 5A,B*** for image examples, and ***Figure 6C*** for quantification) (***Lénárt et al., 2003***). By contrast, in areas closer to the rupture site, we observed regions with gaps in NPC occupancy, the number and size of which increased proximal to this region (***Figure 5C***). In the vicinity of the site, gaps appeared to evolve into 'bumps' and membrane spikes (***Figure 5D***). Although reconstructing the full 3D architecture of these spikes is challenging, even in 300-nm-thick tomographic sections, the most prominent spikes that we observed rose ~1 µm above the level of the NE (***Figure 5D,E***). These spikes contain fibrous densities consistent with actin filaments (***Figure 5D*** and ***Figure 5—figure supplement 1A***) and are even more clearly distinguishable on tomographic reconstructions (***Figure 5E***).

Intriguingly, on both thin sections and tomographic reconstructions, we observed that these spikes were covered by continuous nuclear membranes and almost completely free of NPCs

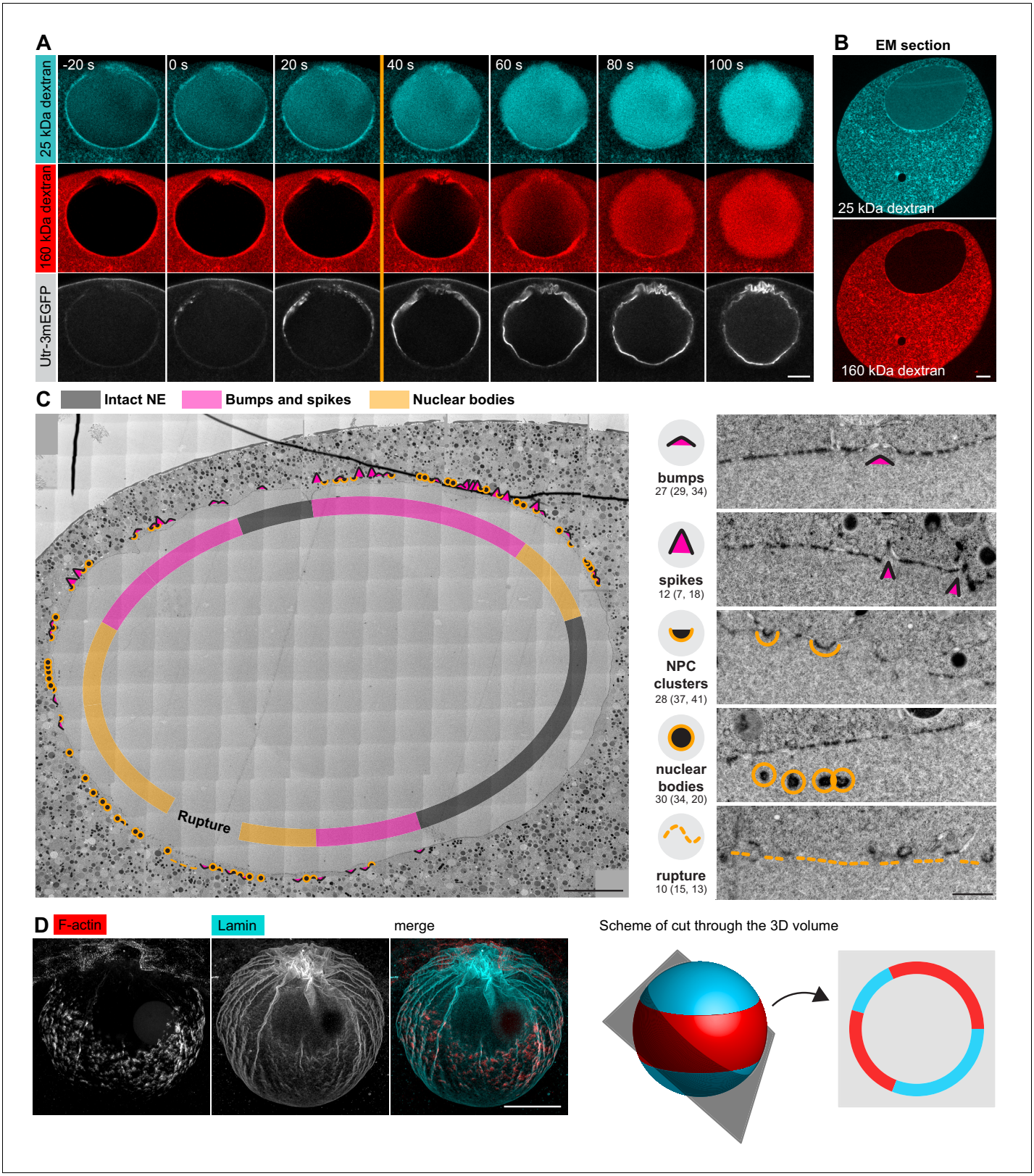

Figure 4. Correlative EM approach captures NE rupture intermediates. (**A**) Live imaging of a starfish oocyte undergoing NEBD and injected with a 25-kDa Cy5-labeled dextran (cyan), a 160-kDa TRITC-labeled dextran (red) and UtrCh-3mEGFP (white).Selected 2-frame projections from a confocal time-series imaged at one frame per second are shown. The orange line marks the moment immediately before rupture of the membrane, corresponding to the predicted time for the EM sample shown in panels (**B**) and (**C**). Scale bar: 20 µm. (**B**) Wide-field fluorescence image of a 70-nm section of a Lowicryl-

Figure 4 continued on next page

Figure 4 continued

embedded oocyte undergoing NEBD and injected with a 25-kDa Cy5-labeled dextran (cyan) and a 160-kDa TRITC-labeled (red) dextran. Scale bar: 20 μm. (**C**) A whole-nucleus tile of transmission EM images stitched automatically for the oocyte section shown in panel (B). Symbols around the nucleus correspond to NE rupture intermediates. A symbol legend with examples (crops from the tiled image) is shown to the right. Under each symbol, numbers correspond to the count of these events in the section shown, and the count in two adjacent sections is given in parentheses (shown in ***Figure 4—figure supplements 1–3***). The band that traces the NE within the nuclear space demarcates areas with color-code for predominant membrane features. For a full resolution image, see ***Figure 4—figure supplement 1***. Scale bar: 10 μm. (**D**) An oocyte fixed and stained with anti-lamin antibody (cyan) and phalloidin-AlexaFluor568 at early shell formation. A maximal Z projection is shown. Right: scheme illustrating the 3D geometry of the EM section. Scale bar: 20 μm.

The online version of this article includes the following figure supplement(s) for figure 4:

Figure supplement 1. High-resolution transmission electron microscropy (TEM) montage of a section through the nuclear region of an oocyte undergoing NEBD (shown on ***Figure 3C***).

Figure supplement 2. High-resolution TEM montage of a section through the nuclear region of an oocyte undergoing NEBD, section adjacent to that shown in ***Figure 4—figure supplement 1***..

Figure supplement 3. High-resolution TEM montage of a section through the nuclear region of an oocyte undergoing NEBD, section from the oocyte also shown in ***Figure 4—figure supplement 1***. Scale bar: 10 μm.

(***Figure 5D***). These pore-free areas are surrounded by NPC-dense adjacent regions (***Figure 5D*** and ***Figure 5—figure supplement 1A,B***). We are unable to estimate the 3D membrane areas from 2D sections, nevertheless, our data suggest that NPC-free areas pushed out by the F-actin shell may cause the crowding of NPCs in juxtaposed regions (***Figure 6C***).

These observations are further supported by light microscopy. AiryScan imaging in live oocytes shows membrane-covered spike-like F-actin protrusions extending from the NE, and these protrusions are consistent in size and number with our observations by EM (***Figure 5F***). In fixed samples imaged by STED, we were unable to visualize membranes directly, but we observed F-actin spikes extending out of the lamina with no NPC staining covering them except for dense NPC clusters at their base, an arrangement that is fully consistent with that seen on EM samples (***Figure 5G***). In addition, we were able to visualize that the lamina runs at the base of the F-actin shell, below but still attached to NPC clusters, suggesting that NPCs might be held back at the base of spikes by their attachments to the lamina (***Figure 5G***).

Together, our data from EM correlated with live cell and immunofluorescence suggest that the growing gaps between NPCs, which then develop into bumps and spikes, are protrusions generated by Arp2/3-driven actin polymerization, which pries nuclear membranes and lamina apart. Membrane evaginations are largely free of NPCs, most probably because NPCs are still attached to the lamina, and thus NPCs are held back and cluster at the base of spikes.

NPC-dense clusters invaginate and segregate from NPC-free regions

In regions closer to rupture sites, we observed an increasing segregation of pore-free and pore-dense segments (***Figure 6A***). Furthermore, accompanying spikes and NPC-rich clusters, we observed additional frequent membrane structures, which we call nucleoplasmic bodies. These are dense, round structures 200–500 nm in diameter beneath the NE in the nucleoplasm (***Figures 5D*** and ***6B***). These bodies often appear in a beads-on-a-string arrangement with a slightly electron-denser material connecting them (***Figure 6B***). Above them, the NE appears to be still intact, consisting mostly of NPC-free nuclear membranes and maintaining the nucleo-cytoplasmic boundary, as judged by the distribution of ribosomes. In pore-dense segments, as well as in nucleoplasmic bodies, our quantification shows that pore-to-pore distance decreased substantially from ~200 nm in intact areas to ~100 nm (***Figure 6C***), suggesting that the NPC-free membranes are generated by redistribution of NPCs.

Careful examination of intermediates suggests that nucleoplasmic bodies may form by invagination of NPC-rich clusters, initially inducing pits that curve into the nucleoplasm and then forming inverted NE tubules filled inside with cytoplasm (***Figure 6A,B*** and ***Figure 5—figure supplement 1B***). Sections capturing these structures *en face* and tomograms confirm that the electron density along the boundary of the bodies corresponds to closely juxtaposed NPCs with an intact central ring structure, similar to NPCs in still-intact areas (see 'nucleoplasmic bodies' in ***Figure 6D,E***).

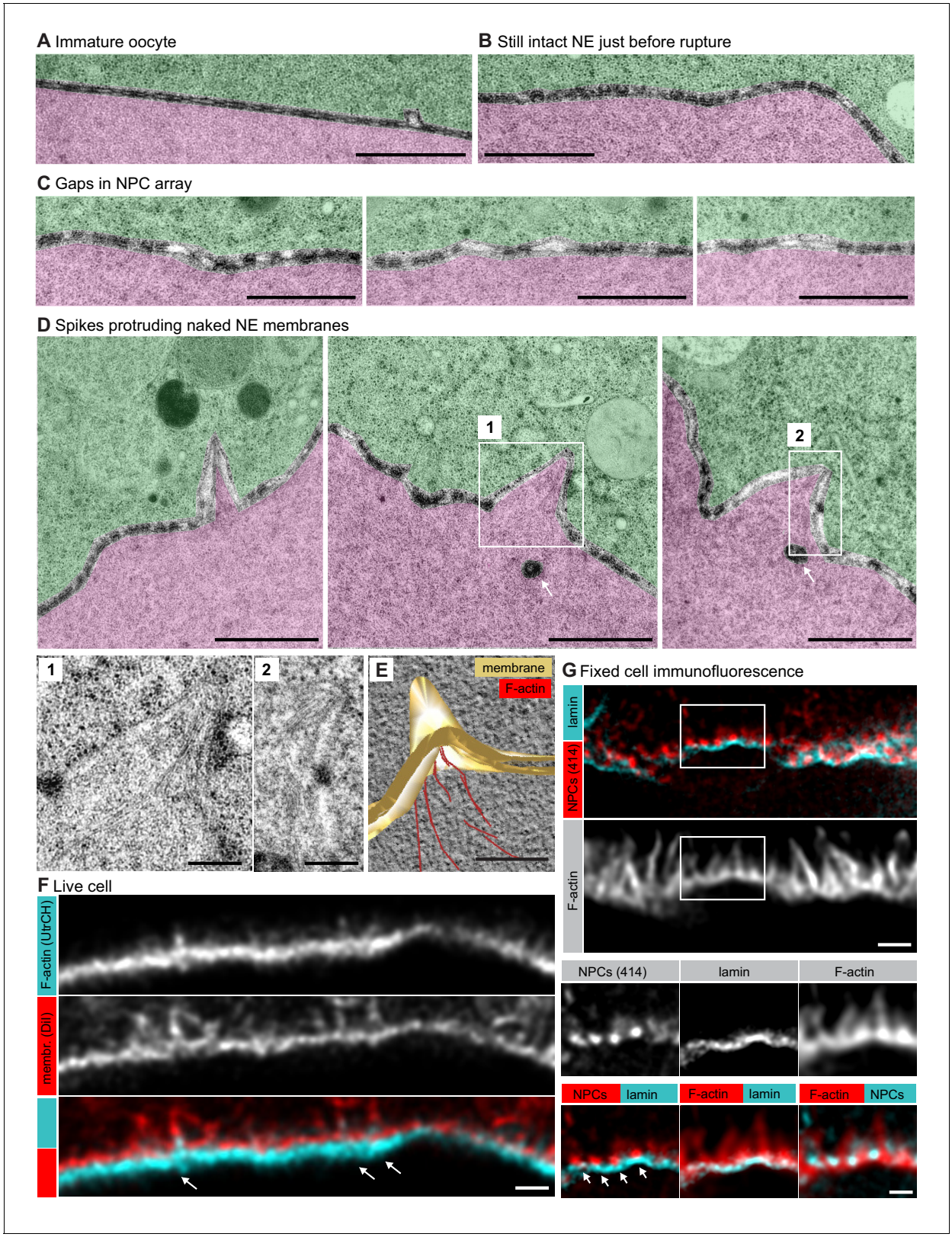

Figure 5. Spikes protrude bare nuclear membranes. (**A–D**) Transmission EM images from the oocyte shown in ***Figure 4C*** showing intermediates of NE rupture. Transparency coloring distinguishes the cytoplasm (green) from the nuclear area (pink) on the basis of the presence of ribosomes. Scale bars are 1 µm, except in the zooms, where they are 250 nm. In panel (D) arrows point to nucleoplasmic bodies. Zooms of the areas outlined with white rectangles are shown below. (**E**) Tomogram of a NE spike from a 300-nm thick section of the oocyte shown in ***Figure 4C***, with model overlay

Figure 5 continued on next page

Figure 5 continued

segmented manually. Scale bar: 200 nm. (**F**) Selected single frame from a deconvolved 3D Airyscan recording at the time of NE rupture. F-actin is labeled with recombinant UtrCH-AlexaFluor488, and endomembranes are stained by $DiIC_{18(3)}$. Arrows mark prominent F-actin spikes. Scale bar: 1 μm. (**G**) STED image of the NE at the shell stage stained for NPCs (mAb414), lamina and phalloidin-Abberior Star Red. Separate channels and overlays are shown in the combinations indicated. Arrows point at nucleoplasmic bodies. Scale bars: 1 μm and 0.5 μm.
The online version of this article includes the following figure supplement(s) for figure 5:

Figure supplement 1. Examples of NPC-rich clusters.

Comparing these structures to membrane intermediates observed in live cells suggests that they correspond to the convoluted morphology seen just before rupture (***Figure 6F***). In fixed samples, large spots of NPC accumulations that appear to be attached to the underlying lamina are also strongly reminiscent of the nucleoplasmic bodies (***Figure 6G***).

Finally, the EM montages revealed that the membranes were interrupted in areas where the segregation of pore-dense and pore-free regions was strongest and NPC invaginations frequent and most dramatic (***Figure 7A***). Here, no continuous membrane boundary was seen to separate cyto- and nucleoplasm, but nucleoplasmic bodies were abundant. Light microscopy of the corresponding stage revealed a complex tubular-vesicular network that was densely labeled by NPC staining, occasionally resolving cross-sections of tubules consistent with our EM data (***Figure 7B***).

Together, our data show that NE rupture proceeds by F-actin-driven sorting of NE membranes into pore-dense and pore-free segments. Pore-dense segments invaginate, forming a network of nucleoplasmic bodies, whereas rupture occurs in evaginating pore-free segments.

Discussion

Here, we resolved structural intermediates of rapid NE rearrangements mediated by the transient F-actin shell by using live-cell imaging, super-resolution light microscopy and correlative EM in starfish oocytes. On the basis of our data, we propose the following model for NE rupture (***Figure 7D***).

The first step is the formation of F-actin foci within the lamina. We hypothesize that these foci form at the time when cytoplasmic components, such as the Arp2/3 complex and actin monomers, reach a critical concentration in the nucleus as a result of the gradual, phosphorylation-driven disassembly and increasing leakiness of the NPCs in the first phase of NEBD. Once triggered, F-actin foci grow rapidly, which is expected as a result of the autocatalytic nature of Arp2/3-mediated nucleation of branched F-actin networks. As the foci spread, they merge to form a continuous shell. The filaments seem to grow preferentially from the shell base in the lamina towards nuclear membranes, and push against them. This asymmetry may be explained by the fact that force imposed on actin filaments promotes the nucleation of a branched meshwork (***Bieling et al., 2016***). Intriguingly, F-actin networks that are nucleated in vitro on micropatterned activated Arp2/3 show a morphology that is strikingly similar to that of the F-actin shell, with filopodia-like bundles pointing away from a base of dense branched network (***Reymann et al., 2010***). This suggests that localized activation of Arp2/3 within the lamina may be sufficient to explain the morphology of the F-actin shell.

Our light and electron microscopy data clearly show that the F-actin shell protrudes pore-free nuclear membranes, separating these from the lamina. We propose that these membranes are cleared of NPCs, because most NPCs are attached to the still-intact lamina at this stage, and thus are held back, while membranes are protruded by actin assembly. Then, as the NPCs accumulate between pore-free spikes, the membranes in these NPC-rich dimples buckle into the nucleoplasm and invaginate to form nucleoplasmic bodies. Our data suggest that pore-free nuclear membranes that are separated from the lamina are unstable, and thus rupture and rearrange into an ER-like reticular structure.

The exact mechanism of rupture remains unclear. However, in agreement with our model, it has been shown in various other physiological contexts that detaching the nuclear membranes from the lamin network leads to NE rupture. For example, NE rupture frequently occurs in cancer cells, in particular in micronuclei, where breaching of the NE barrier is preceded by local lamin disruption (***Hatch et al., 2013***). Recent work shows that the 'breakability' of the nucleus in migrating cells is dependent on lamin composition (***Thiam et al., 2016***; ***Davidson and Lammerding, 2014***; ***Denais et al., 2016***). Indeed, in somatic cells, it has been shown that NEBD proceeds by

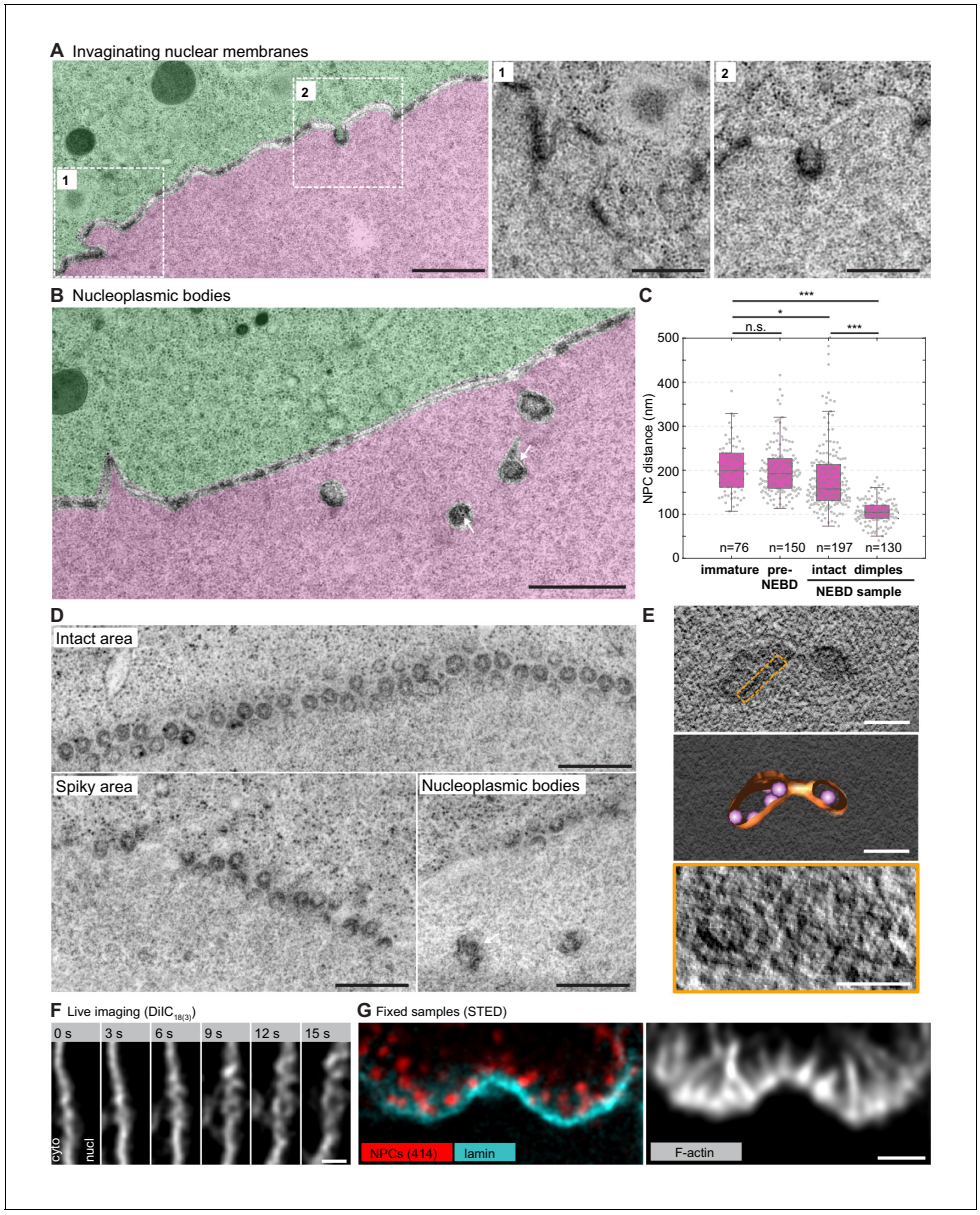

Figure 6. NPC clusters invaginate to form nucleoplasmic bodies. (**A**) Transmission EM images from the oocyte shown in ***Figure 4C*** and colored as in ***Figure 5A–D***, showing invaginating NPC clusters. Zooms of portions outlined with white rectangles are shown below without color transparencies. Scale bars: 1 µm (left) and 500 nm(zooms). See ***Figure 5—figure supplement 1A*** for more examples. (**B**) Transmission EM images as in panel (**A**) showing an area with nucleoplasmic bodies. Arrows point at ribosomes that are present within nucleoplasmic bodies. Scale bar: 1 µm. (**C**) Quantification of pore-to-pore distance on electron micrographs similar to those shown in ***Figure 4—figure supplements 1–3***. n refers to the number of pore-pairs measured in each of the respective samples or regions. n.s. denotes no significant difference, *, $p \leq 0.05$, ***, $p \leq 0.001$, as calculated by Student's T-test. (**D**) *En face* views of NPCs in the indicated regions along the NE. Scale bars: 500 nm. (**E**) Tomogram of a nucleoplasmic body (left), with a model overlaid (middle). Right: re-slicing of the volume perpendicular to the view on the left corresponding to the area outlined with an orange dashed rectangle in the top panel. Scale bars: 200 nm (top and middle) and 100 nm (bottom). (**F**) Selected frames from a live-cell recording of an oocyte injected with $DiIC_{18(3)}$ undergoing NE rupture. Scale bar: 1 µm. (**G**) STED image of the NE at the shell stage stained for NPCs (mAb414) (red), lamina (cyan) and phalloidin-AlexaFluor488 (gray). Scale bar: 1 µm.

microtubule-mediated tearing of the lamina (***Beaudouin et al., 2002***; ***Salina et al., 2002***), but the precise morphology of the NE intermediates at a resolution comparable to that which we achieved in starfish oocytes is not known. Therefore, it is possible that a similar mechanism, based on

the segregation of lamina, NPCs and membranes, plays a critical role in destabilizing the NE during NE rupture in somatic cells.

One possibility is that membranes actually break (fission), but this is complicated by the fact that this process would probably require a coordinated fission of inner nuclear membranes. Another alternative mechanism of NE rupture may be the disassembly of the central ring of a nuclear pore. This could allow the nuclear envelope to rearrange into an ER-like network without the need for an actual change in membrane topology. It is clear that only a small subset of NPCs may undergo such complete disassembly, because we can visualize the majority of NPCs with still intact central ring structure long after rupture. F-actin assembly may facilitate this process by increasing membrane tension in evaginations, or by causing extreme membrane curvatures, for example at the boundary of invaginations, thereby facilitating NE rupture or possibly complete NPC disassembly.

In addition, although this hypothesis remains rather speculative at this point, it is intriguing to consider links between our work and what has been shown for repair of interphase NE rupture, as well as reassembly of NE after division, both instances involving the ESCRT machinery (**Denais et al., 2016**; **Raab et al., 2016**; **Olmos et al., 2015**). In our NEBD intermediates, we observe membrane topologies that are similar to those involved in NE repair, suggesting that the ESCRT complex may also be involved in these membrane rearrangements.

As mentioned in the 'Introduction', there is wide diversity across species and cell types in the extent of NE disassembly during division. For example, the lamina persists much longer in many species as compared to mammalian somatic cells (**Gruenbaum et al., 2003**). Intriguingly, an F-actin shell similar to that in starfish oocytes has been observed in several species, although these structures are yet to be characterized in detail. These species include other echinoderm species, such as sea urchin (**Burkel et al., 2007**), the cnidarian model *Nematostella vectensis* (**DuBuc et al., 2014**), and polychaete worms (**Jacobsohn, 1999**). These examples strongly suggest that F-actin-mediated NE rupture may be widely spread across animal species, and we speculate that the presence or absence of this mechanism may be correlated with differences in NE disassembly dynamics, nuclear size and other differences in physiology.

Finally, the clearing of NPCs off the membrane during NEBD appears to be conserved in organisms with partially open mitosis. Tearing of the NE has been observed in the fungus *Ustilago maydis* and the yeast *Schizosaccharomyces japonicus*. In *U. maydis*, the shearing is caused by microtubules pulling the nucleus through a small opening into the bud of the daughter cell (**Straube et al., 2005**). *Sz. japonicus*, on the other hand, splits the NE by stretching the nucleus between the two poles of a dividing cell (**Aoki et al., 2011**). Thus, NE rupture occurs by different means, but intriguingly, both show evidence of clearing NPCs before the NE is torn: *Sz. japonicus* redistributes the NPCs to the two poles, freeing naked membranes at the NE regions destined to be broken. NPCs of *U. maydis* on the other hand initiate release of nucleoporins prior to rupture just as in higher eukaryotes (**Straube et al., 2005**; **Aoki et al., 2011**; **Theisen et al., 2008**).

Taken together, our data suggest that the F-actin shell destabilizes the NE by segregating pore-dense and pore-free membranes, providing the first mechanistic explanation for the sudden collapse of the NE structure during its breakdown. As discussed above, this mechanism is likely to function in many animal species. In other species, forces may be generated by means other than Arp2/3-mediated actin polymerization, but the segregation of nuclear membranes from the lamin network appears to be a general feature of nuclear rupture observed in dividing mammalian somatic cells, as well as during the interphase NE rupture that is frequent in cancer cells.

Materials and methods

Key resources table

Reagent type or resource	Designation	Source or reference	Identifiers	Additional information
Biological sample (*Patiria miniata*)	starfish oocytes	https://scbiomarine.com/ http://www.marinusscientific.com/		

Continued on next page

Continued

Reagent type or resource	Designation	Source or reference	Identifiers	Additional information
Biological sample (*Patiria pectinifera*)	starfish oocytes	Kazuyoshi Chiba, Ochanomizu University, Tokyo, Japan		
Sequence-based reagent	mEGFP3-UtrCH, 3mCherry-UtrCH	doi: 10.1002/cm.20226		synthetic mRNA (Utrophin CH domain (human))
Peptide, recombinant protein	Importin	doi: 10.1093/emboj/16.6.1153		(Importin-ß (45-462))
Peptide, recombinant protein	UtrCH	doi: 10.1002/cm.20226		(Utrophin CH domain (human))
Antibody, mouse (mAb414)	mAb414, mouse monoclonal	Sigma, BioLegend	Sigma #N8786, Biologend #902907	1:250
Antibody, rabbit (lamin)	lamin, rabbit polyclonal	see 'Materials and methods' for details		1:250
Commercial assay or kit	AmpliCap-Max T7 High Yield Message Maker	CellScript	C-ACM04037	
Commercial assay or kit	Poly(A) tailing kit	CellScript	C-PAP5104H	
Commercial assay or kit	Alexa Fluor 647 maleimide	ThermoFisher	A20347	
Commercial assay or kit	Alexa Fluor 488 maleimide	ThermoFisher	A10254	
Commercial assay or kit	Alexa Fluor 647 NHS Ester	ThermoFisher	A20006	
Commercial assay or kit	Alexa Fluor 488 NHS Ester	ThermoFisher	A20000	
Commercial assay or kit	Cy5 NHS Ester	discontinued		
Chemical compound, drug	$DiIC_{18(3)}$	ThermoFisher	D282	
Chemical compound, drug	1-methyladenine (1-MA)	ACROS organics		
Commercial assay or kit	Phalloidin-Alexa Fluor 488	ThermoFisher	A12379	
Commercial assay or kit	Phalloidin-Alexa Fluor 568	ThermoFisher	A12380	
Commercial assay or kit	Phalloidin-Alexa Fluor 647	ThermoFisher	A22287	
Commercial assay or kit	Abberior STAR RED phalloidin	Abberior		
Chemical compound, drug	CK-666	Merck	182515	
Chemical compound, drug	Amino-dextran 500,000 MW	ThermoFisher	D7144	
Chemical compound, drug	Amino-dextran 70,000 MW	ThermoFisher	D1862	
Chemical compound, drug	TRITC–Dextran 155,000 MW	Sigma	T1287	

Oocyte collection and injection

Starfish (*Patiria miniata* or *P. pectinifera*) were obtained in the springtime from Southern California (South Coast Bio-Marine LLC, Monterey Abalone Company or Marinus Scientific Inc) or were kindly provided by Kazoyushi Chiba (Ochanomizu University, Tokyo, Japan). They were kept at 16˚C for the

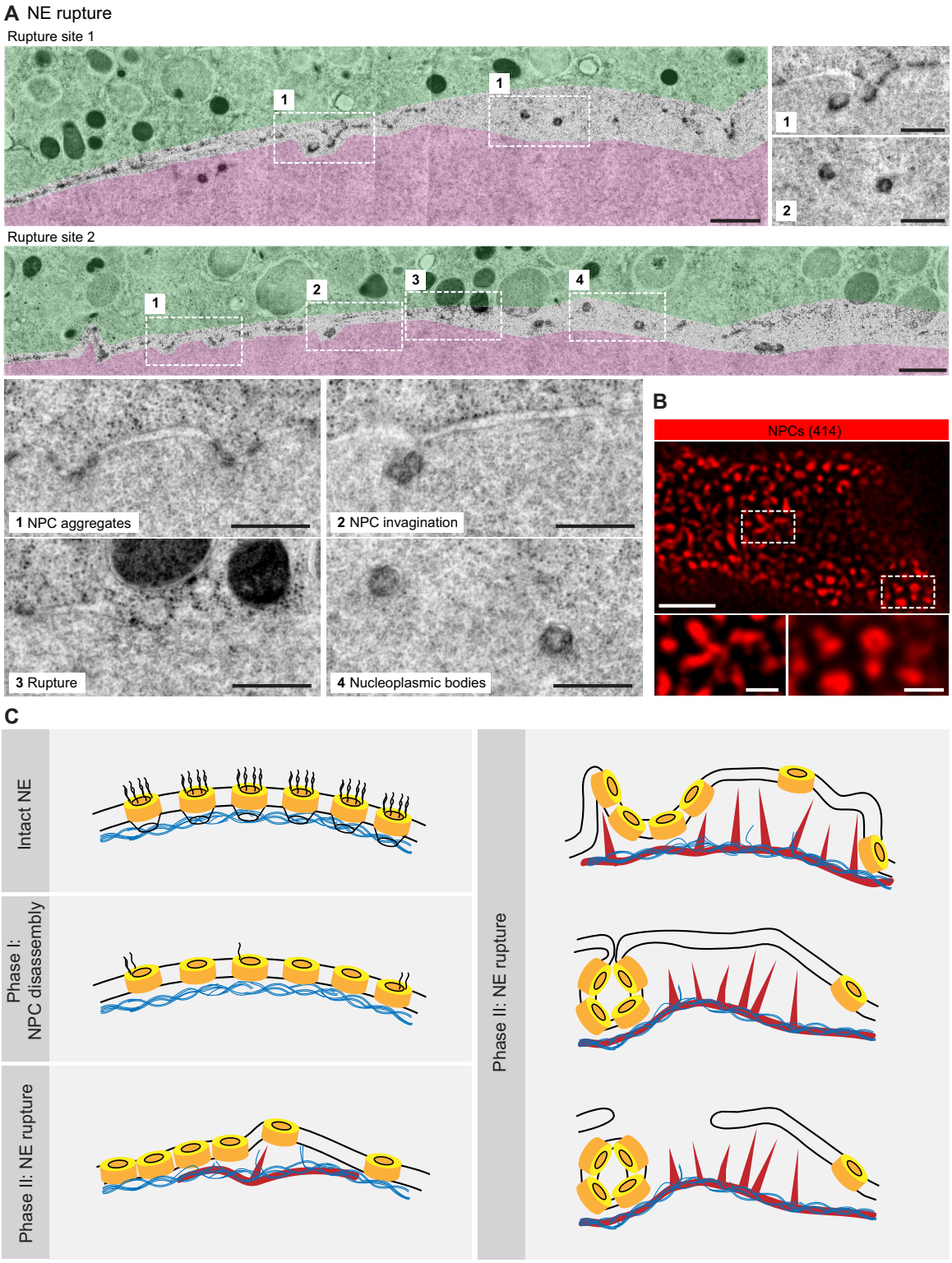

Figure 7. NE rupture occurs in pore-free regions. (**A**) Transmission EM images like those in ***Figure 6A*** showing examples of NE rupture events. Zooms of the areas outlined with white squares are shown below. Scale bars: 1 µm, and 500 nm for zooms. (**B**) *En face* STED image of the NE at the shell stage stained for NPCs (mAb414) (red). Scale bars: 1 µm (top) and 0.5 µm (bottom). (**C**) Model of F-actin-driven NE rupture. Intact NE: interphase organization of nuclear membranes (black lines) with regularly spaced NPCs (yellow cylinders) featuring cytoplasmic filaments and nuclear baskets. Nuclear baskets

Figure 7 continued on next page

Figure 7 continued

are embedded in the lamin network (blue filaments). Phase I of NEBD: peripheral NPC components are gradually released, but the NPC core and the overall NE structure remains intact. Phase II: NE rupture. First, small patches of F-actin (red) form within the lamina. F-actin patches grow and merge to form a shell, pushing apart NPCs that are still partially anchored in the lamina. As frequent F-actin spikes further sever the lamin-to-NE attachments, NPCs segregate into conglomerates, leaving stretches of unstable bare membrane, where breaks appear.

rest of the year in seawater aquariums at EMBL's or MPI-BPC's marine facilities. Oocytes were extracted from the animals fresh for each experiment as described earlier (**Lénárt et al., 2003**). mRNAs and other fluorescent markers were injected using microneedles, as described previously (**Jaffe and Terasaki, 2004**; **Borrego-Pinto et al., 2016**). mRNA was injected the day before to allow protein expression, whereas fluorescently labeled protein markers or dextrans were injected a few hours prior to imaging. Meiosis was induced at the initiation of the experiment by addition of 1-methyladenine (1-MA, 10 µM, Acros Organics). NEBD normally started 20–25 min after 1-MA addition, and only oocytes that initiated NEBD within 40 min of 1-MA addition were considered. Every experiment was repeated at least three times, with oocytes taken from at least two different animals.

Fluorescent markers and antibodies

To label F-actin, 3mEGFP-UtrCH (**Burkel et al., 2007**) mRNA was synthesized in vitro from linearized DNA templates using the AmpliCap-Max T7 High Yield Message Maker kit (Cellscript), followed by polyA-tail elongation (A-Plus Poly(A) Polymerase Tailing Kit, Cellscript). mRNAs were dissolved in water (typical concentration 3–5 µg/µl) and injected into the oocyte up to 5% of the oocyte volume.

Alternatively, the UtrCH domain was cloned and expressed in *E. coli*, purified and labeled with Alexa Fluor 488- or 647-maleimide. Importin-β (45-462)-AlexaFluor488/647 protein was a generous gift from Dirk Görlich.

Phalloidin labeled with the indicated Alexa or Abberior fluorophores (Invitrogen) was dissolved in methanol, and was then air-dried prior to use and dissolved in PBS for immunostaining.

For dextrans, amino-dextrans were labeled with succinimidyl ester dye derivatives (Cy5 or AlexaFluor647) or purchased in already labeled form (TRITC), purified and injected into oocytes as described earlier (**Lénárt et al., 2003**). $DiIC_{18(3)}$ (ThermoFisher) was dissolved in sunflower oil to saturation and injected to oocytes.

For CK-666 (Merck) treatments, oocytes were treated at 0.5 mM final concentration and incubated for 1 hr prior to hormone addition.

The pan-NPC antibody mAb414 was purchased from BioLegend or Sigma (catalogue #902907 or #N8786, respectively). To produce the anti-starfish-lamin antibody, the *Patiria miniata* lamin sequence was first identified by BLAST searches in our transcriptome-based database by comparisons to the human lamin B amino acid sequence, and then confirmed by reverse searches to other species. Furthermore, the corresponding mRNA was expressed as a mEGFP fusion and showed the expected localization to the NE in starfish oocytes (not shown). Peptide antibodies were then produced against the 'histone-interaction peptide' region of starfish lamin (GTKRRRLDEEE SMVQSS), which was used as the antigen for rabbit immunization. Antibody production and affinity purification was performed by Cambridge Research Biochemicals. The antibody's specificity was confirmed by Western blots, which showed an expected-sized band, and by immunostaining, which showed localization to the nuclear rim in starfish oocytes.

Immunostaining

Oocytes were fixed at the desired times in a PFA/GA fixative (100 mM HEPES [pH 7.0], 50 mM EGTA, 10 mM $MgSO_4$, 0.5% Triton-X100, 1 or 2% formaldehyde, 0.2 or 0.4% glutaraldehyde) modified from **Strickland et al. (2004)**. Active aldehyde groups that remained post fixation were quenched by 0.1% solution of $NaBH_4$ or by 200 mM NH_4Cl and 200 mM glycine. Subsequently, samples were permeabilized and blocked in PBS+0.1% Triton-X100 plus 3% BSA and the Image-IT reagent (ThermoFisher Scientific). Antibody staining was done overnight for the primary antibody and for 2–3 hr for the secondary antibody in PBS+0.1% Triton-X100 at room temperature. Oocytes were mounted with the antifade agent ProLongGold (ThermoFisher Scientific) under a coverslip pressed quite firmly onto tiny pillars of grease or double-sided tape (Scotch).

Light microscopy

Live-cell movies were acquired on a Leica SP5 confocal microscope using a 40x HCX PL AP 1.10 NA water immersion objective lens (Leica Microsystems), or a Zeiss LSM880 AiryScan microscope using a C-Apochromat 40 × 1.20 NA water immersion objective lens. For live-cell imaging experiments, at least 3–5 oocytes were recorded per session.

Fixed oocytes were imaged on a Leica SP8 microscope equipped with the HC PL APO 1.40 NA 100x oil immersion objective according to Nyquist criteria. For STED imaging, suitable Abberior STAR 580 and Abberior STAR RED or Abberior STAR 635P secondary antibodies or nanobodies were used (Abberior, NanoTag). Samples were imaged on a Leica SP8 STED microscope, with the HC PL APO CS2 1.40 NA 100x oil immersion objective and using the 775 nm depletion laser. Alternatively, we used an Abberior Instruments STEDYCON scan head mounted onto a Nikon Ti2 microscope equipped with a 100x CFI Plan Apochromat Lambda NA 1.45 oil immersion objective lens, or with an Abberior Instruments Expert Line STED microscope using an Olympus 100x UPLSAPO 100XS NA 1.4 oil immersion objective. At least five oocytes were recorded per sample.

Live and fixed oocyte images were processed and deconvolved using the Huygens software (Scientific Volume Imaging) with either confocal, AiryScan or STED settings as appropriate.

Electron microscopy

The electron microscopy protocol is described in detail in ***Burdyniuk et al. (2018)***. In brief, oocytes were injected with a mixture of dextrans and a small batch was tested for meiosis timing. At the approximate time of NEBD, they were transferred into a carrier (three oocytes in 0.3 µl of sea water) and most of the water was removed with filter paper. Oocytes were immediately covered with a drop of 1-hexedecene, and immediately high-pressure frozen. Oocytes were freeze-substituted into Lowicryl HM-20. To stage the oocytes, light microscopy of EM sections was used to determine the progress of dextran entry. Selected sections were then post-stained with lead citrate and imaged using a BioTwin CM120 Philips transmission electron microscope at 120 kV. Large TEM montages were acquired using a JEOL JEM-2100Plus transmission electron microscope at 120 kV. Tomograms were reconstructed from tilt series acquired on a FEI Tecnai F30 transmission electron microscope at 300 kV with 1.554 nm pixel size.

More than 50 oocytes were processed by the above described method, and a few of these oocytes were found to be at the correct stage, showing NE rupture intermediates. The data shown in the figures are from a single oocyte that had perfect preservation throughout and has been sectioned through the entire nuclear volume. Of these sections, more than ten have been imaged and have been scanned as a large montage, and analyzed carefully. Three of these montages are shown as figure supplements.

Acknowledgements

We thank the members of the Lénárt laboratory at EMBL for reagents and support, in particular Kálmán Somogyi, Andrea Callegari, Johanna Bischof, Joana Borrego-Pinto and Philippe Bun. We also thank EMBL's Advanced Light Microscopy Facility for essential support, specifically Marko Lampe for help with STED imaging. We thank the Electron Microscopy Core Facility, Yannick Schwab and Paolo Ronchi for sharing expertise during development of the EM protocol. We thank EMBL's Laboratory Animal Resources and Kresimir Crnokic in particular. We thank the members of the Lénárt group at MPI-BPC, in particular Jasmin Jakobi and Antonio Politi, as well as the staff of MPI-BPC's animal facility, in particular Ulrike Teichmann and Sascha Krause. We would like to thank Dirk Görlich and members of his laboratory for providing reagents and advice.

Research in PL's laboratory was funded by the European Molecular Biology Laboratory (EMBL) and the Deutsche Forschungsgemeinschaft (DFG) through grant GZ LE 2926/1–1 AOBJ 603520 of the Priority Programme SPP 1464. The laboratory is currently funded by the Max Planck Society.

Additional information

Funding

Funder	Grant reference number	Author
Deutsche Forschungsgemeinschaft	SPP 1464	Natalia Wesolowska
European Molecular Biology Laboratory		Natalia Wesolowska Pedro Machado Celina Geiss Hiroshi Kondo Masashi Mori Peter Lenart
Max Planck Society		Ivan Avilov Peter Lenart

The funders had no role in study design, data collection and interpretation, or the decision to submit the work for publication.

Author contributions

Natalia Wesolowska, Conceptualization, Data curation, Investigation, Visualization, Methodology, Writing - original draft, Writing - review and editing; Ivan Avilov, Investigation, Visualization, Writing - review and editing; Pedro Machado, Data curation, Investigation, Methodology; Celina Geiss, Data curation; Hiroshi Kondo, Masashi Mori, Investigation; Peter Lenart, Conceptualization, Data curation, Supervision, Funding acquisition, Investigation, Visualization, Methodology, Writing - original draft, Project administration, Writing - review and editing

Author ORCIDs

Peter Lenart https://orcid.org/0000-0002-3927-248X

Decision letter and Author response

Decision letter https://doi.org/10.7554/eLife.49774.sa1
Author response https://doi.org/10.7554/eLife.49774.sa2

Additional files

Supplementary files

- Transparent reporting form

Data availability

Full resolution EM montages are provided as supplementary files.

References

Aoki K, Hayashi H, Furuya K, Sato M, Takagi T, Osumi M, Kimura A, Niki H. 2011. Breakage of the nuclear envelope by an extending mitotic nucleus occurs during anaphase in Schizosaccharomyces japonicus. *Genes to Cells* **16**:911–926. DOI: https://doi.org/10.1111/j.1365-2443.2011.01540.x, PMID: 21733045

Beaudouin J, Gerlich D, Daigle N, Eils R, Ellenberg J. 2002. Nuclear envelope breakdown proceeds by microtubule-induced tearing of the Lamina. *Cell* **108**:83–96. DOI: https://doi.org/10.1016/S0092-8674(01)00627-4, PMID: 11792323

Bieling P, Li TD, Weichsel J, McGorty R, Jreij P, Huang B, Fletcher DA, Mullins RD. 2016. Force feedback controls motor activity and mechanical properties of Self-Assembling branched actin networks. *Cell* **164**:115–127. DOI: https://doi.org/10.1016/j.cell.2015.11.057, PMID: 26771487

Borrego-Pinto J, Somogyi K, Lénárt P. 2016. Live imaging of centriole dynamics by fluorescently tagged proteins in starfish oocyte meiosis. *Methods in Molecular Biology* **1457**:145–166. DOI: https://doi.org/10.1007/978-1-4939-3795-0_11, PMID: 27557579

Burdyniuk M, Wesolowska N, Fleszar M, Karreman MA, Machado P, Borrego-Pinto J, Ruthensteiner B, Schwab Y, Lénárt P. 2018. Correlated light and electron microscopy of cell division in large marine oocytes, eggs, and

embryos. *Methods in Cell Biology* **145**:293–313. DOI: https://doi.org/10.1016/bs.mcb.2018.03.031, PMID: 29957211

Burke B, Ellenberg J. 2002. Remodelling the walls of the nucleus. *Nature Reviews Molecular Cell Biology* **3**:487–497. DOI: https://doi.org/10.1038/nrm860, PMID: 12094215

Burkel BM, von Dassow G, Bement WM. 2007. Versatile fluorescent probes for actin filaments based on the actin-binding domain of utrophin. *Cell Motility and the Cytoskeleton* **64**:822–832. DOI: https://doi.org/10.1002/cm.20226, PMID: 17685442

Davidson PM, Lammerding J. 2014. Broken nuclei–lamins, nuclear mechanics, and disease. *Trends in Cell Biology* **24**:247–256. DOI: https://doi.org/10.1016/j.tcb.2013.11.004, PMID: 24309562

Denais CM, Gilbert RM, Isermann P, McGregor AL, te Lindert M, Weigelin B, Davidson PM, Friedl P, Wolf K, Lammerding J. 2016. Nuclear envelope rupture and repair during Cancer cell migration. *Science* **352**:353–358. DOI: https://doi.org/10.1126/science.aad7297, PMID: 27013428

DuBuc TQ, Dattoli AA, Babonis LS, Salinas-Saavedra M, Röttinger E, Martindale MQ, Postma M. 2014. In vivo imaging of *Nematostella vectensis* embryogenesis and late development using fluorescent probes. *BMC Cell Biology* **15**:44. DOI: https://doi.org/10.1186/s12860-014-0044-2, PMID: 25433655

Dultz E, Zanin E, Wurzenberger C, Braun M, Rabut G, Sironi L, Ellenberg J. 2008. Systematic kinetic analysis of mitotic dis- and reassembly of the nuclear pore in living cells. *The Journal of Cell Biology* **180**:857–865. DOI: https://doi.org/10.1083/jcb.200707026, PMID: 18316408

Goldberg MW, Allen TD. 1995. Structural and functional organization of the nuclear envelope. *Current Opinion in Cell Biology* **7**:301–309. DOI: https://doi.org/10.1016/0955-0674(95)80083-2, PMID: 7662358

Gruenbaum Y, Goldman RD, Meyuhas R, Mills E, Margalit A, Fridkin A, Dayani Y, Prokocimer M, Enosh A. 2003. The nuclear Lamina and its functions in the nucleus. *International Review of Cytology* **226**:1–62. DOI: https://doi.org/10.1016/s0074-7696(03)01001-5, PMID: 12921235

Hatch EM, Fischer AH, Deerinck TJ, Hetzer MW. 2013. Catastrophic nuclear envelope collapse in Cancer cell micronuclei. *Cell* **154**:47–60. DOI: https://doi.org/10.1016/j.cell.2013.06.007, PMID: 23827674

Hetzer MW. 2010. The nuclear envelope. *Cold Spring Harbor Perspectives in Biology* **2**:a000539. DOI: https://doi.org/10.1101/cshperspect.a000539, PMID: 20300205

Jacobsohn S. 1999. Characterization of novel F-actin envelopes surrounding nuclei during cleavage of a polychaete worm. *The International Journal of Developmental Biology* **43**:19–26. PMID: 10213079

Jaffe LA, Terasaki M. 2004. Quantitative microinjection of oocytes, eggs, and embryos. *Methods in Cell Biology* **74**:219–242. DOI: https://doi.org/10.1016/s0091-679x(04)74010-8, PMID: 15575609

Lénárt P, Rabut G, Daigle N, Hand AR, Terasaki M, Ellenberg J. 2003. Nuclear envelope breakdown in starfish oocytes proceeds by partial NPC disassembly followed by a rapidly spreading fenestration of nuclear membranes. *The Journal of Cell Biology* **160**:1055–1068. DOI: https://doi.org/10.1083/jcb.200211076, PMID: 12654902

Linder MI, Köhler M, Boersema P, Weberruss M, Wandke C, Marino J, Ashiono C, Picotti P, Antonin W, Kutay U. 2017. Mitotic disassembly of nuclear pore complexes involves CDK1- and PLK1-Mediated phosphorylation of key interconnecting nucleoporins. *Developmental Cell* **43**:141–156. DOI: https://doi.org/10.1016/j.devcel.2017.08.020, PMID: 29065306

Martino L, Morchoisne-Bolhy S, Cheerambathur DK, Van Hove L, Dumont J, Joly N, Desai A, Doye V, Pintard L. 2017. Channel nucleoporins recruit PLK-1 to nuclear pore complexes to direct nuclear envelope breakdown in *C. elegans*. *Dev Cell* **43**:157–171. DOI: https://doi.org/10.1016/j.devcel.2017.09.019

Mori M, Somogyi K, Kondo H, Monnier N, Falk HJ, Machado P, Bathe M, Nédélec F, Lénárt P. 2014. An Arp2/3 nucleated F-actin shell fragments nuclear membranes at nuclear envelope breakdown in starfish oocytes. *Current Biology* **24**:1421–1428. DOI: https://doi.org/10.1016/j.cub.2014.05.019, PMID: 24909322

Mühlhäusser P, Kutay U. 2007. An in vitro nuclear disassembly system reveals a role for the RanGTPase system and microtubule-dependent steps in nuclear envelope breakdown. *The Journal of Cell Biology* **178**:595–610. DOI: https://doi.org/10.1083/jcb.200703002, PMID: 17698605

Olmos Y, Hodgson L, Mantell J, Verkade P, Carlton JG. 2015. ESCRT-III controls nuclear envelope reformation. *Nature* **522**:236–239. DOI: https://doi.org/10.1038/nature14503, PMID: 26040713

Raab M, Gentili M, de Belly H, Thiam HR, Vargas P, Jimenez AJ, Lautenschlaeger F, Voituriez R, Lennon-Duménil AM, Manel N, Piel M. 2016. ESCRT III repairs nuclear envelope ruptures during cell migration to limit DNA damage and cell death. *Science* **352**:359–362. DOI: https://doi.org/10.1126/science.aad7611, PMID: 27013426

Reymann AC, Martiel JL, Cambier T, Blanchoin L, Boujemaa-Paterski R, Théry M. 2010. Nucleation geometry governs ordered actin networks structures. *Nature Materials* **9**:827–832. DOI: https://doi.org/10.1038/nmat2855, PMID: 20852617

Salina D, Bodoor K, Eckley DM, Schroer TA, Rattner JB, Burke B. 2002. Cytoplasmic dynein as a facilitator of nuclear envelope breakdown. *Cell* **108**:97–107. DOI: https://doi.org/10.1016/S0092-8674(01)00628-6, PMID: 11792324

Straube A, Weber I, Steinberg G. 2005. A novel mechanism of nuclear envelope break-down in a fungus: nuclear migration strips off the envelope. *The EMBO Journal* **24**:1674–1685. DOI: https://doi.org/10.1038/sj.emboj.7600644, PMID: 15861140

Strickland L, von Dassow G, Ellenberg J, Foe V, Lenart P, Burgess D. 2004. Light microscopy of echinoderm embryos. *Methods in Cell Biology* **74**:371–409. DOI: https://doi.org/10.1016/s0091-679x(04)74016-9, PMID: 15575615

Terasaki M, Campagnola P, Rolls MM, Stein PA, Ellenberg J, Hinkle B, Slepchenko B. 2001. A new model for nuclear envelope breakdown. *Molecular Biology of the Cell* **12**:503–510. DOI: https://doi.org/10.1091/mbc.12.2.503, PMID: 11179431

Theisen U, Straube A, Steinberg G. 2008. Dynamic rearrangement of nucleoporins during fungal "open" mitosis. *Molecular Biology of the Cell* **19**:1230–1240. DOI: https://doi.org/10.1091/mbc.e07-02-0130, PMID: 18172026

Thiam HR, Vargas P, Carpi N, Crespo CL, Raab M, Terriac E, King MC, Jacobelli J, Alberts AS, Stradal T, Lennon-Dumenil AM, Piel M. 2016. Perinuclear Arp2/3-driven actin polymerization enables nuclear deformation to facilitate cell migration through complex environments. *Nature Communications* **7**:10997. DOI: https://doi.org/10.1038/ncomms10997, PMID: 26975831

Ungricht R, Kutay U. 2017. Mechanisms and functions of nuclear envelope remodelling. *Nature Reviews Molecular Cell Biology* **18**:229–245. DOI: https://doi.org/10.1038/nrm.2016.153, PMID: 28120913

Author contributions

Chapter 1 (How does the Mos-MAPK pathway control oocyte meiosis?).

Together with Dr. Peter Lenart, I conceptualized the review and wrote the original draft.

Chapter 2 (Phospho-proteomics identifies translation and spindle organization as the main targets of Mos-MAPK in oocyte meiosis).

Together with Dr. Peter Lenart, I was responsible for the conceptualization of the manuscript, writing the original draft, and assembling the figures. I performed all experiments and analyzed the data with the following exceptions:

The phospho-proteomics analysis of the samples from starfish oocytes as well as the MaxQuant search was done by Luisa Welp and Henning Urlaub. All the following analysis of the MS data was done by Yehor Horokhovskyi and Juliane Liepe except the manual classification of the MS hits into the functional modules. Isolation of oocytes, immunofluorescence optimization, and sample preparation for the experiments shown in Fig. 1C and Fig. 3 were done by Aleksander Orzechowski. Immunofluorescence experiments shown in Fig.1D, Fig2A, and Fig. 9 were done by Mingfang Cai. Quantification of 3D distances of the spindle poles at different stages of meiosis I, shown in Fig. 8B were done by Dr. Peter Lenart

Chapter 3 (Actin assembly ruptures the nuclear envelope by prying the lamina away from nuclear pores and nuclear membranes in starfish oocytes).

As a co-author, I was responsible for writing and editing the manuscript. I performed experiments and analyzed the data that was shown in Fig. 1E, Fig. 3D,E, Fig. 5F,G, Fig. 6G, Fig. 7B.

Discussion

In my PhD project, I took advantage of starfish oocytes to study meiotic processes by combining mass spectrometry and high-resolution imaging. I studied the conserved Mos-MAPK pathway that controls meiotic progression across animal species. I characterized the Mos-MAPK inhibition phenotype in starfish that confirmed and further expanded previous studies in this animal (Mori et al., 2006; Tachibana et al., 2000; Ucar et al., 2013). I found that in oocytes Mos-MAPK is activated at metaphase I, and showed that at this stage Mos-MAPK regulates translation and cytoskeleton that drives the second meiosis and renders divisions asymmetric – the key features of meiosis. Additionally, I studied the actin-mediated mechanism of nuclear envelope breakdown (NEBD) in starfish oocyte meiosis.

Proteomics as a powerful tool to identify molecular mechanisms of meiosis

In the last decade, mass spectrometry (MS) became a powerful tool in studying the oocyte meiosis. Proteomics experiments have recently been carried out in oocytes of *Drosophila* (Casas-Vila et al., 2017; Fabre et al., 2016), starfish (Swartz et al., 2021), sea urchin (Guo et al., 2015), *Xenopus* (Ge et al., 2017), zebrafish (Shaik et al., 2014), mouse (Israel et al., 2019; Rosas-Salvans et al., 2018) and human (Virant-Klun et al., 2016). The high-throughput systems biology methods like proteomics or *de novo* transcriptome sequencing has the potential to substitute thousands of western blot or qPCR assays. In unusual animal model systems like starfish oocytes, proteomics has an additional advantage in overcoming the limited repertoire of antibodies available for western blots. On the other hand, in animals with less characterized proteomes, proteomics is more challenging since the number of identified hits strictly depends on the quality of proteome annotation. However, now there are web interfaces to automatic annotation pipelines available, like TRAPID that already at present can almost completely solve this limitation, and it is expected that with further development of these tools, this limitation will soon be fully eliminated (Bucchini et al., 2021).

In my PhD work I took advantage of proteomics in starfish oocytes that revealed core molecular modules controlling essential, meiosis-specific functions under the control of the conserved meiotic regulator, Mos-MAPK.

Mos-MAPK drives MII progression by stimulation of Cyclin B synthesis

A model of Mos-MAPK-mediated S-phase skipping between the two meiotic divisions was first proposed in starfish oocytes (Tachibana et al., 2000). According to this model, the oocytes in meiosis I are already competent for the embryonic cell cycle (Tachibana et al., 2000). After the first meiotic division, Mos-MAPK reactivates the Cdk1-Cyclin B complex that prevents replication and drives the second meiotic division. This model is based on evidence that inhibition of Mos-MAPK pathway components results in DNA replication after meiosis I, similar to preventing Cdk1-Cyclin B activation. In *Xenopus* and starfish oocytes, inhibition of Cdk1-Cyclin B activity by Cdk1 inhibitor treatment (Iwabuchi et al., 2000; Picard et al., 1996) or preventing Cyclin B translation (Hochegger et al., 2001; Picard et al., 1996) results in DNA replication after the first meiotic division. On the other hand, injection of non-degradable Cyclin B prevents DNA replication (Hochegger et al., 2001; Picard et al., 1996), and in *Xenopus* it restores the second meiotic division (Hochegger et al., 2001). However, would the activation of Cdk1-Cyclin B, mediated by the Mos-MAPK be sufficient to drive MII or there are additional mechanisms that ensure S-phase skipping in meiosis?

In my studies, I confirmed this model by live imaging. Firstly, in Mos-MAPK-inhibited oocytes, I evidenced meiosis exit and nucleus reformation after MI, followed by mitosis, as predicted by Tachibana and coworkers (Tachibana et al., 2000). I supported previous biochemical studies by the observation of nuclear reformation when I inhibited Cyclin B translation. Inhibition of Cyclin B translation showed an overall strikingly similar phenotype to Mos-MAPK inhibition. I then attempted to rescue the Mos-MAPK-inhibited oocytes by injection of active Cdk1-Cyclin B complex shortly after meiosis I. Intriguingly, the rescued oocytes proceed to the second meiotic division without reforming a nucleus, similarly to normal meiosis. My experiments clearly indicate that in starfish Cdk1-Cyclin B activity depends on Mos-MAPK and is necessary and sufficient for driving the second meiotic division. Consistent with studies in *Xenopus*, this indicates that the Cdk1-Cyclin B activity required to drive the second meiotic division is strictly dependent on additional Cyclin B translation (Hochegger et al., 2001; Picard et al., 1996). This leads to the conclusion that one of the main functions of Mos-MAPK is controlling Cyclin B translation at the meiosis I to II transition. What are the mechanisms that control Mos-MAPK dependent Cyclin B translation?

Generally, translation in starfish oocytes is very restricted during meiosis (Lapasset et al., 2008; Swartz et al., 2021). Proteomic analysis in starfish oocytes identified only 108 proteins affected by translation inhibition with emetine (Swartz et al., 2021). Among these, very few regulatory proteins have been found to change the abundance during meiosis: CPEB, Importin-8 (the importer of eIF4E), PIM1, and Cyclin B (Swartz et al., 2021). In another study, treatment with eIF4E-mediated translation inhibitor rapamycin identified Cyclin B as the only protein significantly expressed during starfish oocyte meiosis (Lapasset et al., 2008).

My phospho-proteomics data identified that Mos-MAPK is responsible for the phosphorylation of multiple proteins involved in eIF4E-mediated translation as well as phosphorylation of CPEB. CPEB together with TACC3 and eIF4ENIF1/eIF4E forms a complex that inhibits Cyclin B mRNA polyadenylation, crucial for translation (Arumugam et al., 2009; Stebbins-Boaz et al., 1999, 1996; Yang et al., 2014). CPEB phosphorylation followed by degradation releases the inhibitory effect of this complex (Stebbins-Boaz et al., 1999). Thereby my findings are consistent with previous evidence showing that in starfish Cyclin B translation depends on CPEB phosphorylation (Lapasset et al., 2005). Additionally, in *Xenopus* Mos-mediated CPEB phosphorylation stimulates the Cyclin B mRNA polyadenylation (Moor and Richter, 1997). However, in mice, Cyclin B translation appear to depend rather on MAPK-mediated CPEB degradation than phosphorylation (Cao et al., 2020). In starfish, CPEB degradation seems to be more critical (Lapasset et al., 2005; Swartz et al., 2021), CPEB seems not to be required for Cyclin B synthesis during meiotic progression (Lapasset et al., 2005). Together, my phospho-proteomics experiment comprehensively identified the entire CPEB translational module, including a number of phosphorylation sites. This will in the future allow the elucidation of the detailed molecular mechanism of translational regulation.

Another direction towards clarifying the mechanism of Mos-MAPK mediated translational regulation in starfish oocytes would be to test whether the Cyclin B translation is indeed controlled by Mos-MAPK through CPE-elements contained in the 3'UTR which in turn is regulated by CPEB. This can be tested by the injection of starfish oocytes with mRNA encoding for reporter fluorescent protein fused to 3'UTR of Cyclin B or Cyclin A. Cyclin A is not translated in meiosis and serves as a control. I would expect a stronger fluorescent signal accumulation from mRNA with 3'UTR of Cyclin B in non-treated oocytes rather than Mos-MAPK-inhibited. The signal of mRNA with 3'UTR of Cyclin A will not be affected by Mos-MAPK-inhibition.

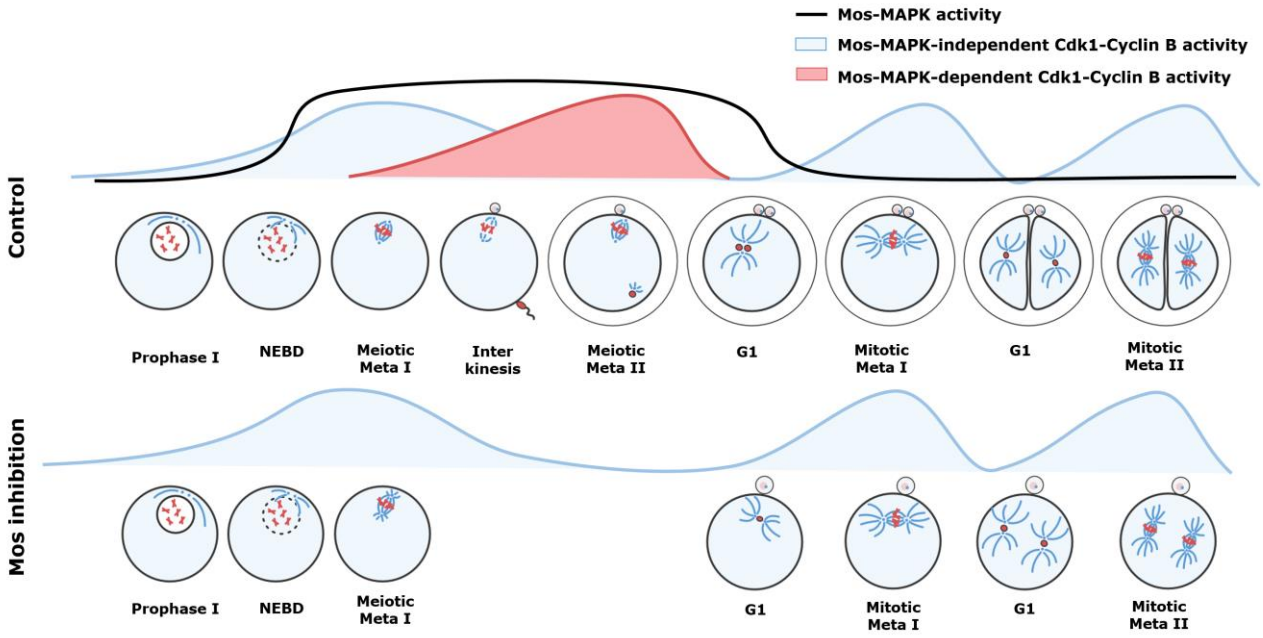

Figure 4. MOS-MAPK-dependent Cdk1-Cyclin B activity after MI ensures skipping of the S-phase and progression to MII instead of mitosis.

Asymmetric division in meiosis depends on Mos-MAPK

The second major function of Mos-MAPK is the regulation of asymmetric divisions. Here I combined phospho-proteomics with a detailed morphometric analysis of the microtubule spindle in control and Mos-MAPK-inhibited oocytes, by imaging of fixed and live oocytes. These experiments allowed me to identify three meiosis-specific features of spindle architecture mediated by Mos-MAPK that ensure asymmetric divisions in meiosis.

Firstly, Mos-MAPK is responsible for the reduction of the astral and interpolar microtubule growth. This microscopic observation is in good agreement with the phospho-proteomic candidates that include the microtubule plus-end stabilizing proteins. Long astral microtubules push the spindle away from the oocyte cortex resulting in substantially larger polar bodies or abortion of polar body extrusion. An increase in the number of astral microtubules, followed by a large polar body is indeed consistent with observations in Mos-MAPK-inhibited oocytes of several other species (Dupré et al., 2011). Additionally, stabilization of microtubules with Taxol treatment resulted in a similar phenotype with a large polar body or abortion of polar body extrusion in starfish oocytes (Kikuchi and Hamaguchi, 2012).

Secondly, Mos-MAPK downregulates pericentriolar material proteins (PCM), resulting in the observed reduction of centrosome size. This serves as an additional mechanisms to reduce the number of astral microtubules. Consistently with this observation, in my phospho-proteomic data, I have identified components of the PCM and centriolar proteins responsible for PCM recruitment. In starfish oocytes as well as other echinoderms (Holland, 1981; Nakashima and Kato, 2001; Sluder et al., 1993) and some mollusks (Wu and Palazzo, 1999) meiotic divisions characterized by having centrioles, but they are eliminated before pronuclear fusion (Borrego-Pinto et al., 2016). Although this feature is not conserved in vertebrates, this allowed me to observe the Mos-MAPK effect on PCM by microscopy and directly comparing meiotic to mitotic cleavages.

Thirdly, in meiosis, Mos-MAPK inhibits anaphase B. In the oocytes, chromosome separation is mainly based on the shortening of the kinetochore fibers, referred as anaphase A, and separation of the

spindle poles due to the pushing force of the interpolar microtubules or anaphase B is inhibited. This contrasts meiosis from mitosis where both anaphase A and anaphase B are present. Mos-MAPK inhibition seems to restore anaphase B, observed as an increase of interpolar microtubule density and progressive spindle elongation. Consistently, in my phospho-proteomic survey, I identified kinesin-4, that in mouse known to control the spindle elongation in anaphase (Heath and Wignall, 2019). Although the live data on spindle morphology dynamics upon Mos-MAPK inhibition is limited, in mice the anti-Mos-MAPK treatment also results in spindle elongation during meiosis I (Verlhac et al., 2000).

Taken together, my experiments consistently show that Mos-MAPK specifically downregulates PCM, reduces the growth as well as the amount of astral and interpolar microtubules, and prevents Anaphase B. Mitotic spindle has along asters that play a crucial role in orienting the spindle in the middle of the cell. Mos-MAPK helps to convert the mitotic spindle into the practically anastral meiotic one. The meiotic spindle is able to closely attach to the oocyte cortex and complete division as compactly as possible, resulting in an asymmetric cell division – extrusion of the polar body.

Maskin/TACC3 as a potential link between microtubule regulation and localized translation

Maskin/TACC3 may link the two functions of Mos in spindle organization and translational regulation. On the one hand, Maskin/TACC3 is known to interact with CPEB and eIF4ENIF1 to inhibit the translation of CPE-containing mRNAs, such as the Cyclin B transcript (Cao and Richter, 2002; Stebbins-Boaz et al., 1999). On the other hand, Maskin/TACC3 is an important microtubule regulator (Ding et al., 2017). In *Xenopus*, Maskin/TACC3 plays a role in microtubule minus end stabilization and spindle pole maintenance and is a binding partner of XMAP215/chTOG possibly involved in loading XMAP215 at the spindle pole (Barros et al., 2005; Kinoshita et al., 2005). Thereby Maskin/TACC3 may regulate the length and abundance of astral microtubules. In mouse oocytes, Maskin/TACC3 is also the main component of the recently discovered phase-separated spindle domain, LISH, which contains several aMTOC proteins including the main pericentriolar material component, PCM1 (Kinoshita et al., 2005; So et al., 2019).

Thus, Maskin/TACC3 is involved in translational regulation and organization of the (centrosomal or acentrosomal) spindle pole. These two functions of Maskin/TACC3 appear to be conserved at least to vertebrates (Albee and Wiese, 2008). This raises the intriguing possibility that these two functions co-evolved in order to coordinate spindle pole organization with localized Cyclin B synthesis on the meiotic spindle. Such a mechanism would automatically ensure that Cdk1-Cyclin B reactivation to drive the second meiotic division occurs not only at the right time but also at the right place. This is particularly relevant in large oocytes, where it is known that cell cycle transitions form spatial waves (Bischof et al., 2017; Chang and Jr, 2013). This would also provide a straightforward explanation for why in biochemical assays an apparently very small Cdk1-Cyclin B activity peak is sufficient to drive meiosis II. This hypothesis is supported by data from *Xenopus* oocytes in which both Maskin/TACC3 and CPEB have been shown to localize to the spindle poles (Albee and Wiese, 2008; Eliscovich et al., 2008), although in starfish oocytes I was unable to localize these proteins to the spindle. In rat oocytes phosphorylated $p38^{MAPK}$ also localizes to the spindle (Cui et al., 2012), and in porcine oocytes the localization of phosphorylated $p38^{MAPK}$ is distinct in mitosis and meiosis (Lee et al., 2000). Additionally, there is evidence from multiple species, including *Xenopus*, zebrafish, and starfish that Cyclin B mRNA is localized to the animal pole of the oocyte (Galas et al., 1993; GROISMAN et al., 2001; Kondo et al., 2001; Kotani et al., 2013; Takahashi et al., 2018), and Cyclin B is known to localize to the spindle not only in oocytes (Huo et al., 2005; Ookata et al., 1995, 1993), but also in somatic cells (Nakamura et al., 2005). Together, these data suggest tight coordination between spindle organization and localized regulation of the cell cycle by localized translation.

References

Adhikari D, Diril MK, Busayavalasa K, Risal S, Nakagawa S, Lindkvist R, Shen Y, Coppola V, Tessarollo L, Kudo NR, Kaldis P, Liu K. 2014. Mastl is required for timely activation of APC/C in meiosis I and Cdk1 reactivation in meiosis II. *J Cell Biol* 206:843–853. doi:10.1083/jcb.201406033

Albee AJ, Wiese C. 2008. Xenopus TACC3/Maskin Is Not Required for Microtubule Stability but Is Required for Anchoring Microtubules at the Centrosome. *Mol Biol Cell* 19:3347–3356. doi:10.1091/mbc.e07-11-1204

Alberts AS. 2001. Identification of a Carboxyl-terminal Diaphanous-related Formin Homology Protein Autoregulatory Domain*. *J Biol Chem* 276:2824–2830. doi:10.1074/jbc.m006205200

Almonacid M, Ahmed WW, Bussonnier M, Mailly P, Betz T, Voituriez R, Gov NS, Verlhac M-H. 2015. Active diffusion positions the nucleus in mouse oocytes. *Nat Cell Biol* 17:470–479. doi:10.1038/ncb3131

Álvarez-Fernández M, Sánchez-Martínez R, Sanz-Castillo B, Gan PP, Sanz-Flores M, Trakala M, Ruiz-Torres M, Lorca T, Castro A, Malumbres M. 2013. Greatwall is essential to prevent mitotic collapse after nuclear envelope breakdown in mammals. *Proc National Acad Sci* 110:17374–17379. doi:10.1073/pnas.1310745110

Amiel A, Houliston E. 2009. Three distinct RNA localization mechanisms contribute to oocyte polarity establishment in the cnidarian Clytia hemisphærica. *Dev Biol* 327:191–203. doi:10.1016/j.ydbio.2008.12.007

Anaphase A Seminars in Cell and Developmental Biology. n.d.

Arumugam K, Wang Y, Hardy LL, MacNicol MC, MacNicol AM. 2009. Enforcing temporal control of maternal mRNA translation during oocyte cell-cycle progression. *Embo J* 29:387–397. doi:10.1038/emboj.2009.337

Barros TP, Kinoshita K, Hyman AA, Raff JW. 2005. Aurora A activates D-TACC–Msps complexes exclusively at centrosomes to stabilize centrosomal microtubules. *J Cell Biology* 170:1039–1046. doi:10.1083/jcb.200504097

Baudat F, Imai Y, Massy B de. 2013. Meiotic recombination in mammals: localization and regulation. *Nat Rev Genet* 14:794–806. doi:10.1038/nrg3573

Beaudouin J, Gerlich D, Daigle N, Eils R, Ellenberg J. 2002. Nuclear Envelope Breakdown Proceeds by Microtubule-Induced Tearing of the Lamina. *Cell* 108:83–96. doi:10.1016/s0092-8674(01)00627-4

Bieber FR, Nance WE, Morton CC, Brown JA, Redwine FO, Jordan RL, Mohanakumar T. 1981. Genetic Studies of an Acardiac Monster: Evidence of Polar Body Twinning in Man. *Science* 213:775–777. doi:10.1126/science.7196086

Bischof J, Brand CA, Somogyi K, Májer I, Thome S, Mori M, Schwarz US, Lénárt P. 2017. A cdk1 gradient guides surface contraction waves in oocytes. *Nat Commun* 8:849. doi:10.1038/s41467-017-00979-6

Booth AJ, Yue Z, Eykelenboom JK, Stiff T, Luxton GG, Hochegger H, Tanaka TU. 2019. Contractile acto-myosin network on nuclear envelope remnants positions human chromosomes for mitosis. *Elife* 8:e46902. doi:10.7554/elife.46902

Borrego-Pinto J, Somogyi K, Karreman MA, König J, Müller-Reichert T, Bettencourt-Dias M, Gönczy P, Schwab Y, Lénárt P. 2016. Distinct mechanisms eliminate mother and daughter centrioles in meiosis of starfish oocytesCentriole elimination in starfish oocytes. *J Cell Biology* 212:815–827. doi:10.1083/jcb.201510083

Boveri T. 1895. Ueber das Verhalten der Centrosomen bei der Befruchtung des Seeigel-Eies : nebst allgemeinen Bemerkungen über Centrosomen und Verwandtes. *Verhandl Phys-Med Ges Würzburg* 29:1–75.

Brunet S, Verlhac MH. 2011. Positioning to get out of meiosis: the asymmetry of division. *Hum Reprod Update* 17:68–75. doi:10.1093/humupd/dmq044

Bucchini F, Del Cortona A, Kreft Ł, Botzki A, Van Bel M, Vandepoele K. 2021. TRAPID 2.0: a web application for taxonomic and functional analysis of de novo transcriptomes. *Nucleic Acids Res* 49:gkab565-. doi:10.1093/nar/gkab565

Bun P, Dmitrieff S, Belmonte JM, Nédélec FJ, Lénárt P. 2018. A disassembly-driven mechanism explains F-actin-mediated chromosome transport in starfish oocytes. *Elife* 7:e31469. doi:10.7554/elife.31469

Burdyniuk M, Callegari A, Mori M, Nédélec F, Lénárt P. 2018. F-Actin nucleated on chromosomes coordinates their capture by microtubules in oocyte meiosis. *J Cell Biol* 217:2661–2674. doi:10.1083/jcb.201802080

Campellone KG, Welch MD. 2010. A nucleator arms race: cellular control of actin assembly. *Nat Rev Mol Cell Bio* 11:237–251. doi:10.1038/nrm2867

Cao L-R, Jiang J-C, Fan H-Y. 2020. Positive Feedback Stimulation of Ccnb1 and Mos mRNA Translation by MAPK Cascade During Mouse Oocyte Maturation. *Frontiers Cell Dev Biology* 8:609430. doi:10.3389/fcell.2020.609430

Cao Q, Richter JD. 2002. Dissolution of the maskin–eIF4E complex by cytoplasmic polyadenylation and poly(A)-binding protein controls cyclin B1 mRNA translation and oocyte maturation. *Embo J* 21:3852–3862. doi:10.1093/emboj/cdf353

Casas-Vila N, Bluhm A, Sayols S, Dinges N, Dejung M, Altenhein T, Kappei D, Altenhein B, Roignant J-Y, Butter F. 2017. The developmental proteome of Drosophila melanogaster. *Genome Res* 27:1273--1285. doi:10.1101/gr.213694.116

Chang JB, Jr JEF. 2013. Mitotic trigger waves and the spatial coordination of the Xenopus cell cycle. *Nature* 500:603–607. doi:10.1038/nature12321

Chenevert J, Roca M, Besnardeau L, Ruggiero A, Nabi D, McDougall A, Copley RR, Christians E, Castagnetti S. 2020. The Spindle Assembly Checkpoint Functions during Early Development in Non-Chordate Embryos. *Cells* 9:1087. doi:10.3390/cells9051087

Chen Z, Borek D, Padrick SB, Gomez TS, Metlagel Z, Ismail AM, Umetani J, Billadeau DD, Otwinowski Z, Rosen MK. 2010. Structure and control of the actin regulatory WAVE complex. *Nature* 468:533–538. doi:10.1038/nature09623

Costache V, McDougall A, Dumollard R. 2014. Cell cycle arrest and activation of development in marine invertebrate deuterostomes. *Biochem Bioph Res Co* 450:1175–1181. doi:10.1016/j.bbrc.2014.03.155

Cox J, Mann M. 2008. MaxQuant enables high peptide identification rates, individualized p.p.b.-range mass accuracies and proteome-wide protein quantification. *Nat Biotechnol* 26:1367–1372. doi:10.1038/nbt.1511

Cui W, Zhang J, Lian H-Y, Wang H-L, Miao D-Q, Zhang C-X, Luo M-J, Tan J-H. 2012. Roles of MAPK and Spindle Assembly Checkpoint in Spontaneous Activation and MIII Arrest of Rat Oocytes. *Plos One* 7:e32044. doi:10.1371/journal.pone.0032044

Cundell MJ, Bastos RN, Zhang T, Holder J, Gruneberg U, Novak B, Barr FA. 2013. The BEG (PP2A-B55/ENSA/Greatwall) Pathway Ensures Cytokinesis follows Chromosome Separation. *Mol Cell* 52:393–405. doi:10.1016/j.molcel.2013.09.005

Dassow G von, Valley J, Robbins K. 2018. Microinjection of oocytes and embryos with synthetic mRNA encoding molecular probes. *Methods Cell Biol* 150:189–222. doi:10.1016/bs.mcb.2018.10.012

Dayon L, Affolter M. 2020. Progress and pitfalls of using isobaric mass tags for proteome profiling. *Expert Rev Proteomic* 17:149--161. doi:10.1080/14789450.2020.1731309

Dayon L, Hainard A, Licker V, Turck N, Kuhn K, Hochstrasser DF, Burkhard PR, Sanchez J-C. 2008. Relative Quantification of Proteins in Human Cerebrospinal Fluids by MS/MS Using 6-Plex Isobaric Tags. *Anal Chem* 80:2921–2931. doi:10.1021/ac702422x

Dehapiot B, Carrière V, Carroll J, Halet G. 2013. Polarized Cdc42 activation promotes polar body protrusion and asymmetric division in mouse oocytes. *Dev Biol* 377:202–212. doi:10.1016/j.ydbio.2013.01.029

Deng M, Suraneni P, Schultz RM, Li R. 2007. The Ran GTPase Mediates Chromatin Signaling to Control Cortical Polarity during Polar Body Extrusion in Mouse Oocytes. *Dev Cell* 12:301–308. doi:10.1016/j.devcel.2006.11.008

Ding Z, Huang C, Jiao X, Wu D, Huo L. 2017. The role of TACC3 in mitotic spindle organization. *Cytoskeleton* 74:369–378. doi:10.1002/cm.21388

Dultz E, Zanin E, Wurzenberger C, Braun M, Rabut G, Sironi L, Ellenberg J. 2008. Systematic kinetic analysis of mitotic dis- and reassembly of the nuclear pore in living cells. *J Cell Biology* 180:857–865. doi:10.1083/jcb.200707026

Dumont J, Million K, Sunderland K, Rassinier P, Lim H, Leader B, Verlhac M-H. 2007. Formin-2 is required for spindle migration and for the late steps of cytokinesis in mouse oocytes. *Dev Biol* 301:254–265. doi:10.1016/j.ydbio.2006.08.044

Dupré A, Haccard O, Jessus C. 2011. Mos in the Oocyte: How to Use MAPK Independently of Growth Factors and Transcription to Control Meiotic Divisions. *J Signal Transduct* 2011:350412. doi:10.1155/2011/350412

Eliscovich C, Peset I, Vernos I, Méndez R. 2008. Spindle-localized CPE-mediated translation controls meiotic chromosome segregation. *Nat Cell Biol* 10:858–865. doi:10.1038/ncb1746

Fabre B, Korona D, Groen A, Vowinckel J, Gatto L, Deery MJ, Ralser M, Russell S, Lilley KS. 2016. Analysis of Drosophila melanogaster proteome dynamics during embryonic development by a combination of label-free proteomics approaches. *Proteomics* 16:2068--2080. doi:10.1002/pmic.201500482

Farmer JB, Moore JES. 1905. On the maiotic phase (reduction divisions) in animals and plants. *Q J Microsc Sci* 48:489–557.

FitzHarris G. 2012. Anaphase B Precedes Anaphase A in the Mouse Egg. *Curr Biol* 22:437–444. doi:10.1016/j.cub.2012.01.041

Flemming W. 1882. Zellsubstanz, Kern und Zelltheilung. F. C. W. Vogel, Leipzig. doi:doi.org/10.5962/bhl.title.168645

Galas S, Barakat H, Dorée M, Picard A. 1993. A nuclear factor required for specific translation of cyclin B may control the timing of first meiotic cleavage in starfish oocytes. *Mol Biol Cell* 4:1295–1306. doi:10.1091/mbc.4.12.1295

Gard DL. 1992. Microtubule organization during maturation of Xenopus oocytes: Assembly and rotation of the meiotic spindles. *Dev Biol* 151:516–530. doi:10.1016/0012-1606(92)90190-r

Ge C, Lu W, Chen A. 2017. Quantitative proteomic reveals the dynamic of protein profile during final oocyte maturation in zebrafish. *Biochem Bioph Res Co* 490:657--663. doi:10.1016/j.bbrc.2017.06.093

Glotzer M, Murray AW, Kirschner MW. 1991. Cyclin is degraded by the ubiquitin pathway. *Nature* 349:132–138. doi:10.1038/349132a0

GROISMAN I, HUANG Y-S, MENDEZ R, CAO Q, RICHTER JD. 2001. Translational Control of Embryonic Cell Division by CPEB and Maskin. *Cold Spring Harb Sym* 66:345–352. doi:10.1101/sqb.2001.66.345

Guo H, Garcia-Vedrenne AE, Isserlin R, Lugowski A, Morada A, Sun A, Miao Y, Kuzmanov U, Wan C, Ma H, Foltz K, Emili A. 2015. Phosphoproteomic network analysis in the sea urchin Strongylocentrotus purpuratus reveals new candidates in egg activation. *Proteomics* 15:4080--4095. doi:10.1002/pmic.201500159

Güttinger S, Laurell E, Kutay U. 2009. Orchestrating nuclear envelope disassembly and reassembly during mitosis. *Nat Rev Mol Cell Bio* 10:178–191. doi:10.1038/nrm2641

Hara M, Abe Y, Tanaka T, Yamamoto T, Okumura E, Kishimoto T. 2012. Greatwall kinase and cyclin B-Cdk1 are both critical constituents of M-phase-promoting factor. *Nat Commun* 3:1059. doi:10.1038/ncomms2062

Hara M, Mori M, Wada T, Tachibana K, Kishimoto T. 2009. Start of the embryonic cell cycle is dually locked in unfertilized starfish eggs. *Dev Camb Engl* 136:1687--1696. doi:10.1242/dev.035261

Harasimov K, Uraji J, Mönnich EU, Holubcová Z, Elder K, Blayney M, Schuh M. 2023. Actin-driven chromosome clustering facilitates fast and complete chromosome capture in mammalian oocytes. *Nat Cell Biol* 25:439–452. doi:10.1038/s41556-022-01082-9

Hartwell LH, Weinert TA. 1989. Checkpoints: Controls That Ensure the Order of Cell Cycle Events. *Science* 246:629–634. doi:10.1126/science.2683079

Heath CM, Wignall SM. 2019. Chromokinesin Kif4 promotes proper anaphase in mouse oocyte meiosis. *Mol Biol Cell* 30:1691–1704. doi:10.1091/mbc.e18-10-0666

Hochegger H, Klotzbücher A, Kirk J, Howell M, Guellec K le, Fletcher K, Duncan T, Sohail M, Hunt T. 2001. New B-type cyclin synthesis is required between meiosis I and II during Xenopus oocyte maturation. *Development* 128:3795–3807. doi:10.1242/dev.128.19.3795

Holland ND. 1981. Electron Microscopic Study of Development in a Sea Cucumber, Stichopus tremulus (Holothuroidea), from Unfertilized Egg through Hatched Blastula. *Acta Zool-stockholm* 62:89–111. doi:10.1111/j.1463-6395.1981.tb00618.x

Hunt DF, Yates JR, Shabanowitz J, Winston S, Hauer CR. 1986. Protein sequencing by tandem mass spectrometry. *Proc National Acad Sci* 83:6233–6237. doi:10.1073/pnas.83.17.6233

Huo L-J, Yu L-Z, Liang C-G, Fan H-Y, Chen D-Y, Sun Q-Y. 2005. Cell-cycle-dependent subcellular localization of cyclin B1, phosphorylated cyclin B1 and p34cdc2 during oocyte meiotic maturation and fertilization in mouse. *Zygote* 13:45–53. doi:10.1017/s0967199405003060

Israel S, Ernst M, Psathaki OE, Drexler HCA, Casser E, Suzuki Y, Makalowski W, Boiani M, Fuellen G, Taher L. 2019. An integrated genome-wide multi-omics analysis of gene expression dynamics in the preimplantation mouse embryo. *Sci Rep-uk* 9:13356. doi:10.1038/s41598-019-49817-3

Iwabuchi M, Ohsumi K, Yamamoto TM, Sawada W, Kishimoto T. 2000. Residual Cdc2 activity remaining at meiosis I exit is essential for meiotic M–M transition in Xenopus oocyte extracts. *Embo J* 19:4513–4523. doi:10.1093/emboj/19.17.4513

Jessus C, Munro C, Houliston E. 2020. Managing the Oocyte Meiotic Arrest—Lessons from Frogs and Jellyfish. *Cells* 9:1150. doi:10.3390/cells9051150

KANATANI H, SHIRAI H, NAKANISHI K, KUROKAWA T. 1969. Isolation and Identification of Meiosis Inducing Substance in Starfish Asterias amurensis. *Nature* 221:273–274. doi:10.1038/221273a0

Kikuchi Y, Hamaguchi Y. 2012. The effect of taxol microinjection on the microtubular structure in polar body formation of starfish oocytes. *Cytoskeleton* 69:125–132. doi:10.1002/cm.21004

Kinoshita K, Noetzel TL, Pelletier L, Mechtler K, Drechsel DN, Schwager A, Lee M, Raff JW, Hyman AA. 2005. Aurora A phosphorylation of TACC3/maskin is required for centrosome-dependent microtubule assembly in mitosis. *J Cell Biology* 170:1047–1055. doi:10.1083/jcb.200503023

KISHIMOTO T. 2018. MPF-based meiotic cell cycle control: Half a century of lessons from starfish oocytes. *Proc Jpn Acad Ser B* 94:180–203. doi:10.2183/pjab.94.013

Kishimoto T. 2015. Entry into mitosis: a solution to the decades-long enigma of MPF. *Chromosoma* 124:417–428. doi:10.1007/s00412-015-0508-y

Kondo T, Kotani T, Yamashita M. 2001. Dispersion of Cyclin B mRNA Aggregation Is Coupled with Translational Activation of the mRNA during Zebrafish Oocyte Maturation. *Dev Biol* 229:421–431. doi:10.1006/dbio.2000.9990

Kotani T, Yasuda K, Ota R, Yamashita M. 2013. Cyclin B1 mRNA translation is temporally controlled through formation and disassembly of RNA granules. *J Cell Biol* 202:1041–1055. doi:10.1083/jcb.201302139

Kronja I, Yuan B, Eichhorn SW, Dzeyk K, Krijgsveld J, Bartel DP, Orr-Weaver TL. 2014. Widespread Changes in the Posttranscriptional Landscape at the Drosophila Oocyte-to-Embryo Transition. *Cell Reports* 7:1495–1508. doi:10.1016/j.celrep.2014.05.002

Lapasset L, Pradet-Balade B, Lozano J-C, Peaucellier G, Picard A. 2005. Nuclear envelope breakdown may deliver an inhibitor of protein phosphatase 1 which triggers cyclin B translation in starfish oocytes. *Dev Biol* 285:200–210. doi:10.1016/j.ydbio.2005.06.016

Lapasset L, Pradet-Balade B, Vergé V, Lozano J, Oulhen N, Cormier P, Peaucellier G. 2008. Cyclin B synthesis and rapamycin-sensitive regulation of protein synthesis during starfish oocyte meiotic divisions. *Mol Reprod Dev* 75:1617–1626. doi:10.1002/mrd.20905

Lee J, Miyano T, Moor RM. 2000. Localisation of phosphorylated MAP kinase during the transition from meiosis I to meiosis II in pig oocytes. *Zygote* 8:119--125. doi:10.1017/s0967199400000897

Lénárt P, Bacher CP, Daigle N, Hand AR, Eils R, Terasaki M, Ellenberg J. 2005. A contractile nuclear actin network drives chromosome congression in oocytes. *Nature* 436:812–818. doi:10.1038/nature03810

Lénárt P, Rabut G, Daigle N, Hand AR, Terasaki M, Ellenberg J. 2003. Nuclear envelope breakdown in starfish oocytes proceeds by partial NPC disassembly followed by a rapidly spreading fenestration of nuclear membranes. *J Cell Biology* 160:1055–1068. doi:10.1083/jcb.200211076

Lew DJ, Kornbluth S. 1996. Regulatory roles of cyclin dependent kinase phosphorylation in cell cycle control. *Curr Opin Cell Biol* 8:795–804. doi:10.1016/s0955-0674(96)80080-9

Linder MI, Köhler M, Boersema P, Weberruss M, Wandke C, Marino J, Ashiono C, Picotti P, Antonin W, Kutay U. 2017. Mitotic Disassembly of Nuclear Pore Complexes Involves CDK1- and PLK1-Mediated Phosphorylation of Key Interconnecting Nucleoporins. *Dev Cell* 43:141-156.e7. doi:10.1016/j.devcel.2017.08.020

MacLennan M, Crichton JH, Playfoot CJ, Adams IR. 2015. Oocyte development, meiosis and aneuploidy. *Semin Cell Dev Biol* 45:68–76. doi:10.1016/j.semcdb.2015.10.005

Malumbres M, Barbacid M. 2005. Mammalian cyclin-dependent kinases. *Trends Biochem Sci* 30:630–641. doi:10.1016/j.tibs.2005.09.005

Martino L, Morchoisne-Bolhy S, Cheerambathur DK, Hove LV, Dumont J, Joly N, Desai A, Doye V, Pintard L. 2017. Channel Nucleoporins Recruit PLK-1 to Nuclear Pore Complexes to Direct Nuclear Envelope Breakdown in C. elegans. *Dev Cell* 43:157-171.e7. doi:10.1016/j.devcel.2017.09.019

Masters TA, Kendrick-Jones J, Buss F. 2016. The Actin Cytoskeleton. *Handb Exp Pharmacol* 235:77–122. doi:10.1007/164_2016_29

Mochida S, Ikeo S, Gannon J, Hunt T. 2009. Regulated activity of PP2A–B55δ is crucial for controlling entry into and exit from mitosis in Xenopus egg extracts. *Embo J* 28:2777–2785. doi:10.1038/emboj.2009.238

Mogessie B, Schuh M. 2017. Actin protects mammalian eggs against chromosome segregation errors. *Science* 357. doi:10.1126/science.aal1647

Moor CH de, Richter JD. 1997. The Mos pathway regulates cytoplasmic polyadenylation in Xenopus oocytes. *Mol Cell Biol* 17:6419–6426. doi:10.1128/mcb.17.11.6419

Mori M, Hara M, Tachibana K, Kishimoto T. 2006. p90Rsk is required for G1 phase arrest in unfertilized starfish eggs. *Development* 133:1823--1830. doi:10.1242/dev.02348

Mori M, Somogyi K, Kondo H, Monnier N, Falk HJ, Machado P, Bathe M, Nédélec F, Lénárt P. 2014. An Arp2/3 Nucleated F-Actin Shell Fragments Nuclear Membranes at Nuclear Envelope Breakdown in Starfish Oocytes. *Curr Biol* 24:1421–1428. doi:10.1016/j.cub.2014.05.019

Nakamura N, Tokumoto T, Ueno S, Iwao Y. 2005. The cytoskeleton-dependent localization of cdc2/cyclin B in blastomere cortex during Xenopus embryonic cell cycle. *Mol Reprod Dev* 72:336–345. doi:10.1002/mrd.20348

Nakashima S, Kato KH. 2001. Centriole behavior during meiosis in oocytes of the sea urchin Hemicentrotus pulcherrimus. *Dev Growth Differ* 43:437–445. doi:10.1046/j.1440-169x.2001.00580.x

Nigg EA. 2001. Mitotic kinases as regulators of cell division and its checkpoints. *Nat Rev Mol Cell Bio* 2:21–32. doi:10.1038/35048096

Nurse P. 2000. A Long Twentieth Century of the Cell Cycle and Beyond. *Cell* 100:71–78. doi:10.1016/s0092-8674(00)81684-0

Okumura E, Sekiai T, Hisanaga S, Tachibana K, Kishimoto T. 1996. Initial triggering of M-phase in starfish oocytes: a possible novel component of maturation-promoting factor besides cdc2 kinase. *J Cell Biology* 132:125–135. doi:10.1083/jcb.132.1.125

Olsen JV, Vermeulen M, Santamaria A, Kumar C, Miller ML, Jensen LJ, Gnad F, Cox J, Jensen TS, Nigg EA, Brunak S, Mann M. 2010. Quantitative Phosphoproteomics Reveals Widespread Full Phosphorylation Site Occupancy During Mitosis. *Sci Signal* 3:ra3–ra3. doi:10.1126/scisignal.2000475

Ookata K, Hisanaga S, Bulinski JC, Murofushi H, Aizawa H, Itoh TJ, Hotani H, Okumura E, Tachibana K, Kishimoto T. 1995. Cyclin B interaction with microtubule-associated protein 4 (MAP4) targets p34cdc2 kinase to microtubules and is a potential regulator of M-phase microtubule dynamics. *J Cell Biology* 128:849–862. doi:10.1083/jcb.128.5.849

Ookata K, Hisanaga S, Okumura E, Kishimoto T. 1993. Association of p34cdc2/cyclin B complex with microtubules in starfish oocytes. *J Cell Sci* 105:873–881. doi:10.1242/jcs.105.4.873

Otsuki J, Nagai Y, Lopata A, Chiba K, Yasmin L, Sankai T. 2012. Symmetrical division of mouse oocytes during meiotic maturation can lead to the development of twin embryos that amalgamate to form a chimeric hermaphrodite. *Hum Reprod* 27:380–387. doi:10.1093/humrep/der408

Pappireddi N, Martin L, Wühr M. 2019. A Review on Quantitative Multiplexed Proteomics. *Chembiochem* 20:1210–1224. doi:10.1002/cbic.201800650

Paul AS, Pollard TD. 2009. Review of the mechanism of processive actin filament elongation by formins. *Cell Motil Cytoskeleton* 66:606–617. doi:10.1002/cm.20379

Peters J-M. 2006. The anaphase promoting complex/cyclosome: a machine designed to destroy. *Nat Rev Mol Cell Bio* 7:644–656. doi:10.1038/nrm1988

Picard A, Galas S, Peaucellier G, Dorée M. 1996. Newly assembled cyclin B-cdc2 kinase is required to suppress DNA replication between meiosis I and meiosis II in starfish oocytes. *Embo J* 15:3590–3598. doi:10.1002/j.1460-2075.1996.tb00728.x

Pleiner T, Bates M, Görlich D. 2018. A toolbox of anti–mouse and anti–rabbit IgG secondary nanobodies. *J Cell Biol* 217:1143–1154. doi:10.1083/jcb.201709115

Pollard TD. 2016. Actin and Actin-Binding Proteins. *Csh Perspect Biol* 8:a018226. doi:10.1101/cshperspect.a018226

Prodon F, Chenevert J, Sardet C. 2006. Establishment of animal–vegetal polarity during maturation in ascidian oocytes. *Dev Biol* 290:297–311. doi:10.1016/j.ydbio.2005.11.025

Robinson RC, Turbedsky K, Kaiser DA, Marchand J-B, Higgs HN, Choe S, Pollard TD. 2001. Crystal Structure of Arp2/3 Complex. *Science* 294:1679–1684. doi:10.1126/science.1066333

Rosas-Salvans M, Cavazza T, Espadas G, Sabido E, Vernos I. 2018. Proteomic profiling of microtubule self-organization in M-phase. *Mol Cell Proteomics* 17:mcp.RA118.000745. doi:10.1074/mcp.ra118.000745

Rotty JD, Wu C, Bear JE. 2013. New insights into the regulation and cellular functions of the ARP2/3 complex. *Nat Rev Mol Cell Bio* 14:7–12. doi:10.1038/nrm3492

Rouiller I, Xu X-P, Amann KJ, Egile C, Nickell S, Nicastro D, Li R, Pollard TD, Volkmann N, Hanein D. 2008. The structural basis of actin filament branching by the Arp2/3 complex. *J Cell Biology* 180:887–895. doi:10.1083/jcb.200709092

Sagata N. 1996. Meiotic metaphase arrest in animal oocytes: its mechanisms and biological significance. *Trends Cell Biol* 6:22–28. doi:10.1016/0962-8924(96)81034-8

Saiki T, Hamaguchi Y. 1997. Division of Polar Bodies Induced by Their Enlargement in the StarfishAsterina pectinifera. *Exp Cell Res* 237:142–148. doi:10.1006/excr.1997.3772

Schuh M. 2011. An actin-dependent mechanism for long-range vesicle transport. *Nat Cell Biol* 13:1431–1436. doi:10.1038/ncb2353

Schuh M, Ellenberg J. 2008. A New Model for Asymmetric Spindle Positioning in Mouse Oocytes. *Curr Biol* 18:1986–1992. doi:10.1016/j.cub.2008.11.022

Shaik AA, Wee S, Li RHX, Li Z, Carney TJ, Mathavan S, Gunaratne J. 2014. Functional Mapping of the Zebrafish Early Embryo Proteome and Transcriptome. *J Proteome Res* 13:5536--5550. doi:10.1021/pr5005136

Sluder G, Miller FJ, Lewis K. 1993. Centrosome Inheritance in Starfish Zygotes II: Selective Suppression of the Maternal Centrosome during Meiosis. *Dev Biol* 155:58–67. doi:10.1006/dbio.1993.1006

So C, Seres KB, Steyer AM, Mönnich E, Clift D, Pejkovska A, Möbius W, Schuh M. 2019. A liquid-like spindle domain promotes acentrosomal spindle assembly in mammalian oocytes. *Science* 364:eaat9557. doi:10.1126/science.aat9557

Stebbins-Boaz B, Cao Q, Moor CH de, Mendez R, Richter JD. 1999. Maskin Is a CPEB-Associated Factor that Transiently Interacts with eIF-4E. *Mol Cell* 4:1017–1027. doi:10.1016/s1097-2765(00)80230-0

Stebbins-Boaz B, Hake LE, Richter JD. 1996. CPEB controls the cytoplasmic polyadenylation of cyclin, Cdk2 and c-mos mRNAs and is necessary for oocyte maturation in Xenopus. *Embo J* 15:2582–92.

Strączyńska P, Papis K, Morawiec E, Czerwiński M, Gajewski Z, Olejek A, Bednarska-Czerwińska A. 2022. Signaling mechanisms and their regulation during in vivo or in vitro maturation of mammalian oocytes. *Reprod Biol Endocrin* 20:37. doi:10.1186/s12958-022-00906-5

Swartz SZ, Nguyen HT, McEwan BC, Adamo ME, Cheeseman IM, Kettenbach AN. 2021. Selective dephosphorylation by PP2A-B55 directs the meiosis I - meiosis II transition in oocytes. *Elife* 10:e70588. doi:10.7554/elife.70588

Tachibana K, Tanaka D, Isobe T, Kishimoto T. 2000. c-Mos forces the mitotic cell cycle to undergo meiosis II to produce haploid gametes. *Proc National Acad Sci* 97:14301--14306. doi:10.1073/pnas.97.26.14301

Takahashi K, Ishii K, Yamashita M. 2018. Staufen1, Kinesin1 and microtubule function in cyclin B1 mRNA transport to the animal polar cytoplasm of zebrafish oocytes. *Biochem Bioph Res Co* 503:2778–2783. doi:10.1016/j.bbrc.2018.08.039

Terasaki M, Campagnola P, Rolls MM, Stein PA, Ellenberg J, Hinkle B, Slepchenko B. 2001. A New Model for Nuclear Envelope Breakdown. *Mol Biol Cell* 12:503–510. doi:10.1091/mbc.12.2.503

Ucar H, Tachibana K, Kishimoto T. 2013. The Mos–MAPK pathway regulates Diaphanous-related formin activity to drive cleavage furrow closure during polar body extrusion in starfish oocytes. *J Cell Sci* 126:5153--5165. doi:10.1242/jcs.130476

Uraji J, Scheffler K, Schuh M. 2018. Functions of actin in mouse oocytes at a glance. *J Cell Sci* 131:jcs218099. doi:10.1242/jcs.218099

Verlhac M-H, Lefebvre C, Guillaud P, Rassinier P, Maro B. 2000. Asymmetric division in mouse oocytes: with or without Mos. *Curr Biol* 10:1303–1306. doi:10.1016/s0960-9822(00)00753-3

Virant-Klun I, Leicht S, Hughes C, Krijgsveld J. 2016. Identification of Maturation-Specific Proteins by Single-Cell Proteomics of Human Oocytes. *Mol Cell Proteomics* 15:2616--2627. doi:10.1074/mcp.m115.056887

Wang Q, Racowsky C, Deng M. 2011. Mechanism of the chromosome-induced polar body extrusion in mouse eggs. *Cell Div* 6:17. doi:10.1186/1747-1028-6-17

Wang S, Kou Z, Jing Z, Zhang Y, Guo X, Dong M, Wilmut I, Gao S. 2010. Proteome of mouse oocytes at different developmental stages. *P Natl Acad Sci Usa* 107:17639--17644. doi:10.1073/pnas.1013185107

Weber KL, Sokac AM, Berg JS, Cheney RE, Bement WM. 2004. A microtubule-binding myosin required for nuclear anchoring and spindle assembly. *Nature* 431:325–329. doi:10.1038/nature02834

Wessel GM, Reich AM, Klatsky PC. 2010. Use of Sea Stars to Study Basic Reproductive Processes. *Syst Biol Reprod Mec* 56:236–245. doi:10.3109/19396361003674879

Wühr M, Freeman RM, Presler M, Horb ME, Peshkin L, Gygi SP, Kirschner MW. 2014. Deep Proteomics of the Xenopus laevis Egg using an mRNA-Derived Reference Database. *Curr Biol* 24:1467--1475. doi:10.1016/j.cub.2014.05.044

Wu X, Palazzo RE. 1999. Differential regulation of maternal vs. paternal centrosomes. *Proc National Acad Sci* 96:1397–1402. doi:10.1073/pnas.96.4.1397

Xu Y, Moseley JB, Sagot I, Poy F, Pellman D, Goode BL, Eck MJ. 2004. Crystal Structures of a Formin Homology-2 Domain Reveal a Tethered Dimer Architecture. *Cell* 116:711–723. doi:10.1016/s0092-8674(04)00210-7

Yamagishi Y, Abe H. 2018. Actin assembly mediated by a nucleation promoting factor WASH is involved in MTOC–TMA formation during Xenopus oocyte maturation. *Cytoskeleton* 75:131–143. doi:10.1002/cm.21428

Yang G, Smibert CA, Kaplan DR, Miller FD. 2014. An eIF4E1/4E-T Complex Determines the Genesis of Neurons from Precursors by Translationally Repressing a Proneurogenic Transcription Program. *Neuron* 84:723–739. doi:10.1016/j.neuron.2014.10.022

Yi K, Unruh JR, Deng M, Slaughter BD, Rubinstein B, Li R. 2011. Dynamic maintenance of asymmetric meiotic spindle position through Arp2/3-complex-driven cytoplasmic streaming in mouse oocytes. *Nat Cell Biol* 13:1252–1258. doi:10.1038/ncb2320

Zhong Z, Huo L, Liang C, Chen D, Sun Q. 2005. Small GTPase RhoA is required for ooplasmic segregation and spindle rotation, but not for spindle organization and chromosome separation during mouse oocyte maturation, fertilization, and early cleavage. *Mol Reprod Dev* 71:256–261. doi:10.1002/mrd.20253